Dissertation

Water-Rock Interaction and Geochemistry of Groundwater in Axum Area (Northern Ethiopia)

By

Tewodros Alemayehu Tesfamichael

Graz University of Technology

Institute of Applied Geosciences

May, 2011

Dissertation

Water-Rock Interaction and Geochemistry of Groundwater in Axum Area (Northern Ethiopia)

By

Tewodros Alemayehu TESFAMICHAEL

Supervisor and reviewer

Univ.-Prof. Dipl.-Min. Dr.rer.nat. Martin DIETZEL

Institute of Applied Geosciences, Graz University of Technology

Second reviewer

Dipl.Chem. Dr. Albrecht LEIS

Laboratory Centre for Isotope Hydrology and Environmental Analytics, Joanneum Research

“The love of a family is life's greatest blessing”

Dedication

To my wife Tigist Teame and my lively daughters Niyat and Eliana
I dedicate this to you. Thank you for all that you have done for me.

Declaration

I hereby declare that the Doctoral thesis, entitled “water-rock interactions and geochemistry of groundwater in Axum area (Northern Ethiopia)”, represents my own work. To the best of my knowledge and belief, the thesis contains neither material previously published or written by another person nor material which has been previously submitted for the award of any other degree, diploma or other qualification of the university or other institute of higher learning, except where due reference has been made.

Signed .....

Tewodros Alemayehu Tesfamichael

Date .....

Abstract

The thesis investigates the chemical characteristics of groundwater in the Axum area to decipher the hydrogeochemical processes leading to the variability in groundwater quality. A wide range of chemical constituents can be dissolved in groundwater as a result of interaction with the soil and bedrock and from human activities. The variations in groundwater chemistry/quality are discerned from hydrochemical and isotope data.

The result reveals that the groundwater chemistry is generally controlled by uptake of CO_2, weathering of minerals, and precipitation of secondary minerals as well as ion exchange. Elevated concentrations of total dissolved solids (1200-2000 mg l^{-1} TDS) in some deep wells of Axum groundwater are attributed to prolonged water-rock interaction. The high level of nitrate in selected wells indicates that shallow unconfined aquifers are particularly vulnerable to anthropogenic contamination.

The δ^2H and δ^{18}O values (VSMOW) of all water samples indicate meteoric origin. Apparent variation in isotopic composition of groundwaters is partly attributed to evaporation (surface water) and impact of strong water-silicate interaction (two deep groundwaters). The isotope values suggest that most recharge occurs through basalt fractures with little or no significant evaporation prior to recharge. $\delta^{13}C_{DIC}$ values of shallow groundwaters between -7 and -12 ‰ (VPDB) display uptake of soil CO_2, whereas $\delta^{13}C_{DIC}$ of deep groundwater ranging from +1 to -5‰ attests contribution of CO_2 from volcanic origin. Uptake of volcanic CO_2 stimulates the dissolution of minerals and rocks, and results in elevated solute concentrations in the basaltic aquifer. Deep groundwaters are significantly enriched in concentrations of Ca^{2+}, Mg^{2+}, Na^+ and $Si(OH)_4$ compared to the shallow type groundwater. Weathering of local basalts is documented by $^{87}Sr/^{86}Sr$ ratios from 0.7038 to 0.7059 in the groundwater with possible impact from the basement complex. Besides silicate weathering, the neoformation of, e.g., kaolinite and montmorillonite has to be considered as reaction products. The δ^{34}S range (VCDT) of dissolved sulfate from +6 to +19 ‰ can be explained by leaching of volcanic sulfur with subsequent bacterial induced sulfate reduction. The concentration of iron and manganese responds to the groundwater redox conditions.

In several solutions supersaturation with respect to calcite is reached by degassing of CO_2 leading to the precipitation of calcium carbonates. Inverse geochemical modelling validates the reaction mechanisms observed by (isotope) chemical composition of the groundwater.

Kurzfasssung

Die vorliegende Arbeit umfasst die chemische Charakterisierung von Grundwässern aus der Region Axum zur Darstellung der hydrogeochemischen Prozesse, die für die Variation der Grundwasserzusammensetzung verantwortlich sind. Die im Grundwasser gelösten Komponenten werden im Wesentlichen über die Wechselwirkung mit Böden, anstehenden Gesteinen und anthropogene Aktivitäten eingetragen. Die Variabilität in der Chemie/Qualität des Grundwassers kann über hydrogeochemische und isotopenchemische Daten abgeleitet werden.

Die Ergebnisse zeigen, dass die Grundwasserchemie wesentlich durch die Aufnahme von CO_2, die Verwitterung von Mineralen und die Abscheidungen von Sekundärmineralen sowie durch Ionen-Austausch-Prozesse geprägt ist. Hohe Konzentrationen an total gelösten Feststoffen (1200-2000 mg l^{-1} TDS) in einigen tiefen Brunnen sind an starke Wasser-Gesteins Wechselwirkungen gebunden. Der hohe Gehalt an Nitrat in einigen Brunnen indiziert, dass insbesonders seichte Brunnen durch anthropogene Kontaminationen gefährdet sind.

Die $\delta^{2}H$ und $\delta^{18}O$ Werte (VSMOW) aller Wasserproben zeigen meteorische Herkunft an. Die auftretenden Wertebereiche sind zum Teil an Evaporationsprozessse (Oberflächenwasser) und an verstärkte Wasser-Silikat Reaktionen (2 tiefere Brunnenwässer) gebunden. Die Isotopenwerte vermitteln ferner, dass die Grundwassererneuerung über Bruchstrukturen im Basalt stattfindet mit nur sehr geringer Evaporation vor der Infiltration. Die $\delta^{13}C_{DIC}$ Werte von seichten Grundwässern zwischen -7 und -12 ‰ (VPDB) ergeben sich durch die Aufnahme von Boden CO_2. Demgegenüber sind die $\delta^{13}C_{DIC}$ Werte der tieferen Grundwässer von +1 bis -5‰ an CO_2 vulkanogener Herkunft gebunden. Die Aufnahme von CO_2 verstärkt die Auflösung von Mineralen und Gesteinen und verursacht erhöhte Konzentrationen an Ca^{2+}, Mg^{2+}, Na^{+} und $Si(OH)_4$ im Vergleich zu den seichten Grundwässern. Die Verwitterung des lokalen Basalts ist durch die $^{87}Sr/^{86}Sr$ Verhältnisse von 0.7038 bis 0.7059 dokumentiert, wobei ein Eintrag über die Verwitterung von Gesteinen des Basements möglich ist. Neben der Verwitterung von Silikaten ist die Neubildung von z.B. Kaolinit und Montmorillonit zu berücksichtigen. Der $\delta^{34}S$ Wertebereich (VCDT) des gelösten Sulfates von +6 bis +19 ‰ kann durch die Aufnahme von vulkanogenem CO_2 und nachfolgender bakteriell induzierter Sulfatreduktion erklärt werden.

Die Konzentrationen an Eisen und Mangan reflektieren die Redoxbedingungen des Grundwassers.

In einigen Lösungen wird eine Übersättigung in Bezug auf Kalzit über die Entgasung von CO_2 beobachtet. Dies kann zur Abscheidung von Kalziumkarbonat führen. Inverse geochemische Modellierungen bestätigen die Rektionsmechanismen, die aus den Isotopendaten und chemischen Zusammensetzungen der Grundwässer abgeleitet wurden.

Key words: Axum; groundwater; geochemical modelling; stable isotopes; water-rock interaction

Acknowledgements

A lot of people have contributed in many ways to the success of this work and as part of my appreciation to their contribution I would like to extend my gratitude to all of those who generously supported me along the way.

First, I am heartily thankful to my supervisor, Prof. Dr. Martin Dietzel, whose unceasing guidance, encouragement and support made working on this dissertation a real pleasure. This work could not have been materialized without his significant input, constructive criticisms, valuable advice, and fruitful discussions. I would also like to thank Dr. Albrecht Leis for his assistance in isotope analysis and geochemical modelling. I am grateful to Prof. Dr. Aberra Mogessie for his encouragement, practical advice and for reviewing the manuscript.

I am thankful to all the staff of the Institute of Applied Geosciences for their technical support in the laboratory, in particularly Prof. Dr. Dietmar Klammer, Judith Jernej, Maria Hierz, Dipl. Min. Daniel Hoellen and Dr. Christine Latal for their unreserved help during the water and solid sample analysis. I thank Prof. Dr. Anton Eisenhauer (GEOMAR, Kiel) and Prof. Dr. Michael Böttcher (IOW, Warnemünde) for support of strontium and sulfur isotope analyses, respectively. I have to thank Peter Schreiber for his support in providing computer and software related facilities. I am thankful to Anna Maria Pendl and Daniela Sobian for all administrative assistances during my stay at the institute.

Our stay (family) in Austria would have not been lively if not for many good friends in Graz. Sincere thanks to Dr. Abraham Abebe, Sara Gebremedhin, Tewodros Teklu, Azeb Assefa and their families for supporting us. I also highly value the support I have received from Sabine Prem and her family. I want to offer my warm thanks to all of them for making our stay in Austria feel as home-away-from-home.

I would like to acknowledge the Austrian Agency for International Cooperation in Education and Research (OeAD-GmbH) for PhD grant. I am grateful to NAWI Graz for enabling me to take part in conferences by providing financial supports and for partial funding of my field work in Ethiopia.

Collecting the water and rock samples would not have been possible without the efforts of several organizations and persons. Here, I want to offer my sincere thanks to Axum Water and Sewerage Authority for allowing access to the municipal wells for sampling. A special thanks to Abadi Romha, Gebrekidan Gebretatios and Luel Teame for their friendly assistance in the field. I would like also to thank Mekelle University for granting me leave of absence to pursue my study and providing me a vehicle during the field work.

Finally, I would like to thank my family: my wife Tigist Teame for her support, patience and unwavering love that would be undeniably a source of my strength and inspiration, and my lively kids Niyat and Eliana. I could not ask for more, and I will always love and cherish their affection. I am grateful to my brothers Elias and Daniel for their encouragement and support. Last but not least I want to thank my parents, Alemayehu and Kidan. I would not have managed to come this far without their efforts, support, blessings and unconditional love, and I will forever be thankful for all they have done for me.

Table of contents

List of Figures

1. Introduction

1.1. Background

Groundwater has served as the main source for drinking water supply in many parts of Ethiopia. Especially in the dry areas, where surface water are seasonal and scarce, water from boreholes and springs provides water resource supply for various purposes including drinking, domestic and irrigation use. Groundwater is the only realistic water supply option to meet the growing water demand. For evaluating the suitability of groundwater for respective purposes, knowledge about the individual chemical characteristics of a given groundwater is essential.

The town Axum is located in the northern volcanic plateaux of Ethiopia. Contrary to the presumed good quality of volcanic hosted groundwater in the highlands, Axum groundwater shows elevated dissolved solids. In general the groundwater chemical constitutes display the interactions with hosted rocks, mainly fractured volcanic rocks and associated alluvial sediments. The volcanic rocks represent a complex aquifer system in which the occurrence and quality groundwater is influenced by the local hydrogeological conditions and geochemical reactions. The geochemical reactions depend on several factors including the presence of reactive gas species such as CO_2, solubility of minerals and rocks in the aquifer, water temperature, oxidation-reduction reactions, and precipitation of secondary minerals.

The uptake of gaseous CO_2 generates acidic solutions and favours the dissolution and transformation of minerals and rocks (e.g. Clark and Fritz, 1997; Dietzel and Kirchhoff, 2002; Schofield and Jankowsk, 2004; Oelkers and Schott, 2009). High partial pressures of CO_2 can be gained from various sources. Accordingly, the geochemical evolution of groundwater is influenced by the distribution of aquifer composition and the initial composition of the recharge solutions. In numerous studies, chemical and isotopic approaches have been successfully applied to decipher reaction mechanisms of relevant water-rock interactions and aquifer heterogeneities (e.g. Frape and Fritz, 1984; Kebede et al., 2005; Elango and Kannan, 2007; Sharif et al., 2008; Shand et al., 2009).

In this study the chemical characteristics of the main groundwater fields of Axum area is investigated to identify mechanisms that influence the variability in major and trace element

concentrations. The chemical and isotopic composition of the groundwater is coupled to the mineralogical and (isotope)geochemical properties of the lithology. Conventional hydrochemical investigation and isotopic tracer elucidate the origin of water and dissolved species. Geochemical modelling is also applied to validate the geochemical processes controlling the groundwater chemistry.

1.2. Motivation and objective of the study

Groundwater is the primary source for drinking proposes in Axum area, but it is poorly managed resource mainly due to lack of scientific knowledge on local groundwater evolution and anthropogenic impacts. The water quality problem of Axum area has been addressed by different institutions (Devecon, 1995; Water Well Drilling Enterprise, 1998; Abay Engineering, 2006). The large variation in yield of wells and the presence of poor quality water in domestic water use have been reported. While earlier studies on groundwater quality in study area attempted to identify the potential contaminant that affects the water quality partly (Devecon 1995; Water Well Drilling Enterprise, 1998; Abay Engineering, 2006), they were unable to establish the source of the water and dissolved constituents. Most of former studies are related to implementation projects for water supply infrastructure of the town. No scientific research has been conducted to understand the causes for variation in groundwater quality.

Unlike the rift valley system, where high solute concentrations e.g. of fluoride in local groundwater is expected, majority of the groundwaters from basaltic plateaus are characterized by low total dissolved solids, TDS (Kebede et al., 2005; Ayenew et al., 2008). Thus, the causes for localized high variation in TDS of groundwater of Axum area are not well understood.

The present study aims to get fundamental knowledge on geochemical processes controlling the chemical composition of groundwater form Axum and its geographical distribution. Multiple elemental and isotopic tracers are used to understand the processes. The specific objectives of this thesis, therefore, are to:

- discover the causes for variability in groundwater chemistry in the Axum aquifer.
- elucidate the dominant geochemical processes that control the solute (major and minor elements) concentration.
- determine sources of groundwater and dissolved solutes.

- examine the contribution of anthropogenic impacts on groundwater chemistry against to natural baseline conditions.
- develop a conceptual model for groundwater evolution and validate hydrogeochemical processes using geochemical modelling.

1.3. Research approach and thesis structure

Hydrochemical, hydrogeological and isotope data are obtained to improve knowledge on the evolution of groundwater and of solutes in different types of groundwaters from Axum area. The conventional chemical characterization comprises major and trace elements of the aqueous solutions. Isotope analyses include $^{2}H/H$, $^{18}O/^{16}O$, $^{13}C/^{12}C$, $^{87}Sr/^{86}Sr$ and $^{34}S/^{32}S$ ratios. Hydrogeochemical modelling is used to validate chemical evolution of groundwater.

The thesis comprises eight chapters. The first chapter introduces the research background, motivation and objectives of the study. The theoretical background chapter highlights the occurrence of groundwater in volcanic aquifer, principles of aqueous speciation, solubility and redox condition, geochemical modelling and application of isotope geochemistry. In the following section an overview about the geological and hydrogeological condition of the study area is given. Chapter four presents the methodology to achieve the research objectives. Chapter five focus on the mineralogical and chemical compositions of the rock samples from the study area. The main research work of the thesis is described in chapter six to eight, where the results including hydrogeochemistry, isotope geochemistry and geochemical modelling are discussed. The sections generally deal with the effect of water-rock interaction on groundwater chemistry and its possible reaction control mechanisms and isotopic interpretations of environmental tracers for deciphering water and solute sources in hydrologic systems. The geochemical modelling is employed to support the groundwater evolution are geochemically valid.

1.4. Previous work

In previous studies the genesis and evolution of Neoproterozoic successions of low grade metamorphic rock and syn- and pos-tectonic intrusive rocks of Axum (Tadesse-Alemau, 1998; Tadesse et al*.,* 1999; Tadesse et al*.*, 2000) and the nearest basalt rocks (e.g. Pik et al., 1998; 1999) and the occurrence of sediments and sedimentary rocks (e.g. Getaneh, 2002; Avigad et al*.,* 2007)

have been studied extensively. More recently the petrology and geochemistry characteristics of volcanic rocks of the Axum area is reported (Hagos et al., 2010)

In addition various organizations (e.g. Devecon, 1995; Water Well Drilling Enterprise, 1998; Abay Engineering, 2006) have also attempted to investigate the groundwater quality of the area. These studies were generally initiated by the water quality problems of the area. The first examination of groundwater resource was done by EWE (1973), who examined the potential water supply of volcanic aquifer for Axum. Water Well Drilling Enterprise (1998) tried to document the drilling and pumping test data records of the aquifer and the state of exploration and utilization. A more detailed and comprehensive study was carried out by Abay Engineering (2006) to tackle the water quality problem. High concentrations of dissolved carbon dioxide, iron and manganese at rather low pH and dissolved oxygen content have been detected in several groundwaters.

The groundwater quality of some of the wells has been considered unsuitable for domestic uses because of high concentrations of TDS, in particular of dissolved iron and manganese above WHO recommended values. Poor water quality of the region has been become challenging as it starts to pose health problem (EHNRI/DACA, 2006). Several wells have been either abandoned or used to supply the inhabitant of the town by mixing with freshwater of higher quality. Moreover, the low yielding capacities of several wells within the study area cannot cater the increasing demand of the inhabitants. Previous studies proposed different origin of the contaminants that affect the groundwater quality, but none of the studies were able to identify the distinct sources and mechanisms for elemental contamination.

Recently, hydrochemical and isotope evidence have been widely applied to identify the hydrogeology and hydrochemistry condition in volcanic aquifers of Ethiopia (e.g. Kebede et al., 2005; Ayenew et al., 2007; Kebede et al., 2007; Demlie et al., 2008). These studies are mostly focused on understanding the groundwater flow paths, recharge condition and chemical evolution of groundwaters in the Ethiopian rift system. Studies to delineate chemically and isotopically distinct groundwaters and infer geochemical interactions using hydrochemical and isotopic indicators on highlands of Ethiopia are barely reported in the literature.

2. Theoretical background

2.1. Groundwater in volcanic aquifers of Ethiopia

Hydrogeological conditions of volcanic aquifers are of a great importance for fresh water resource in many parts of the world (e.g. Edmunds et al., 2002; Dafny et al., 2006; Bertrand et al., 2010). Volcanic rocks have also proved to be important aquifer system in Ethiopia (e.g. Kebede et al., 2007; Ayenew et al., 2008; Demlie et al., 2008; Kebede et al., 2010). Ethiopia has enormous groundwater potential in the volcanic terrain of the Rift System and highlands. However, the potential varies considerably owing to the complex geological condition of the volcanic rocks.

The volcanic plateau is dominated by basaltic lava flow (Fig. 1A) developed in response to tectonic movements associated with Oligocene prerift volcanism (Pik et al., 1998; 1999). Unlike the hydrogeology of the Ethiopian Rift System (e.g. Kebede et al., 2007; Demlie et al., 2008, Kebede et al., 2010), the groundwater system and its interaction with hosting rock in the volcanic plateaux have barely been reported. Groundwater resource study in the Ethiopian flood basalt and associated quaternary sediments are confined in fractured and weathered volcanic interbedded with paleosoils and river gravels in the highlands (Ayenew et al., 2008). The spatial and temporal distributions of the volcanic rocks with wide compositional and weathering variability complicate the hydrogeological and hydrochemical behaviour of the volcanic aquifers (Ayenew et al., 2008). Volcanic rocks have a wide range of chemical, mineralogical, structural, and hydraulic properties, mainly due to variability of rock types. The flow and occurrence of groundwater in crystalline rocks is strongly controlled by the structure and the presence of vesicles and their interconnection and geomorphological setup of the volcanic terrain. These crystalline rocks are highly permeable if fractured and, they generally yield small amounts of groundwater to wells.

The groundwater system of the volcanic terrain of Ethiopia is characterized by multi-layer aquifers. Permeability and recharge rates of the basaltic-rock aquifers are extremely variable. Although the basalts develop good permeability due to secondary porosity, the fractured rocks in several cases locally covered with quaternary sediments reducing the permeability of the fractured rock underneath and acting as aquitard (Ayenew et al., 2008). Acidic volcanic rocks tend to weather intensively and generate clay minerals that seal permeable layers. The thickness of the overburden

sediment varies and hence changes the hydrological conditions of the area (i.e. porosity, permeability). Hydraulic conductivity can be rise in areas that are faulted and fractured (Ayenew et al., 2008). Once water starts percolating in the preferential groundwater recharge areas, it can migrate along the rock structures depending on the hydrological conditions. River discharge increases during the wet season suggesting a direct input from rainfall and surface runoff rather than groundwater (Kebede et al., 2005). Volcanic rocks interbedded with paleosoils and ashes in various locations of Ethiopia highlands (Fig. 1B) can serve as groundwater flow barriers and inhibits water from enters into wells (Ayenew et al., 2008). The spatial variation in quality and quantity of groundwater in the northern Ethiopia can be explained by unconnected aquifers in the study area. The highland older trap series volcanoes have lower fracturing and higher clay filling which result in moderate to low productivity although the unit is characterized locally by high permeability conditions as compared to highly variable basaltic and underlying sandstone heterogeneous lithologic unit (Ayenew et al., 2008).

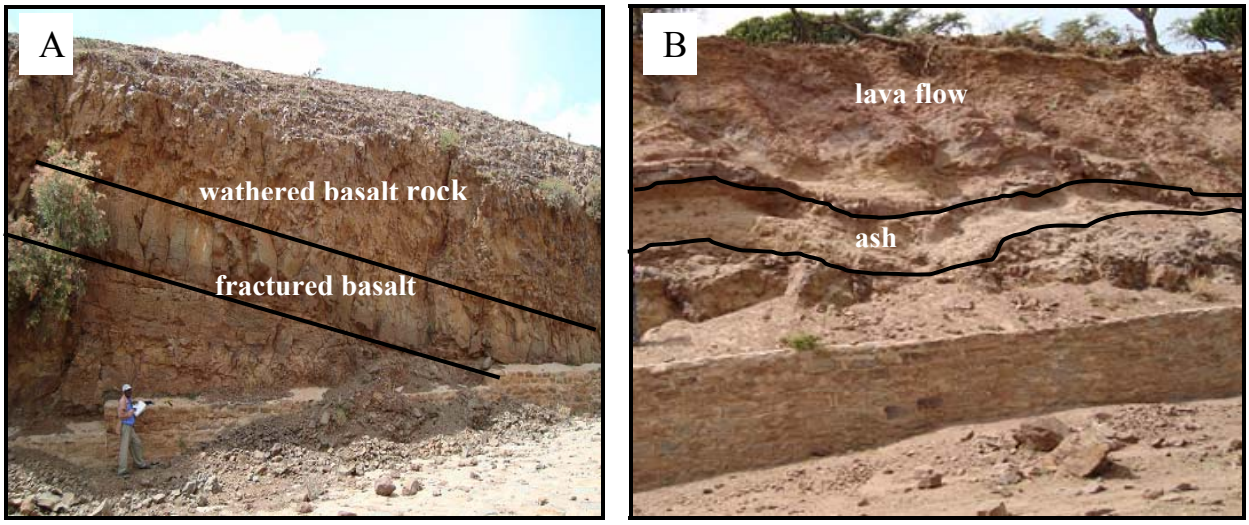

Fig. 1. (A) Typical fissural basaltic lava flow (B) intercalation of lava flow and ash in basaltic aquifer

The hydrochemical signature of groundwater in volcanic terrains indicates wide spatial variation owing to differences in rock-water interactions. The Ethiopian Rift Valley waters are dominantly sodium-bicarbonate type with high salinity and fluoride content (Kebede et al., 2010). Groundwater in the rift zone is influenced by geothermal waters with abnormally high concentrations of fluoride from leaching acid volcanic rocks. In the volcanic plateaux, Ca and Mg ions are the dominant dissolved constitutes, with total dissolved solids often ranging from 50 to 1200 mg/l (Ayenew et al., 2008). Less variation in concentrations of major ions, narrow range in

Mg/Ca ratio and near-neutral pH characterised the groundwater of basaltic aquifer. The groundwater of the deep aquifer is commonly complex mixtures of groundwater recharged through diverse aquifer rocks of water masses. Nevertheless, larger portion of the groundwater system of the basaltic terrain has moderately hard and potable water.

2.2. Water-rock interaction and its control on chemical composition

The chemical composition of the groundwater is influenced by the reaction between the recharging water, mineral of surrounding rocks and gas phases. The effect of aquifer heterogeneity and water-rock interaction for groundwater evolution was documented by e.g. Frape and Fritz, 1984; Edmund et al., 2002; Kebede et al., 2005; Elango and Kannan, 2007; Sharif et al., 2008; Shand et al., 2009. Geochemical reactions such as dissolution and precipitation of solids, cation exchange, and adsorption contribute considerably to the variation of elemental concentrations in the groundwater. Hence, the concentrations of major ions of groundwater can be used to identify the intensity of water-rock interaction and chemical reactions (Elango and Kannan, 2007). Alkalinity is also frequently used to indicate the extent of water-rock interaction (Kim et al., 2002). The nature and extent of interactions can greatly influence the spatial variation in the dissolved solids.

Silicate weathering can be indicated by general relationships between the concentrations of major cations. The degree to which the mineral phases react with the groundwater depends on the internal partial pressure of CO_2 in the groundwater as pH is crucial for silicate weathering. The solubility of CO_2 in the aqueous solutions is of major importance for the reactivity of the system as CO_2 reacts with the water to form carbonic acids. Groundwater properties and time dependent water-rock interactions can greatly affect the chemistry of the water. Understanding of the water-rock interaction and associated reactions is essential to identify variability in groundwater chemical composition.

2.3. Aqueous speciation and solubility

Aqueous speciation comprises the distribution and concentration of individual components in an aqueous solution which can be established based on equilibrium constant. The dissolved species in the aqueous phase are assumed to be in thermodynamic equilibrium to calculate the activities of ions and uncharged compounds.

Gaseous CO_2 is dissolved in water according to the equation

$$CO_{2(g)} \rightarrow CO_{2(aq)} \quad (1)$$

The solubility of CO_2 is defined by Henry's law that describes the equilibrium between vapor and liquid. The dependence of PCO_2 on $H_2CO_3^*$ and equilibrium constant is

$$PCO_2 = \frac{\left(H_2CO_3^*\right)}{K_0} \quad (2)$$

($H_2CO_3^* = CO_{2(aq)} + H_2CO_3$).

The other inorganic carbon species can be related by respective equilibrium constants

$$CO_{2(gas)} + H_2O = H_2CO_3^* \qquad K_0 \quad (3)$$

$$H_2CO_3^* = H^+ + HCO_3^- \qquad K_1 \quad (4)$$

$$HCO_3^- = H^+ + CO_3^{2-} \qquad K_2 \quad (5)$$

where K_0, K_1, and K_2 are the equilibrium constants for CO_2 dissolution into water, and the first and the second dissociation constant, respectively.

The solubility of a solid is the quantity that dissolves in a solution. The solubility product constant (K_{sp}) is the equilibrium constant between a solid and its respective components in a solution according to the general reaction

$$aA + bB = cC + dD \quad (6)$$

The mass action describes the equilibrium mass distribution can thus be written as

$$K_{sp} = \frac{(C)^c (D)^d}{(A)^a (B)^b} \quad (7)$$

where (A),(B),(C), and (D) denote the molar activities and K_{sp} is the solubility product constant. K_{sp} is temperature dependent

The activity of a species is related to its molar concentration according to the equation

$$(A) = \gamma_a [A] \tag{8}$$

where γ_a is the activity coefficient and $[A]$ is the molar concentration of the species A.

The simplest model to predict ion activity coefficients is the Davies or extended Debye-Hückel equation. In PHREEQC, the Davies equation is used for calculating the activity coefficient of charged species in solution according to

$$log\ \gamma_i = -AZ_i^2 \left(\frac{\sqrt{I}}{1+\sqrt{I}} - 0.3I \right) \tag{9}$$

where A is a constant, Z_i is the ion charge, and I is the ionic strength of the solution. The ionic strength of a solution is a function of the concentration of all ions present in a solution and given by

$$I = \frac{1}{2} \sum_i^n M_i Z_i^2 \tag{10}$$

where (M_i) is the molar concentration of the species i.

The relation between the solubility product and the ion activities product of the water constituents is given by the saturation index (SI), defined as:

$$SI = log \left(\frac{IAP}{K_{sp}} \right) \tag{11}$$

where IAP is the ion activity product and K_{sp} is the equilibrium constant at a given temperature. When $SI < 0$ the system is in undersaturated, whereas for $SI > 0$ the solution is supersaturated with respect to the respective solid.

For calculation of aqueous speciation and solubilities the computer code *PHREEQC* (Parkhurst and Appelo, 1999) is used with "phreeqc database" which includes the aqueous species $H_2CO_3^*$, HCO_3^-, CO_3^{2-}, $MgCO_3^o$, $NaHCO_3^o$, $CaCO_3°$, $FeCO_3°$, $MgHCO_3^+$, $CaHCO_3^+$, and $FeHCO_3^+$ for the

carbonate system. *PHREEQC* is also designed to perform a wide variety of hydrogeochemical calculations including speciation, saturation-index and charge balance calculations.

2.4. Oxidation-reduction reactions

Reduction-oxidation (redox) reactions in aquifer are among the one of the most important factors controlling chemical composition, solubility, reactivity and the formation and precipitation of mineral phases in groundwater. The redox potential can directly influence the concentrations redox sensitive elements in groundwater. Such reactions can also modify the pH of solutions, and occasionally induce secondary dissolution of rock-bearing minerals (e.g., Appelo and Postma, 2005). Thus, monitoring oxidation-reduction processes in groundwater systems can be viewed as an integrated assessment of hydrogeochemical processes.

Several elements can occur in more than one oxidation state in solution which influences chemical speciation. A general equation for a redox reaction is described by Nernst (e.g. Stumm and Morgan, 1996).

$$Ox + ne^{-} \rightarrow red \tag{12}$$

where reaction constant is defined as

$$K = \frac{(red)}{(ox)\ \ e^{-n}} \tag{13}$$

(*red*) and (*ox*) refers to reductant and oxidant, respectively and *n* is the number of exchanged electrons. From the equation 13, the following can be derived

$$logK = log\frac{[(ox)]}{[(red)]} - nlog\left(e^{-}\right) \tag{14}$$

Rearranging Eq. (14) gives

$$p\varepsilon = \frac{1}{n} log\, K + \frac{1}{n} log\, \frac{[(ox)]}{[(red)]} \tag{15}$$

The calculation of $p\varepsilon$ (= -log(e^-)) is based on the assumption that all redox reactions in an aqueous system are in a state of thermodynamic equilibrium. The redox potential can also be described using Nernst equation to get *Eh*.

$$Eh = Eh^0 + \frac{2.3RT}{nF} log \frac{[(ox)]}{[(red)]} \quad (16)$$

where *R* is the gas constant, *T* is the absolute temperature in Kelvin, *F* is the Faraday's constant, *n* is the number of transferred electrons in the reaction, and Eh^0 is redox potential under normal conditions.

PHREEQC was used to calculate the *Eh* and $p\varepsilon$ by means of the redox speciation with the Nernst Equation according to

$$Eh = \frac{2.3RT}{F} p\varepsilon \quad (17)$$

Eh can conveniently be measured directly or calculated from the measurements of individual redox species concentrations (e.g. O/O(II)). In natural water, redox couples are not necessarily in equilibrium with each other (Stumm and Morgan, 1996). Consequently, practical measurements rarely correlate with calculated values. Nevertheless, the interpretations of geochemical data by means of *Eh-pH* diagram are frequently used to characterize the redox state assuming the solution is in equilibrium (Peiffer et al., 1992).

2.5. Basic principles of inverse geochemical modelling

Mass balance modelling has been used to validate the chemical evolution of groundwater (e.g. Bowser and Jones, 1990; Parkhurst, 1997; Hidalgo and Cruz-Sanjulian, 2001; Sharif et al., 2008). In the present study so-called inverse geochemical modelling is applied depending on both mass and charge balance. Using such modelling approach water-rock interactions can be re-calculated assuming potential geochemical reactions for the chemical evolution of the local groundwater.

The basic principle of inverse geochemical modelling lays on the mass transfer reactions between two consecutive chemical compositions of aqueous solutions along a flow path. The overall mass

balance equation is given by the initial water components + reactants = final water components + products according to the equation

$$\sum_{p=1}^{p} a_p b_{p,k} = m_{T,k(\,final\,)} - m_{T,k(initial\,)} = \Delta m_{T,k} \qquad (18)$$

(Appelo and Postma, 2005). p denotes number of mineral phases (reactants + products); α_p is the number of moles of the p^{th} mineral transferred into (+) or out of (–) in 1 L solution; $b_{p,k}$ denotes the stoichiometric coefficient of the master species k in the mineral p; $\Delta\, m_{T.k}$, is the change in total molality of the element k between final and initial solution.

The representative chemical contents of the initial and final solutions have to be defined based on the local hydrogeological situation. The respective solutions in the present study area were chosen considering the hydraulic head difference of the aquifer system and observed trends in the chemical composition of the groundwater. The groundwater flows from shallow to deep aquifer of 200 m apart were discerned. Thus shallow (AW23) and deep groundwater (AW16) are considered as initial and final solution, respectively. Inverse geochemical modelling requires mineralogical composition along the flow paths in order to determine the solid phases in the reaction responsible for the observed evolution. The computer code *PHREEQC* with *phreeqc.dat* database (Parkhurst and Appelo, 1999) has been employed to calculate the dissolution and precipitation reaction according to the above modelling approach. The simulation takes into account uncertainty limits that are constrained for mass and charge balance (Parkhurst, 1997).

2.6. Applications of isotope geochemistry

Isotopic composition of groundwater can be used to decipher sources of H_2O and solutes and to identifying geochemical reaction mechanisms. Therefore, applications of isotope analysis have focused on the elements of hydrogen ($^{2}H/H$), oxygen ($^{18}O/^{16}O$), carbon ($^{13}C/^{12}C$), sulfur ($^{34}S/^{33}S$) and strontium ($^{87}Sr/^{86}Sr$). Prior to this study, a detailed record of spatial or temporal isotopic composition of precipitation or groundwater has not existed for the study area. The sources of dissolved inorganic carbon have been investigated using stable carbon isotope records in the dissolved inorganic carbon (DIC). In addition, selected groundwaters were analyzed for $^{34}S/^{33}S$ ratios in dissolved SO_4^{2-} and $^{87}Sr/^{86}Sr$ ratios.

2.6.1. Stable isotopes of oxygen and hydrogen in water

Stable isotope signatures of oxygen and hydrogen in the water molecule provide information about the origin of water, e.g. from individual catchment areas, and on e.g. evaporation and mixing effects (Barnes and Allison, 1988). Stable isotopic composition of the water molecule can be also used to examine the strength of interaction between the groundwater and hosting rocks in the aquifer. Analyses are given in the δ notation as parts per million (‰) with respect to Vienna Standard Mean Ocean Water (V-SMOW). The δ notation is expressed as

$$\delta_{sample\,(‰)} = \frac{\left(R_{sample} - R_{standard}\right)}{R_{standard}} x10^3 \qquad (19)$$

where R_{sample} and R_{standard} represent the ratio of heavy to light isotopes (e.g. ^{2}H/H) of the sample and standard, respectively.

2.6.2. Stable carbon isotopes of DIC

Stable carbon isotopes of total dissolved inorganic carbon (DIC) have been frequently used as groundwater tracers to identify carbon sources and to evaluate chemical reactions within aquifers (Clark and Fritz 1997; Cartwright et al., 2002; Federico et al., 2002; Jin et al., 2009). DIC exists as aqueous carbon dioxide ($CO_{2(aq)}$), carbonic acid ($H_2CO_3°$), bicarbonate (HCO_3^-) and carbonate (CO_3^{2-}) ions. The mole fraction of each species strongly depends on pH of the solution (see section 2.3). HCO_3^- ions are predominant in the near neutral pH range.

The source of DIC may be related to organic or inorganic carbon origins. For instance organic derived soil CO_2 enhances the reactions of recharging soil solution and groundwater with local silicate and carbonate minerals. DIC is generated by dissolution of CO_2 and weathering of carbonates, where carbon isotopes may fractionate. Thus, $\delta^{13}C_{DIC}$ values display source and distinct sources reaction mechanism (e.g. open and closed system with respect to CO_2 gas during limestone dissolution). Considering an open system with respect to CO_2 during the evolution of groundwater the $^{13}C/^{12}C$ isotopic composition of the gaseous CO_2 can be re-calculated by using isotopic equilibrium fractionation according to the expression

$$\delta^{13}C_{CO_2} = \frac{\left(\delta^{13}C_{DIC} + 10^3\right)}{\alpha_{DIC}} - 10^3 \quad (20)$$

where

$$\alpha_{DIC} = \frac{\left({}^{13}C/{}^{12}C\right)_{DIC}}{\left({}^{13}C/{}^{12}C\right)_{CO_2}} = x_f.\alpha_f + x_b.\alpha_b + x_c.\alpha_c \quad (21)$$

is the equilibrium $^{13}C/^{12}C$ fractionation coefficient between DIC and gaseous CO_2 obtained from the individual $^{13}C/^{12}C$ fractionation coefficients α_f, α_b, and α_c (Vogel et al., 1970; Mook et al., 1974; Thode et al., 1965; respectively) and the molar proportions x_f, x_b, and x_c for H_2CO_3*, HCO_3^-, and CO_3^{2-}, respectively. Within the temperature (12 – 29°C) and pH (6.8 – 7.8) range of the groundwaters, the value of α_{DIC} ranges from 1.006 to 1.008 (see Dietzel and Kirchhoff, 2002; Clark and Fritz, 1997).

Stable isotope composition of carbon is normally reported as δ values that represents the ratio of heavy isotope to light isotope in the sample over the ratio of a standard-VPDB (Vienna Pee Dee Belemnite)

$$\delta^{13}C(‰) = \left(\frac{\left({}^{13}C/{}^{12}C\right)sample}{\left({}^{13}C/{}^{12}C\right)standard} - 1 \right) * 1000 \quad (22)$$

2.6.3. Strontium isotopic ratios

Strontium isotopes have been widely used to identify the source of dissolved Sr ion and mixing behaviour of the groundwaters. The application of $^{87}Sr/^{86}Sr$ ratio to trace solute sources depends on the fact that water interacted with minerals and rocks of different age and litholigical composition exhibit distinct $^{87}Sr/^{86}Sr$ signatures. The chemical weathering of aquifer material results in distinct $^{87}Sr/^{86}Sr$ values which are used as tracers for water-rock interaction (e.g. Bain and Bacon**,** 1994; Cartwright et al., 2007; Shand et al., 2009). Sr derived from a mineral through weathering displays the $^{87}Sr/^{86}Sr$ ratio of this mineral. The concentration of strontium combined with $^{87}Sr/^{86}Sr$ ratios provides a powerful tool for distinguishing the dominant reactions responsible for sources of solutes along reaction paths.

Individual dissolution rates determine the progressive weathering of minerals, e.g. of Sr containing silicates that contribute to the Sr in solution and the respective $^{87}Sr/^{86}Sr$ ratio. Silicate minerals may have different $^{87}Sr/^{86}Sr$ ratios owing to relative proportions of Rb^{+} to Sr^{2+} and time. The variation of the $^{87}Sr/^{86}Sr$ is due to the radioactive decay to ^{87}Rb, which has a half-life of 48.8 $x10^{9}$ years. The $^{87}Sr/^{86}Sr$ is given as a function of the initial $^{87}Sr/^{86}Sr$, the ratio of Rb^{+} to Sr^{2+} ($^{87}Rb/^{86}Sr$) which varies with the age of the rocks.

The $^{87}Sr/^{86}Sr$ ratio in local groundwater will be strongly influenced by the most easily weathered phase. The more plagioclase dissolution in which kinetic rate is faster than that of K-feldspar (Zhu, 2005), the higher solute concentrations but the less radiogenic. The isotope ratios increase as weathering resistance K-feldspar starts to dissolve (Cartwright et al., 2007; Shand et al., 2009).

2.6.4. Stable sulfur isotopes in dissolved sulfate

Isotope ratios are reported as δ-values relative to the standards meteoritic Canyon Diablo Troilite (CDT) for $\delta^{34}S$. The $\delta^{34}S$ values of groundwater are highly variable and depend on the kind of sulfur supply. Thus the application of $\delta^{34}S_{CDT}$ values provided information about the source and geochemical processes for SO_4^{2-} delivery or consumption, e.g. by dissolution of minerals or bacterial sulfate reduction.

Sulfur isotopic composition of dissolved sulfate ions cannot always be used as conservative tracers to differentiate potential S sources in groundwater, as it can be modified by isotopic fractionation (Toran and Harris 1989). Sulfur isotope fractionation occurs e.g. during bacterial induced reduction of S in sulfate to sulfide ions (Brunner and Bernasconi 2005). Bacterial sulfate reduction plays a very important role in sulfur isotope fractionation by depleting of ^{32}S in the remaining dissolved sulfate (Canfield 2001; Brunner and Bernasconi 2005). The degree of sulfur isotope fractionation depends on the repeated oxidation/reduction processes involving sulfur in various oxidation states (Canfield 2001; Brunner and Bernasconi 2005).

3. Geology and hydrogeology of Axum area

3.1. General overview

The study area, Axum, is located in the northern Ethiopia. It is bounded within the limits of 14°00'-14°15' N latitude and 38°36'-38°47'E longitude. Axum is Ethiopia's most ancient city and a place of major historical and tourist attraction sites. Historically, it was a strategic area where it controlled the flow trade routes of the regions during Aksumite kingdoms (800 B.C- 700 A.D.; D'Andrea, 2008).

The area is characterized by a hilly topography and flat plateau surfaces with average elevation of 2100 m above sea level. The elevation ranges from 2600 m at the peak of mountains in the north of Axum and decrease towards the south. The main hydrogeological water-divide in the study area runs along the mountain range of Axum dividing the two major river basins (Mereb River and Tekeze River basins). Distribution of the geomorphological features throughout the study area suggests that the landforms were developed mostly due to volcanic activities and the Quaternary sediment deposits. The ridge to the north of Axum constitutes the main portion of the youngest volcanoes of trachytic and phonolitic plugs stand out as circular hills than the surrounding plateau basalts. In the intermediate sectors it is covered by younger deposits.

The climate is characterized by a long dry season and a summer-rain season with an annual mean average precipitation of 672 mm in Axum, mainly confined to the months from June to September. July and August are months with heavy rainfall (about 65 %). The mean annual temperature in this area is 19.4 ^{o}C with daily average temperatures range from 29 °C to 14 °C.

3.2. Geological setting

The geology of Axum area is characterized by rocks ranging in age from Precambrian basement to Quaternary deposits (Fig. 2). The basement consists of low-grade and deformed Neoproterozoic metamorphic rocks that belong to the Arabian–Nubian Shield (Tadesse et al*.,* 1999). The meta-volcano and meta-sedimentary assemblage of basement rocks displays geochemical characteristics typical of intra oceanic island arc systems (Tadesse et al., 1999). The Pan African magmatism had generated syn- and post-tectonic plutons which have been well studied for their role in the geodynamic evolution of the region (Tadesse-Alemau, 1998; Tadesse

et al., 2000). The Palaeozoic sedimentary rocks consist of Enticho Sandstone and the Edaga Arbi glacial deposits are exposed over the region. The lateral transition facies change from Edaga Arbi glacial unit into the Enticho Sandstone is unclear (Kumpulainen at al*.,* 2006; Avigad et al., 2007) and occasionally interfingering (Schrank et al*.,* 2007). The sedimentary rocks exhibit some fine grained sediment and mineralogical maturity in response to intense chemical weathering (Avigad et al*.,* 2007).

The Mesozoic sedimentary rocks comprise the succession of the Adigrat Sandstone, the carbonate succession, which is composed of the Agula Shale and Antalo Limestone (Asrat, 2002), and the early Cretaceous Sandstone Amba Aradam Formation. While exposed over vast area of the northern region, the quartzose sedimentary rocks of Adigrat Sandstone sequences appear to pinch out towards Axum (Werash, 2002). The undifferentiated intercalation of sand- and siltstones of the study area varies in colour and thickness. The sediments show considerable variation in textural maturity with predominately quartz-rich mineral compositions.

The latest significant geological event in the region was the Cenozoic volcanic eruption occurred during Ethiopian continental flood basalt formation about 30 Ma ago (Pik, et al., 1999). Widespread volcanic activity occurred during Tertiary covered the large part of Ethiopia including the study area with rapid outpouring of fissural basalt layers. The northwestern Ethiopian Oligocene flood basalts trap sequences show diverse magmatic distribution (Pik et al*.,* 1998). These volcanic types exhibit distinctive geochemical signatures indicating different evolution and differentiation.

A widespread volcanic hypabissal igneous terrain is evident in the study area forming steep cliffs. These volcanic material rocks belong to Axum-Adwa phonolite-trachyte plugs and extend to the trachy-rhyolitic Senafe, where they display a similar nepheline and quartz mineral assemblage but with differing magmatic series (Zanettin et al., 2006).

In the study area, the clastic and basement rocks occur as relatively minor outcrops in the predominantly volcanic rock ranges. The thickness of the Quaternary sediments that covers the other formations varies from one area to another.

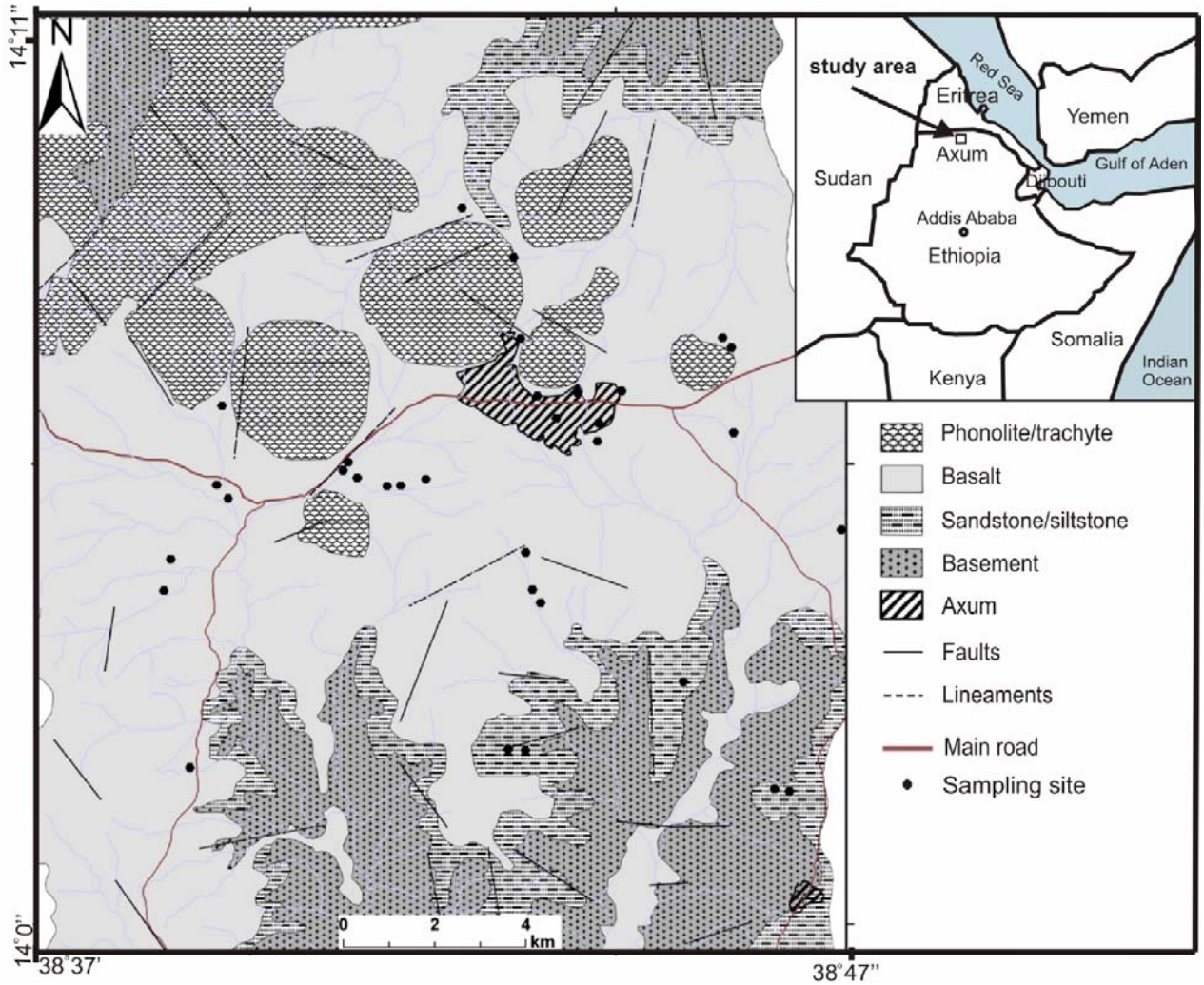

Fig. 2. Simplified geological map of Axum area with water sampling sites; inset shows the location of Axum.

3.3. Hydrogeological condition

The aquifer properties have been determined through examination of water well records, geophysical investigation and geologic descriptions. The shallow aquifer is basically composed of alluvial deposits and weathered vesicular-amygdaloidal basalt with limited interbedded river gravels and sands. The shallow groundwater system has a good network of openings that are favorable for groundwater movement and accumulation. The transmissivity and storage potential of the shallow aquifer depends upon the thickness of the alluvial and weathered volcanic layer. Parts of the fractured permeable materials are covered by a thick blanket of clay that often provides poor condition of water infiltration (German Water Engineering GmbH, 1973).

The deep groundwater system is hosted mainly by fractured basalt that forms the principal component of the groundwater system. The highly fractured and weathered basaltic rocks develop openings enhanced by well-connected fracture network. Evidence indicates that groundwater movement is strongly influenced by the development of secondary permeability (Fig. 3A). Loss of drilling fluid during construction at depth suggests the presence of open joints and fractures (Abay Engineering, 2006). Pumping test conducts in the well-field is interpreted to have high amount of groundwater circulation along major conduits of tilted blocks of basalt (Devecon Engineers and Architects, 1995). Flow in the deep aquifer is likely to be controlled by localised fracture systems related to faulting (Fig. 3B). Alternatively the permeability reduced in other circumstances by the formation of alteration products and clay filling that consequently reduces the productivity (Fig. 3C). The observed lateral variation in groundwater chemistry and yield may suggest lack of connectivity and heterogeneous nature of the aquifer. Generally, the volcanic rocks and associated sediment deposits represent complex aquifer systems where groundwater occurrence and distribution is strongly controlled by both lithology and internal structure of the host rocks. The underlying sandstone formation unit is locally characterized by low aquifer productivity owing to the clay and siltstone intercalation and relatively constricted aquifer. The underlying basement rocks are characterized by low permeability except in the upper weathered horizons.

Groundwater recharge preferentially occurs at unconfined conditions of those elevated topography areas of fractured phonolite and trachyte volcanoes (Fig. 3D; Abay Engineering, 2006). In this situation the surface watershed boundary generally coincides with the boundary of groundwater flow system. Similar to the trap series of volcanoes in the highlands (Ayenew et al., 2008), the volcanic plugs have high transmissivity, low storativity, and localized fault-controlled groundwater flow direction. The flow behaviour is likely to be controlled by geological structures where faulted and fractured can increase the hydraulic conductivity (Ayenew et al., 2008). The groundwater of the deep aquifer of the area is commonly recharged through fractured rocks.

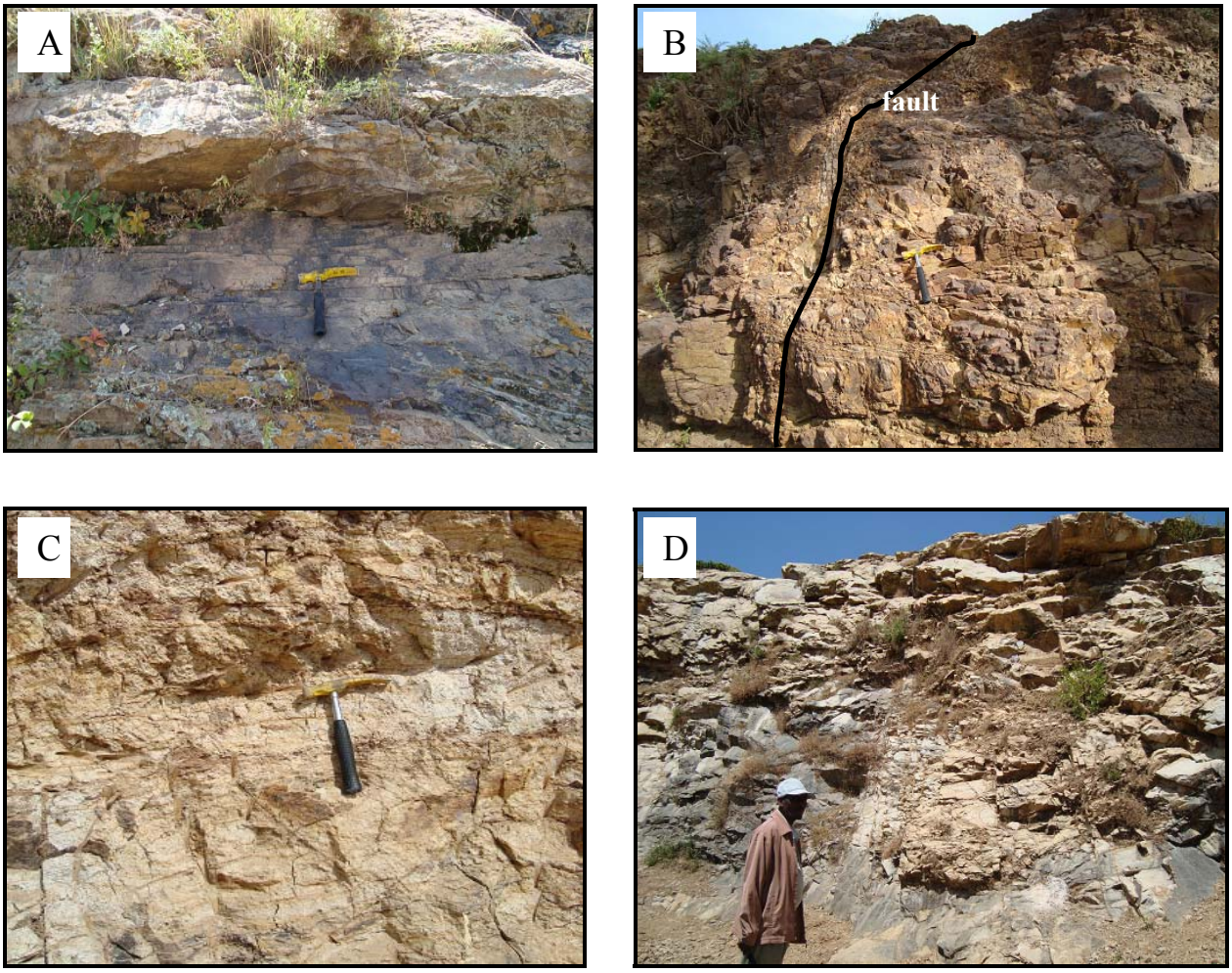

Fig. 3.(A) fractured basaltic rocks (B) localized fault in basalt rocks (C) volcanic ash and altered product of volcanic rocks (D) heavily fractured of the intrusive rocks.

4. Methodology

4.1. Sampling and in-situ parameters

About 42 water samples were collected from Axum for chemical and isotopic analyses (see sampling sites in Fig. 2). Respective sampling campaigns were carried out in December 2008 and May 2009. Samples comprise surface water as well as solutions from springs and boreholes at depth ranging from 10 m to 150 m through out the study area. Some boreholes are active municipal or domestic shallow wells. The wells were sampled close to the well head using available pumps. Prior to sample collection, inactive wells had been pumped for sufficient time for well purging. The bottles were rinsed with sampled water before being filled and were stored in cleaned polyethylene (HDPE) bottles. All samples were filtered through 0.45 μm Nylon membranes (Spartan Syringe filter) in the field. The filtered samples were separated in different aliquots. The solution for cation analysis was preserved by adding ultra-pure 6 N HNO_3 while those used for anion analysis were not acidified.

Sample solutions for analyses of the distribution of stable isotopes of the water molecule ($^{18}O/^{16}O$ and D/H) were stored in HDPE bottles. Carbon isotopes ($^{13}C/^{12}C$) of DIC were collected in 10 ml Na-glass vials (Labco exetainer) preloaded with six droplets of ultrapure phosphoric acid, capped with air-tight caps and flushed with Helium. At the sampling site, a small amount of sample water was injected into the sample vial using a needle syringe. Samples for the determination of sulfur isotopes in dissolved sulphate were collected in clean 0.5 L HDPE bottles. For strontium isotope analysis different aliquots with 50 ml volume were used and the samples were filtered and acidified with ultra-pure HNO_3. Sr isotope ratio measurements were performed in selected samples from springs and deep and shallow wells.

Field measurements, including pH, electrical conductivity and temperature were recorded using a portable WTW pH 330 meter at the time of sample collection in the field. Total alkalinity was measured in the field by titration with HCl (0.05 N), using methyl orange as pH indicator. Dissolved Oxygen Test Kit was used to determine concentrations of dissolved oxygen. The Winkler method requires careful gauging as inaccurate measurements can lead to poor results (White et al., 1991). The analysis involves titration method in which a series of reagents was

added to a sample of water that results in colour change. At the end, the colour change indicates the dissolved oxygen concentration in the sample and given in (mg l^{-1}).

4.2. Analytical techniques for solution analyses

4.2.1. Chemical composition

Major and minor cations were analyzed by multi-element analyser inductively coupled plasma - optical emission spectrometry (ICP-OES, PERKIN ELMER 4300) and trace elements were measured by inductively coupled plasma–mass spectrometer (ICP-MS; Perkin–Elmer Elan 5000) equipped with an ultrasonic nebulization. The ICP-MS was calibrated with multi-element solutions. Anions were analyzed by ion chromatography (DIONEX 600)/HPLC High performance liquid chromatography at the Laboratory of Institute of Applied Geosciences, Graz University of Technology. The quality of water analyses was checked by the relative deviation from charge balance ($\Delta_{meq} = 100 \cdot (\sum_{meq+} - \sum_{meq-}) / (\sum_{meq+} + \sum_{meq-}) < 6$ %).

4.2.2. Isotopes

Oxygen and hydrogen isotopes of H_2O

Oxygen and hydrogen isotopes were analyzed at Laboratory Centre for Isotope Hydrology and Environmental Analytics in Joanneum Research, Graz. The oxygen isotopic composition of the water was measured by the classic CO_2–H_2O equilibrium technique (Epstein and Mayeda, 1953) with a fully automated device adapted from Horita et al. (1989) coupled to a Finnigan DELTA^{plus} mass spectrometer. The isotopes of hydrogen was determined on a continuous flow Finnigan DELTA^{plus} XP mass spectrometer coupled to HEKAtech high-temperature oven by chromium reduction using a ceramic reactor slightly modified from Morrison et al. (2001). Measurement precision was better than ±0.1‰ for $\delta^{18}O$ and ±1‰ for $\delta^{2}H$. Oxygen and hydrogen isotopic results are reported in per mill (‰) relative to VSMOW.

Stable carbon isotopes of DIC

The carbon isotope sample of dissolved inorganic carbon was determined at the Laboratory Centre for Isotope Hydrology and Environmental Analytics in Joanneum Research, Graz. Isotopic composition of DIC was analyzed using a fully automated peripheral continuous-flow gas

preparation device (Gasbench II), which was connected to a Finnigan DeltA^{plus} XP mass spectrometer. The analytical setup is comparable to that used in previous studies (Spötl, 2005).

$^{87/86}$Sr ratios

Aliquots for strontium isotope analysis were filtered through Nylon 0.45 µm Spartan Syringe membrane and acidified with HNO_3. The Sr isotope ratio measurements were performed for selected samples from surface water and deep and shallow groundwaters. Strontium isotope ratios were measured using multi collector inductively coupled plasma mass spectroscopy (MC-ICP-MS) at Leibniz Institute of Marine Sciences, Kiel/Germany, following standard chemical separation (Sr-Spec, 50-100 mesh; 0.3 ml) and measurement procedures. The standard procedure was adopted for chemical separation and mass spectrometry for strontium. After chemical separation, the water samples were analyzed by MC-ICP-MS following a method described in Fietzke and Eisenhauer (2006). On-peak-zero baseline determinations accounted for potential Sr and Rb blanks as well as for the Kr background. The reproducibility of $^{87}Sr/^{86}Sr$ ratio measurements was tested by repeated measurements ($n = 18$) of the NBS 987 standard that yielded a mean value of 0.710248.

Sulfur isotopes in sulfate

For sulfur isotopic analysis, the sample solution was initially acidified to pH < 2 in order to liberate DIC as CO_2 from the solution and prevent formation of barium carbonate for the further procedure. The dissolved SO_4 was precipitated as $BaSO_4$ by adding an excess volume of a 0.3 M $BaCl_2$ solution and left for 24 hours. Subsequently, the precipitated barium sulfate was separated by a 0.45-µm cellulose acetate membrane using a vacuum filtration unit and washed with deionised water. $BaSO_4$ was dried in an oven at 110°C and latter transferred into crucibles with the filters and combusted at 900 °C to remove residual water and organic matter. Finally, the $\delta^{34}S$ value of the $BaSO_4$ was measured by combustion-isotope ratio monitoring mass spectrometry using a methods described by Böttcher and Schnetger (2004). $BaSO_4$ was combusted into SO_2 in Carlo Erba EA 1108 elemental analyzer connected to a Finnigan MAT 252 mass spectrometer.

4.3. Rock sample analyses

Sufficient rock samples were collected during field season from Axum area, where a total of twenty representative rock samples were selected for optical microscope investigation, X-Ray

fluorescence spectrometry (XRF) and X-ray diffraction (XRD) analyses. Detailed petrographic descriptions of thin-sections were made using normal optical microscope. The remaining rock samples were crushed using a jaw crusher with a stainless steel jaw crusher and then pulverized into powder by an agate mortar to carry out XRF and XRD analyses.

XRF (PHILIPS PW 2404) was used for major and trace element analyses. Samples are usually prepared as glass discs for major element analyses and pressed powder pellets for trace-element analyses (detailed preparation procedure is given in Appendix I). Fused glass disks were created in such a way that constituent elements was mixed homogeneously to get accurate and reproducible results (Nakayama and Kakamura, 2005) and eliminating grain size effect and mineralogical effect on mass absorption (La Tour, 1989). The homogenized mixture was compressed at 20 tones yielding a compact disc with a smooth upper surface that can easily be measured in the XRF spectrometer for trace-elements. Loss on ignition (LOI) was considered to make sure the final XRF results are obtained on an anhydrous basis.

In addition to thin-section, mineralogical analysis was carried out by XRD spectrometer (PANalytical X'Pert Pro series diffractometer equipped with a cobalt-target tube anticathode). It provides mineral identification, particularly for fine grained minerals that can not be easily studied by optical microscope. Sample preparation method of XRD analysis is given in Appendix II.

5. Petrology and geochemistry of rocks of the Axum area

5.1. Introduction

The occurrences of compositionally varied volcanic and intrusive rocks represent regional sequence of tectonic and volcanic activities rather than localized eruptive event. The igneous rocks of Axum area are predominantly of basaltic composition with plutonic plugs of phonolite and trachyte rocks emplaced. Mineral composition of fresh and weathered rocks has been investigated to evaluate the alteration during weathering process of water-rock interaction that may bring about change in chemical and mineralogical composition (Eggleton et al., 1987). The petrological and geochemical analysis of this work has primarily focus on these more volcanic rocks. Geochemistry of the rock samples can provide essential information about source and genesis of the rocks and the nature of fluid/rock interaction during weathering processes.

5.2. Tectonic evolution of volcanic rocks

The tectonic evolution of East Africa Rift System is often associated with mantle plume heads impinging on the lithosphere (Hofmann et al., 1997). Based on the interpretation of distinct geochemical variations, it has been noted that the source of basic lavas involves the presence of two mantle plumes, Afar mantle plume and lithospheric mantle. The Ethiopian volcanic province is part of extensive regional Oligocene volcanic belt which are well studied for the source and genesis of magmatic episodes. The geologic history of the Ethiopia volcanic evolution represents magmatism of continental rifting, ranging from prerift continental flood basalts up to sea-floor spreading basalts (Pik et al., 1998). Studies indicate that uplift and magmatism were followed by break-up extension. The Ethiopian volcanic plateau was characterized by eruption of a vast volcanic episode with most intense pulse of volcanism occurred at 30 Ma (Hofmann et al., 1997). Subsequent volcanic activity in the Ethiopian plateau from 22 Ma occurs as large central vent volcanoes or is associated with extension and localized in the rift axis (Pik et al., 1999; Kieffer et al., 2004). Immediately after this peak of activity, a number of large shield volcanoes developed on the surface of the volcanic plateau (Kieffer et al., 2004). The activity has resumed to the present day with eruptions of bimodal suite of basalts and alkaline silicic lavas concentrated within the rift zone (Kieffer et al., 2004; Hagos et al., 2010). The volcanism strongly influenced the regional tectonic setup of the Ethiopian flood basalt (Fig. 4). The Ethiopian highlands of basalt provinces are dominated by fissural flows of Oligocene age overlain by shield volcanoes of

Miocene age, erupted from large central vent volcanoes that are composed predominantly of alkaline basalts, with minor felsic lavas and pyroclastic rocks mainly composed of alkaline lavas (Pik et al., 1998; Kieffer et al., 2004). The youngest magmatism is concentrated in the northern Ethiopian rift valley. The volcanic of main Ethiopian rift and Afar which are characterized by highly alkaline lavas erupted from a number of Quaternary volcanic centres (Beccaluva et al., 2009). The active volcanic activity in the Afar Depression is related to the tectonic dynamic and thermal effects of the Afar hotspot.

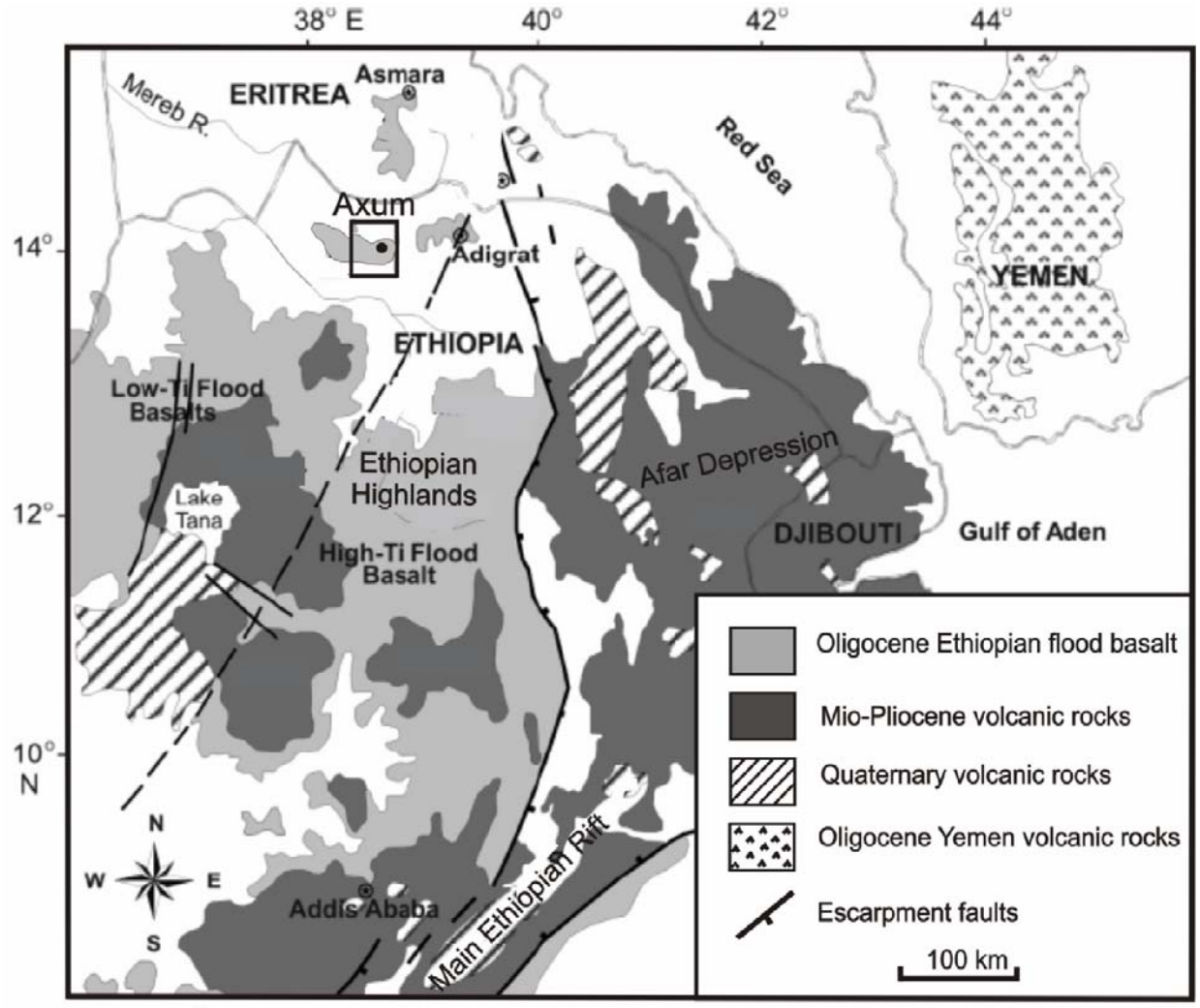

Fig. 4. Schematic map of the Ethiopian flood basalt province. The boundary between the LT and HT provinces is marked by the dashed line (modified from Pik et al. (1999) and Hagos et al. (2010)).

Several workers have attempted to explain the evolution of magma sources and the stratigraphical distribution in Ethiopian flood basalt, in relation to extensional tectonics and mantle plume (e.g. Pik et al., 1998, 1999; Kieffer et al., 2004; Beccaluva et al., 2009). Recently, Beccaluva et al.,

(2009) proposed a striking relationship between the shape, size and location of the melting region in the underlying mantle where magma were generated and the variation of Low-Ti to High-Ti. The Low-Ti (LT: 1.0–2.6 wt. % TiO_2) and high-Ti basalts (HT1: 2.6–4.2 and HT2: 2.6–5.0 wt. % TiO_2) has been identified in Ethiopia flood basalts by Pik et al. (1998; 1999) based on Ti content and trace elements concentrations. According to Beccaluva et al., (2009), the flood basalt was generated at comparable melting degree of LT tholeiites from relatively less metasomatized mantle and HT basalts from the more metasomatized mantle domains closer to the plume axis. The Oligocene basalts from northern Ethiopia bear a closer resemblance to the Yemen basalts with the emplacement of a thick continental flood basalt piles that encircle the Afar depression (Pik et al., 1999). While the Yemen basalts represents HT magma series (Beccaluva et al., 2009), the LT series are restricted to the northwestern part of Ethiopia (Pik et al., 1999).

The volcanic of Axum area are grouped into the Oligocene flood basalt and post-trap (Miocene to Pliocene) volcanism (Hagos et al., 2010). Distinct magma compositions with alkaline magmatic character of the mafic and felsic lavas are distinguished in Axum. The Axum volcanic exhibits diversified rocks, ranging from basanites to trachybasalts and phonolites to trachytes (Hagos, et al., 2010 and this study). The hypabyssal Axum-Adwa phonolite-trachyte plugs of felsic rocks displays different geochemical signatures.

5.3. Petrography and mineralogy

The petrography features of the solid samples were described using optical microscopy. The phonolite rock contains abundant coarse-grained nepheline phenocrysts with fine-grained feldspar as groundmass (Fig. 5A). The nepheline phenocrysts are acicular to tabular in shape and are aligned randomly. Coarse-grained feldspar rich with few pyroxenes are present in trachyte rock samples. The trachytes have no plagioclase phenocrysts but the weathered specimen show alteration of feldspar (Fig. 5B).

The mineralogy of basaltic rock is characterized by a predominance of calcic plagioclase, pyroxene and olivine. The photomicrograph in Fig. 5C demonstrates that sparse phenocrysts of clinopyroxene and olivine with medium-grained size plagioclase dominate most of the basalts in the study area. Lath-shaped plagioclase is typically of the basalt rocks. The most common phenocrysts in basalts are clinopyroxene and olivine. Clinopyroxene phenocrysts show grey colour of intense internal oscillatory zoning and sector growth features. Clinopyroxene is present

among phenocrysts in variable amounts. Samples of this sequence contain considerable accumulation of opaque minerals oxides. The vesiculated and weathered basalts of this sequence also contain some calcite veins or secondary filling of calcite from precipitation of carbonates and silica and zeolites. Vesiculated and weathered basalts can be subjected to mineralogical changes e.g. chlorite, frequently as pseudomorphs after the primary minerals (Eggleton et al., 1987).

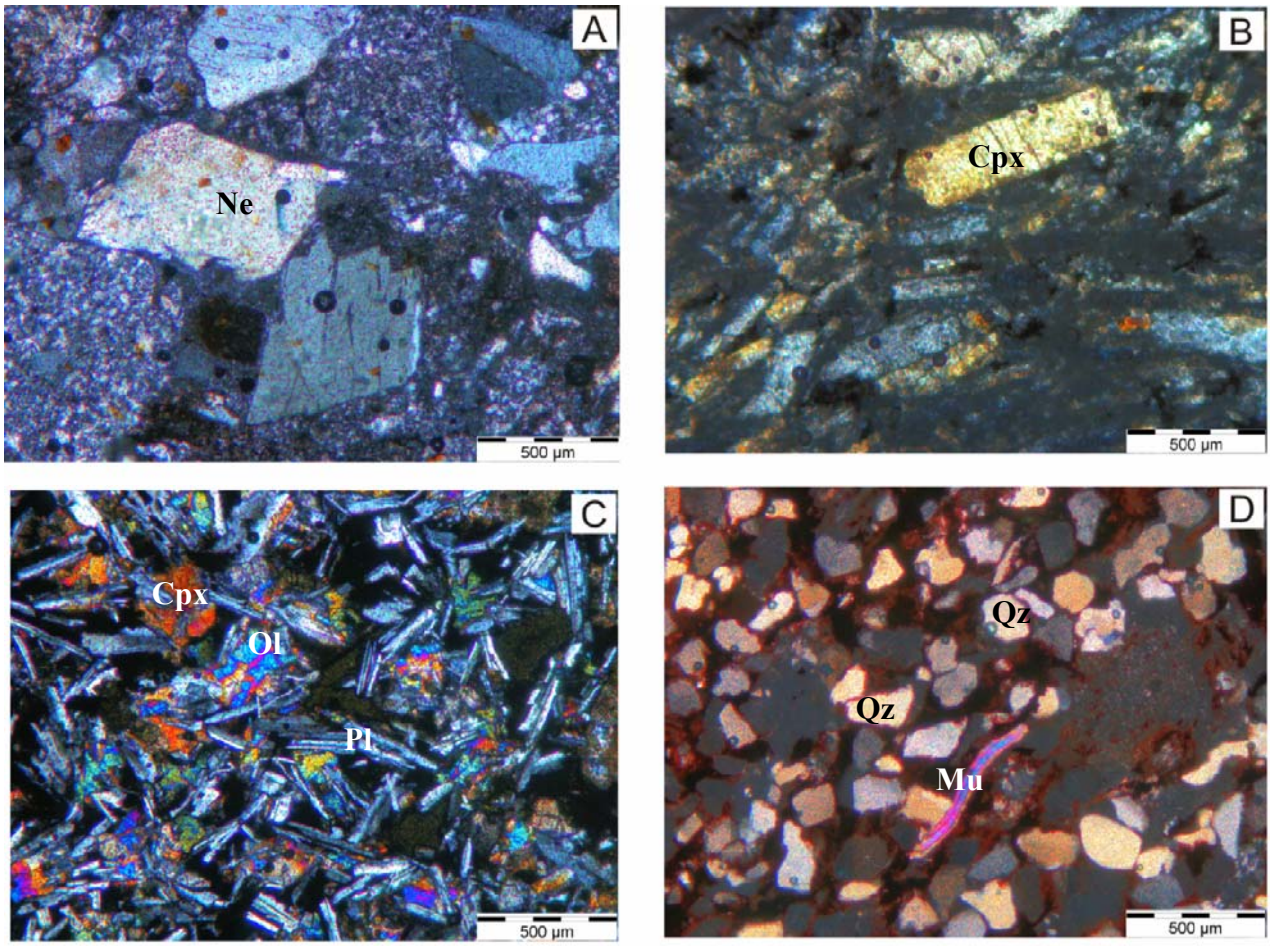

Fig. 5. Petrography analyses of the volcanic and sedimentary rocks of the Axum area. (a) phonolite rocks showing porphyritic texture with nepheline phenocrysts surrounded by fine-grained feldspar (ground mass); (b) large grain of clinopyroxene imbedded in medium-size grained feldspar and altered volcanic and glass in trachyte rocks; (c) medium-grained plagioclase rich alkali basalt with clinopyroxene and olivine; The volcanic glass and Ti oxides are partly filling the interstitial spaces. The plagioclases are lathlike but randomly aligned; (d) local quartz and k-feldspar sandstone with Fe oxides and clay minerals, and elongated muscovite mineral. (Ne-Nepheline; Cpx-Clinopyroxene; Ol-Olivine; Pl-Plagioclase, Qz-Quartz; Mu-Muscovite).

The samples from sedimentary rocks of silt/sandstone are mostly quartz rich. The siltstone consists of quartz and feldspar with clay material as groundmass, e.g. kaolinite and phyrophyllite, with inclusion of muscovite mineral (Fig. 5D). Tiny yellowish or brown crystals generally located

between grains or replacing feldspar grains are clay minerals. In accordance to Schmid et al. (2008) the Quaternary deposit is characterized by the presence of quartz, K–feldspar, kaolinite, smectite, illite, chlorite, and calcite minerals.

Aquifer mineralogical compositions determined by X–ray Diffraction are presented in Appendix II. The X-ray diffraction analysis supports the petrographic observations attesting that plagioclase feldspar, clinopyroxene, forsterite are the dominant minerals in basaltic rock samples. Accessory minerals present in minor amount include Fe and Ti oxides. The investigation reveals that the solid aquifer is composed of Na-feldspar and K-feldspar in the phonolite-trachyte rocks. However, the occurrence and abundance of Fe bearing minerals, chlorite, pyroxene and olivine, vary from site to site. XRD pattern indicates, kaolinite, smectite, and halloysite as major clay minerals gained from the weathering of volcanic rocks. Halloysite is known to be associated with alteration product of feldspar (Eggleton et al., 1987). These results are consistent with the petrographic microscopy observations and previous studies.

Most of the flood basalts are commonly dominated by aphyric to sparsely phyric rocks with plagioclase and clinopyroxene phenocrysts and rare olivine (Kieffer et al., 2004). The phenocryst minerals constitute of euhedral to subhedral pyroxene, olivine, and plagioclase-lath. In the tholeiitic basalt, plagioclase composition varies from An_{50-81} to An_{35-53} in LT and HT basalts, respectively (Beccaluva et al., 2009). Pyroxene in basalts is referred to Mg-rich augite whereas olivine varies in composition in the different magma types ranging from $Fo_{81–77}$ in LT to $Fo_{75–51}$ in HT (Pik et al., 1998; Beccaluva et al., 2009). Basalts mainly consist of dominant plagioclase and scarce olivine with rarely brownish glass is observed in Adigrat sequences, an area very close to Axum (Fig. 4; Beccaluva et al., 2009).

5.4. Geochemistry of the bulk rock

The relative abundances of major oxides and trace elements of the bulk rock by XRF analyses are displayed in Appendix I. The results, plotted on alkali-silica TAS classification scheme of Le Bas et al. (1986), indicate that the prevalent volcanic rocks are trachybasalt and basalt, phonolite and trachyte (Fig. 6). Rock samples comprise a range of chemical composition falling on the alkaline to subalkaline (tholeiitic basalt) groups. Geochemical studies of alkaline basalt have shown that

alkaline rocks evolve along silica-under-saturated. The felsic volcanic rocks are mainly silica-undersaturated phonolite and more silica-saturated trachyte lineage of alkaline nature.

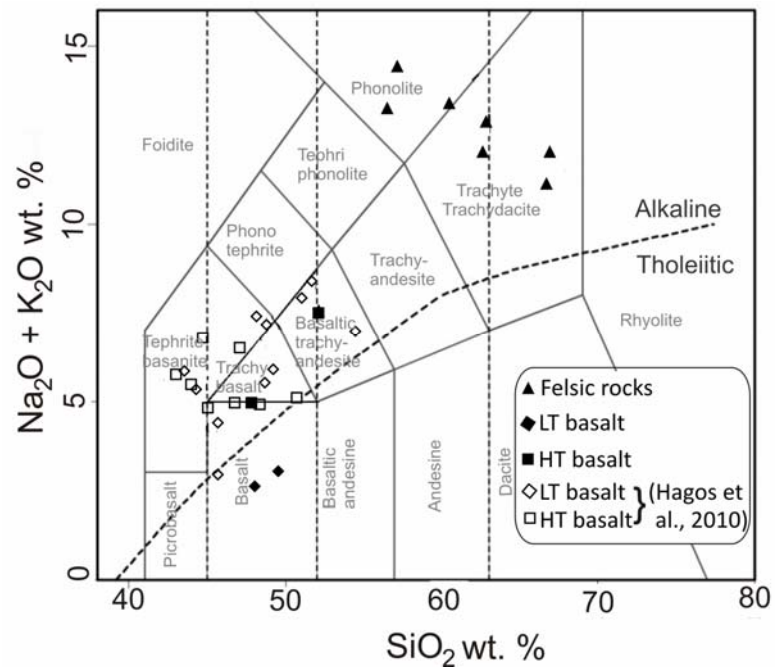

Fig. 6. Total alkali-silica classification diagram (Le Bas et al., 1986) of volcanic rocks. Data points are referred to volcanic rocks from Axum area.

Some of the samples are altered as shown by high values of loss of ignition (LOI; in Appendix I). The alteration of silicate minerals and glassy fractions of the basalts results in the formation of phyllosilicates like the detected kaolinite and smectites. The geochemical data may not show consistent results in weathered basalts because some elements are mobile and can be released during intense weatherizing and alteration (Eggleton et al., 1987). Major elements such as Na_2O and K_2O are generally decreased in the altered sample compared to the less-altered rock. The geochemical variability of SiO_2 content in alkali basalts, phonolite and trachyte is evident from the Figs. 7A to D. Distributions of major elements (given as oxides) show that SiO_2 is more dominant in sand/siltstone, whereas Fe_2O_3 and CaO are abundant in basalts.

All the major oxides are characterized by distinct geochemical trend as SiO_2 progressively increase from 43 – 67 wt. %. The basalts have silica ranging from 48 wt. % to 52 wt. % and MgO from 1.0 wt. % to 5.8 wt. % and CaO from 4.5 wt. % to 10 wt. %. The distribution of TiO_2 in the basalt rocks shows a wide range from 1.7 wt. % to 3.3 wt. % and very low in felsic rocks (phonolites and trachytes). The unaltered basaltic rock samples show relatively high TiO_2 content

from 2.7 to 3.3 wt. % and correspond to flood basalt sequence. The high TiO_2 basalts have high Fe_2O_3 content as well as low MgO content. An elevated content of Fe_2O_3, MgO and CaO coincides with weathered or altered volcanic rock sample, suggesting addition of these components to the rock from the weathering solutions. The weathered basalt concentrations of Na_2O, K_2O, Al_2O_3 and MnO appear to drop markedly from those of the unaltered basalt, while CaO and MgO concentrations increase significantly with weathering. In general, the concentration of Fe_2O_3 increases progressively during the weathering volcanic rocks.

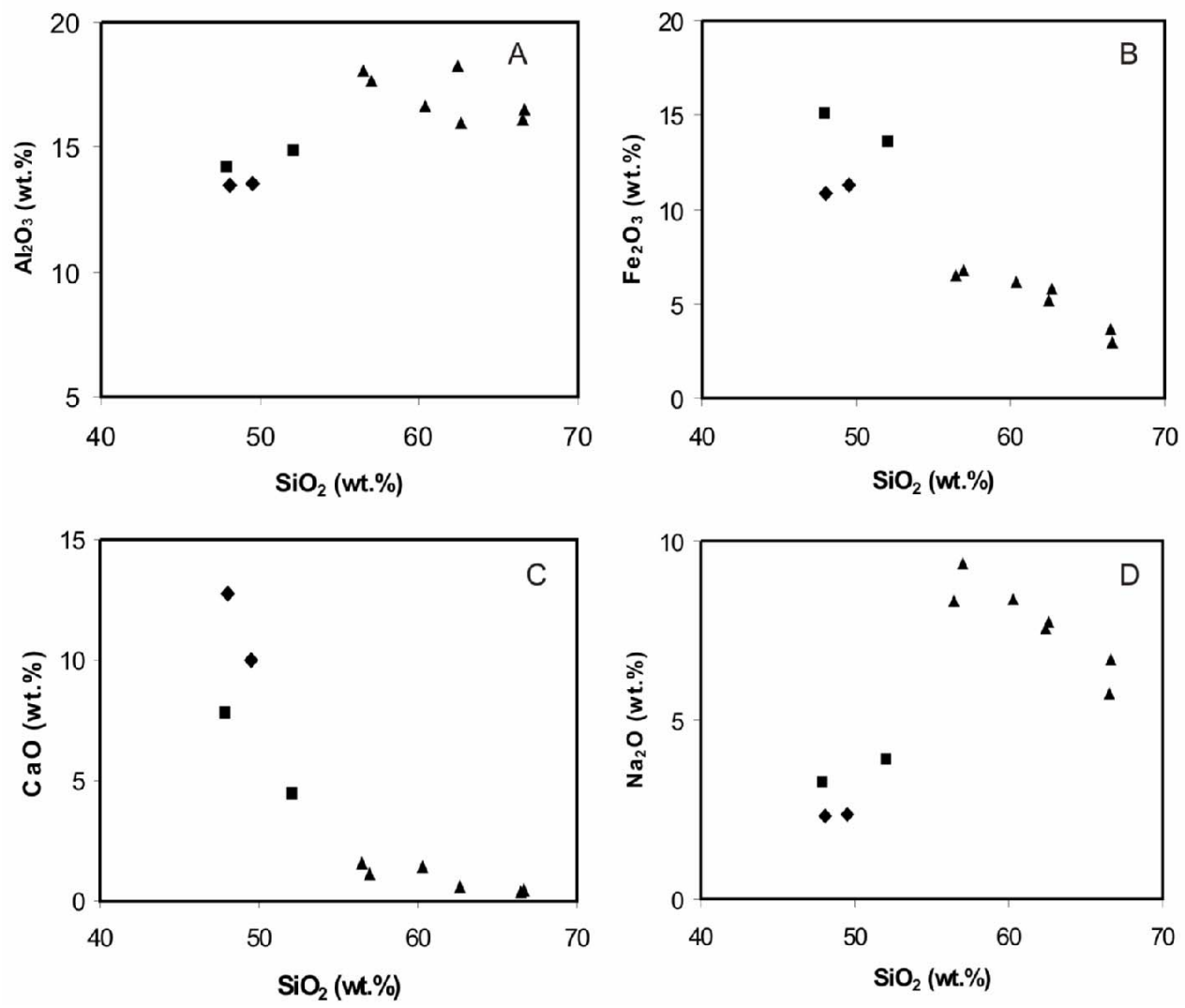

Fig. 7. Variability of selected major oxides with silica content; (▲) felsic rock; (■) HT basalts; (♦) LT basalts.

Figs. 7B and C display a significant decrease in Fe_2O_3 and CaO with increasing silica concentration. The compositions of the felsic rocks correlate inversely to the total alkali (Na_2O

+K_2O) with phonolites showing higher content. The phonolites have SiO_2 between 56 and 62 wt. %, whereas trachytes range from 62 to 67 wt. % SiO_2. But phonolite samples display nearly as much variation with respect to other oxides as trachytes. The phonolites have higher Fe_2O_3 content (5.8–6.7 wt. %), whereas the trachytes show lower Fe_2O_3 content (2.9–5.1 wt. %) with increasing silica concentration (Fig. 7B). The trachyte group is characterized by lower CaO and MgO concentration compared to the phonolitic group. Phonolite and trachyte samples confirm the presence of intermediate sodium-rich rocks (6.7–9.4 wt. % Na_2O) and K_2O (4.5–5.4 wt. %) with low content of TiO_2, CaO and MgO compared to basalts.

Trace elements can be used to identifying igneous rock series and geochemical evolution of magmatic differentiation processes and to determine their behaviour during weathering. The trace and minor elements for the samples show significant variation among the different rocks. Obviously, the sandstone/siltstone rocks have mostly lower concentrations of trace and minor elements compared to volcanic rocks and hence excluded from discussion.

Some trace elements (e.g. Rb and Zr) are positively correlated with SiO_2 content, whereas Sr, Ni and Ba concentrations are inversely correlated to the respective SiO_2 concentration (Fig. 8). Basalts have lower Zr, Rb and La (also in Zn, Pb, and Nd, not shown) vs. SiO_2 content than felsic rocks but higher content of Ni, Cr and Sr (also in Cu, Co and As, not shown) vs. SiO_2. The Axum basalts have Ni and Cr contents ranging from 5–85 and 1–270 ppm, respectively. Ni varies between 20 ppm and 85 ppm in basalts and very low in felsic rocks. Sr content ranges from 10 to 707 with an average of 212 ppm (the highest values are in the basalts). The basalts have Zr content 277 ppm while the felsic rocks have 1180 ppm in average. The average Nb content is 13 and 220 ppm in basalts and the felsic rocks, respectively. The phonolites/trachytes are characterized by enrichment in most trace elements, including Rb, Zr and La. The relative depletion of Sr in phonolite-trachyte is consistent with the dominance of alkali feldspar over plagioclase feldspar in these samples due to significant plagioclase fractionation at early stage (Ayalew and Gibson, 2009). Cr and Ni are compatible elements that can be easily incorporated in the crystallization of olivine in basalt and hence commonly having values low amount in felsic magmas (Nesbitt and Young, 1984). However the weathering of silicates at latter stage can determine the mobility of these elements. Hence, trace elements such as Rb, Ba, Sr and La are often subjected to significant leaching during weathering. Cr and Ni are generally considered to

be relatively conservative that preferentially retained in the solid residue of weathering (Christidis, 1998).

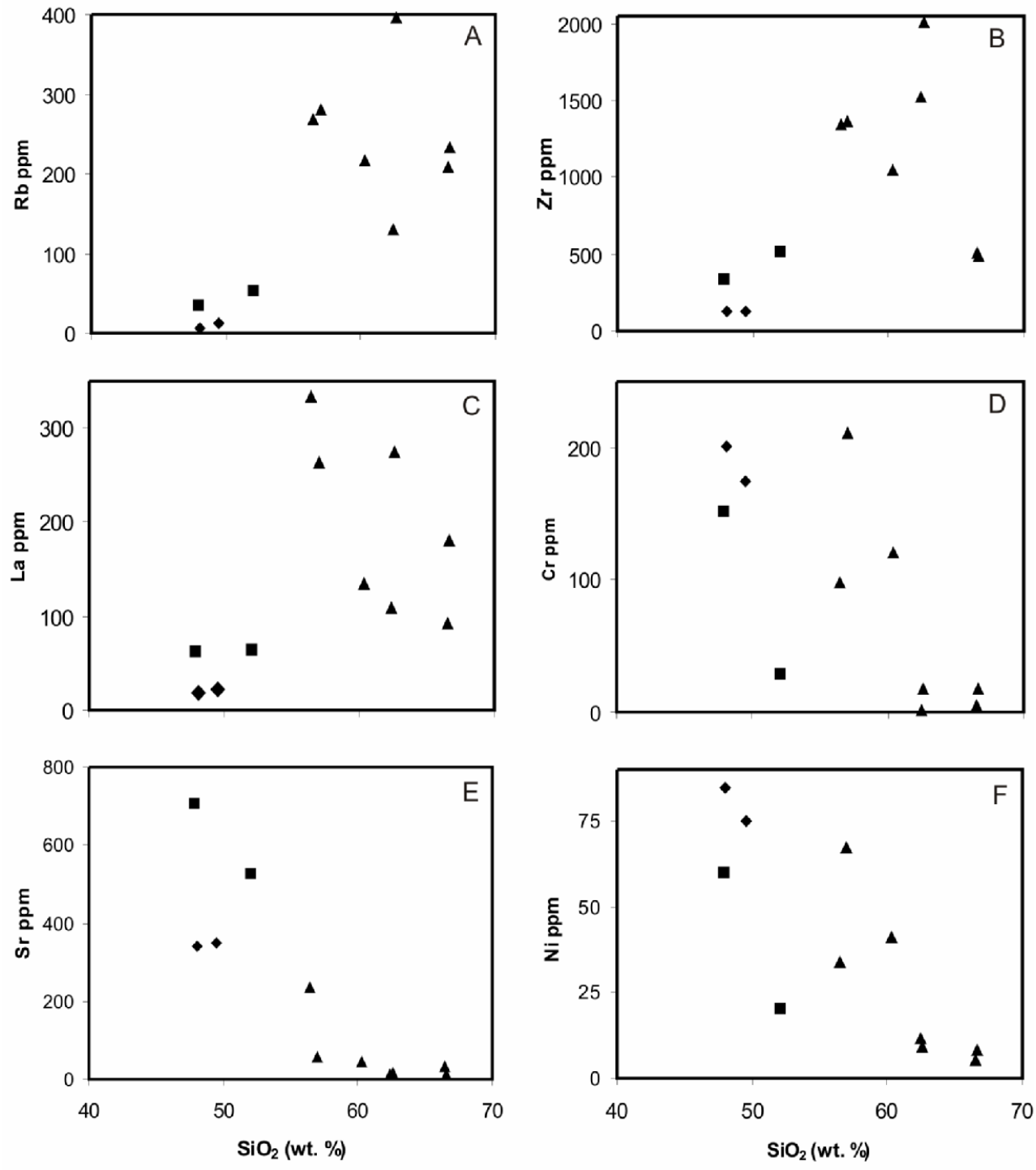

Fig. 8. Plots of concentrations of selected trace elements versus SiO_2 for Axum volcanic rocks. (▲) felsic rock; (■) HT basalts; (♦) LT basalts

5.5. Discussion

The results of this study are limited in terms of the amount of data used to constrain the geochemical trend of the Axum volcanic. Nevertheless, the results permit to compare the data with the previous studies having wider composition ranges. The petrological and geochemical characteristics of Axum volcanic exhibit resemblance to those of the northwestern Ethiopia flood basalt. Recent investigations showed that the basalt rocks occurring in the area are closely related to two geochemical distinct rock suites volcanic episodes (Hagos et al., 2010). Based on Ti-oxides and trace element studies, flood basalt sequence and post-trap basalt sequence and associated felsic rocks have been identified (Hagos et al., 2010). Although the geochronological of Axum has not been determined, field observation and geochemical study indicate that post-trap basalts appear to be younger than the flood basalt sequences. In agreement with the previous studies (Pik et al., 1998; Beccaluva et al., 2009), the LT basalts mostly plot in the tholeiitic field and the HT group shows alkaline magmatic character. But the HT and LT alkali basalts of Hagos et al. (2010) appear to have alkaline affinities with distinct geochemical characteristics (see Fig. 6). The flood basalt sequence is basanites and trachy-basalts with some of the samples having tholeiite magmatic tendency.

Variations of incompatible element ratios in the basalts suggest heterogeneous sources and significant interaction with the crust. The LT basalts exhibit important variations of incompatible element abundances including Nb, Zr, Rb and La and resemble those of other continental alkali basalt suites. The regional LT basalts show a strong lithospheric signature with relative depletions in Nb, Ta, Th, and Rb compared to oceanic basalts (Pik et al., 1999). The geochemical signatures are consistent with crystal fractionation processes from distinct mantle source accompanied by crustal contamination. The HT alkali basalts tends to display high enrichment in most of the same elements compared to LT basalts and it exhibits relatively higher concentration of the light incompatible trace elements (Hagos et al., 2010). The distinctive geochemical characteristics of HT lava indicated that it was derived from a more fractionated magma as reflected by its low MgO (1.1–3.6 wt. %) concentration and the relatively low Ni and Cr concentrations. The different elemental compositions of post-trap basalt and flood basalt sequences together with HT and LT and felsic rocks are plotted in Fig. 9. The LT major geochemistry of basalts is different from Hagos et al. (2010) but coincides with wider LT lava compositions of Kieffer et al. (2004) (see Fig. 9a). The phonolites and trachytes of Axum exhibit different geochemical characteristics than

basalts. The phonolite-trachyte of Axum rocks have higher incompatible trace elements (e.g. La and Nb) and similar degree of fractionation that is characterized by very low MgO and TiO_2 contents with genetically linked to the post-trap basalt sequence (Hagos et al., 2010).

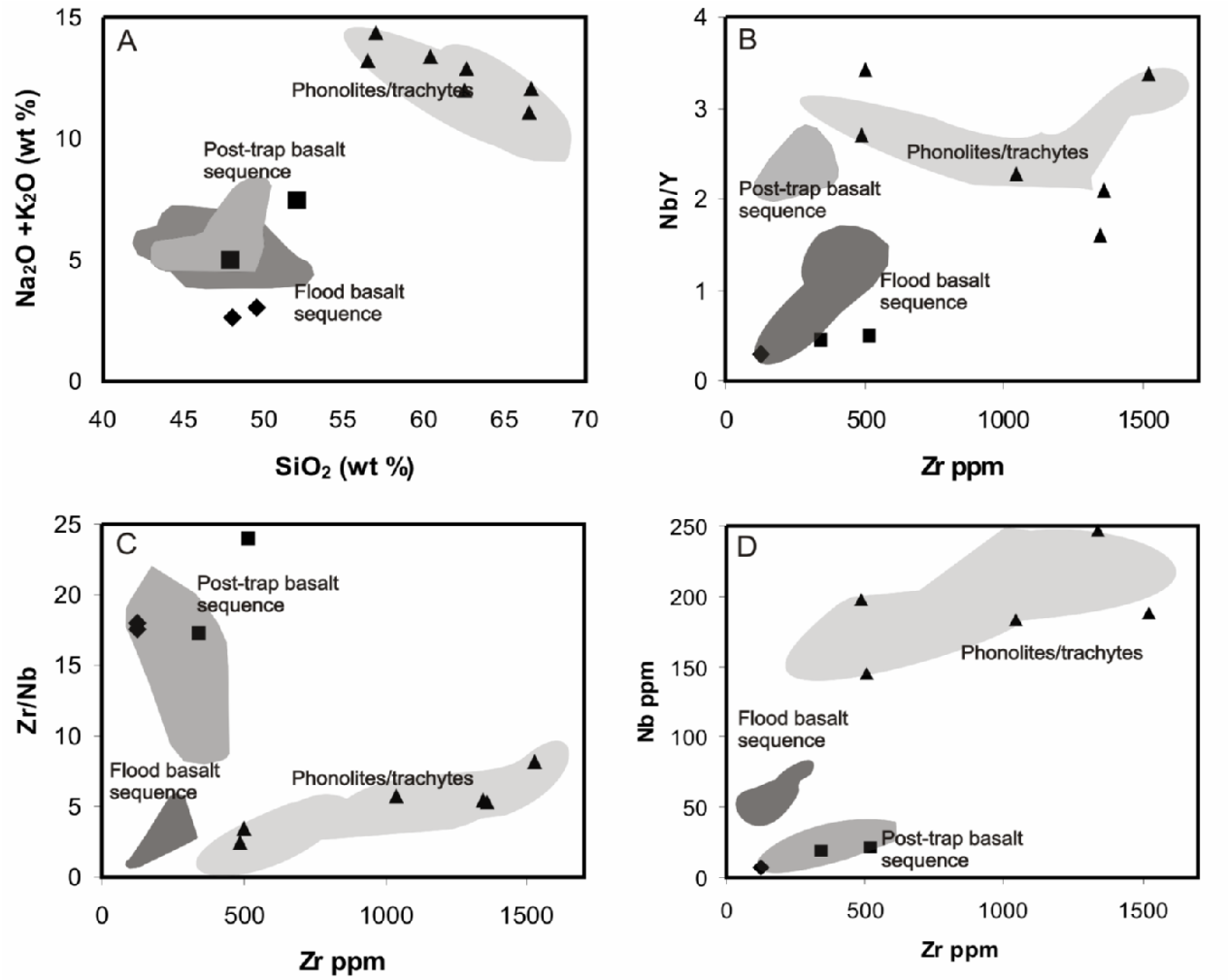

Fig. 9. Variation in selected major and trace elements Axum volcanic, compared with flood basalt and post-trap basalt sequence of the northern plateau. Data from this study (▲) felsic rock; (■) HT basalts; (♦) LT basalts, and Hagos et al. (2010) shaded area.

The HT and LT of the Axum area exhibit minor geochemical differences in terms of Nb and Zr contents and Zr/Nb and Nb/Y ratios (Figs. 9b, c and d). The basalts samples have low to moderate contents of Nb and Zr. The tholeiitic basalts of the Ethiopian flood volcanic have persistently low Nb/Y ratios and higher Zr/Nb ratios suggesting crustal contamination or variation in degree of partial melting (Hagos et al., 2010).

6. Hydrogeochemical characterization of groundwater and water-rock interaction

6.1. Introduction

To examine the water-rock interaction processes in aqueous solutions, the chemical composition of the solution has to be characterized. In general rainfall infiltrates to the soil horizons and subsequently enters the host rock. In the study area, the groundwater passes through a considerable thickness of basaltic rock that influences its hydrochemical signatures. In such a volcanic aquifer, the apparent incongruent weathering of silicate minerals in the groundwater system tend to release cations, especially Ca^{2+}, $Mg^{2+}$and Na^{+}, which results in high content of HCO_3^- and raises pH (Appello and Postma, 2005). The physico-chemical parameters of the analysed groundwater from the Axum area are given in Appendix III. The pH ranges from 6.8 to 7.8, with a mean value of 7.3. Concentrations of dissolved solids change with distance and more predominantly with depth along the flow paths. In general, deeper groundwater (40–150 m) contains higher concentration of major and minor component compared to shallow groundwater. Water chemistry allows identifying the dominant geochemical reactions characterizing the groundwaters evolution. In the study area, evidences for geochemical reaction can be explained by the relationships of major and minor ions in groundwater.

The changes in concentrations of redox-sensitive species such as dissolved oxygen, NO_3^-, Fe^{2+}, and Mn^{2+} in the groundwater vary spatially and are related to increasingly oxic/anoxic conditions along the flowpaths. On another point of view, groundwater quality can be considered unsuitable for different propose if the presence of these dissolved species exceeds permissible limit. Moreover, elevated concentrations of naturally occurring heavy metals in groundwater can even pose health risk on local human communities. From previous studies, little is known about the distribution of these elements in the groundwater of Axum area.

6.2. Major components

The major components of groundwater represent the distribution of aquifer composition and geochemical reaction as well as the local processes including human activities that influence water chemistry. The relative distribution of major dissolved cations and anions are illustrated in Figs. 10A and B.

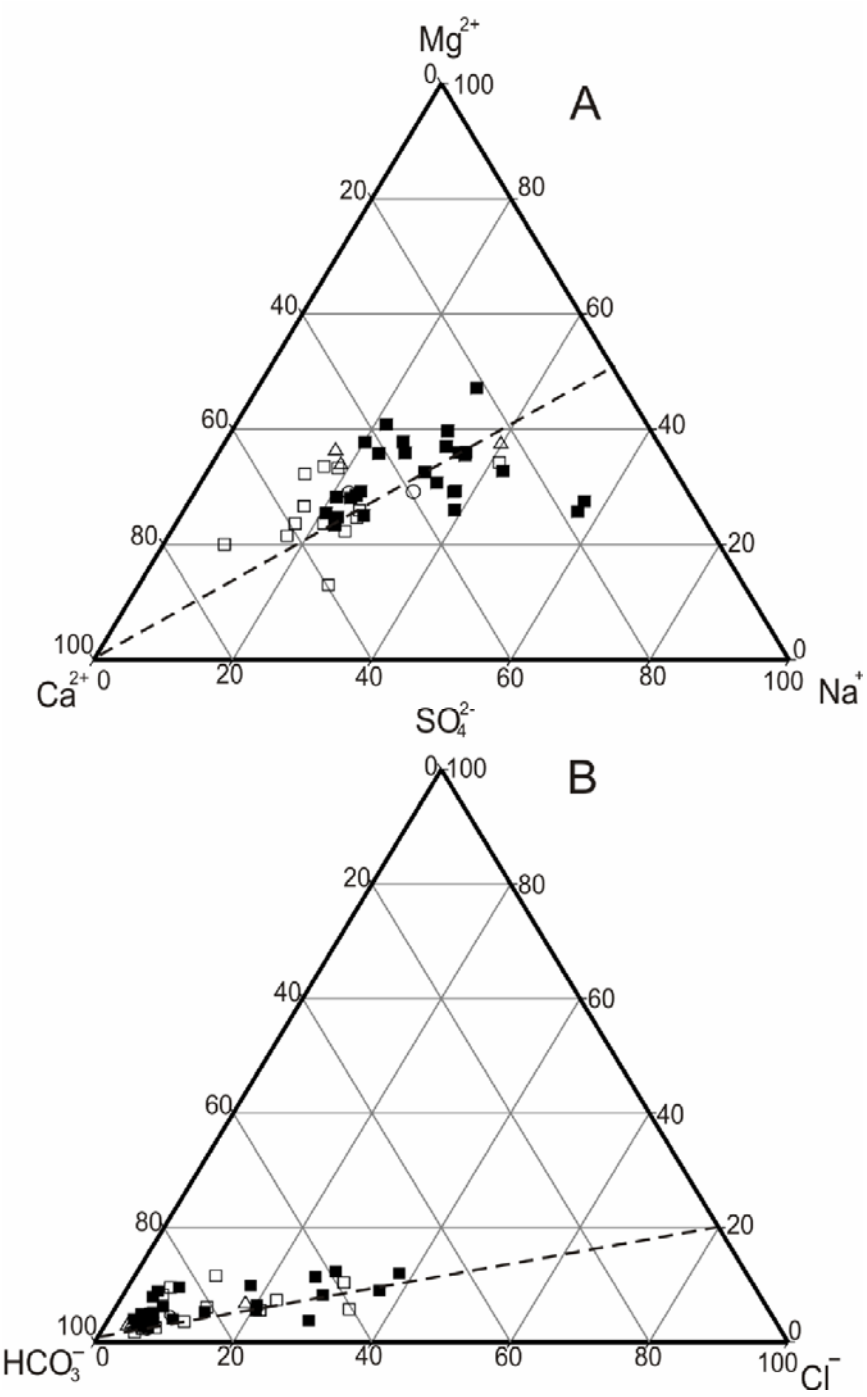

Fig. 10. Ternary plot with major ion chemistry of groundwater from deep wells (■) and shallow wells (□), spring water (Δ) and surface water (o) from the Axum area on a charge-equivalent basis.

In Fig. 10A dissolved cations are mostly dominated by Ca^{2+} followed by Na^{+} and Mg^{2+}. The relative amount of Ca^{2+} ranges from about 20 to 70 equimol %, whereas the equimolar $[Na^{+}]/[Mg^{2+}]$ ratio is rather constant at about 0.5 (see dashed line in Fig. 10A). High relative Ca^{2+} content of groundwater is mostly referred to the shallow aquifer, whereas less Ca^{2+} is prevailed in

groundwater from the deep aquifer. Dissolved anions of the groundwater are strongly dominated by HCO_3^-, followed by Cl^- and SO_4^{2-} (Fig. 10B). The equimolar $[Cl^-]/[SO_4^{2-}]$ ratio is close to 4 for most of the sampled solutions, which is indicated by the dashed line in Fig. 10B. Accordingly, the chemical composition of the analysed groundwater is dominated by HCO_3^- and Ca^{2+} or $Na^+ + Mg^{2+}$ as cations in shallow or deep groundwater, respectively. The major-ion chemistry of certain wells, located in Axum town, may be greatly influenced by anthropogenic source. Accordingly, the elevated content of NO_3^- and Cl^- in shallow aquifers is referred to anthropogenic impact (see Appendix III).

The chemical evolution of the groundwater displays distinct differences between bedrock and alluvium groundwater. Most shallow wells hosted within quaternary alluvial deposits have a composition representing "fresh water" type. Infiltration of precipitation and surface water initially results in dilute, less evolved, Ca–HCO_3^- type water. The average concentration of TDS of this group is very low compared to the mineralized deep groundwaters. In deeper groundwater, the contact time between water and minerals is much longer than it is in shallow flow systems. Among major ions, the average concentration of Ca^{2+} and Mg^{2+} varies from 1.0 to 1.8 mmol l^{-1} in shallow wells and 2.1 to 2.2 mmol l^{-1} in deep wells. The concentrations of Ca^{2+} and Mg^{2+} are typical for basaltic aquifer hosted groundwater and are nearly balanced by alkalinity.

6.3. Hydrogeochemical characterization and weathering reactions

The relationship between major cations (Ca^{2+}, Mg^{2+}, Na^+ and K^+) and alkalinity is commonly used to describe the extent of water-rock interaction as the weathering of silicate contribute to these major ion concentrations in the solution (Kim 2002). The enrichment in Mg^{2+} and Na^+ as well as in silicic acid appears to reflect the chemical evolution mostly related to basalt-water interaction (Appello and Postma, 2005). Carbonic acid hydrolysis of silicate minerals may be suggested as the dominant process controlling the water chemistry. But other processes, such as precipitation of solids and ion-exchange reactions can modify the water chemistry e.g. by removing calcium and liberating sodium, resulting in more evolved Na–HCO_3 type water.

Exemplarily, the incongruent dissolution of anorthite and albite as Ca^{2+} and Na^+ plagioclase endmembers can be described by the overall reactions:

$$CaAl_2Si_2O_8 + 2CO_2 + 3H_2O \rightarrow Al_2Si_2O_5(OH)_4 + Ca^{2+} + 2HCO_3^- \quad (23)$$

$$2NaAlSi_3O_8 + 2CO_2 + 3H_2O \rightarrow Al_2Si_2O_5(OH)_4 + 2Na^+ + 2HCO_3^- + 4Si(OH)_4 \quad (24)$$

where a CO_2-rich solution and kaolinite as a secondary silicate phase are considered. Pursuant to the reactions 23 and 24 a Ca^{2+}– and Na^+–HCO_3^- solution can be obtained. A transfer of Mg^{2+} into the groundwater can be derived e.g., by the dissolution of the end member of olivine according to the overall reaction

$$MgFeSiO_4 + 4H_2O + 4CO_2 \rightarrow Mg^{2+} + Fe^{2+} + 4HCO_3^- + Si(OH)_4 \quad (25)$$

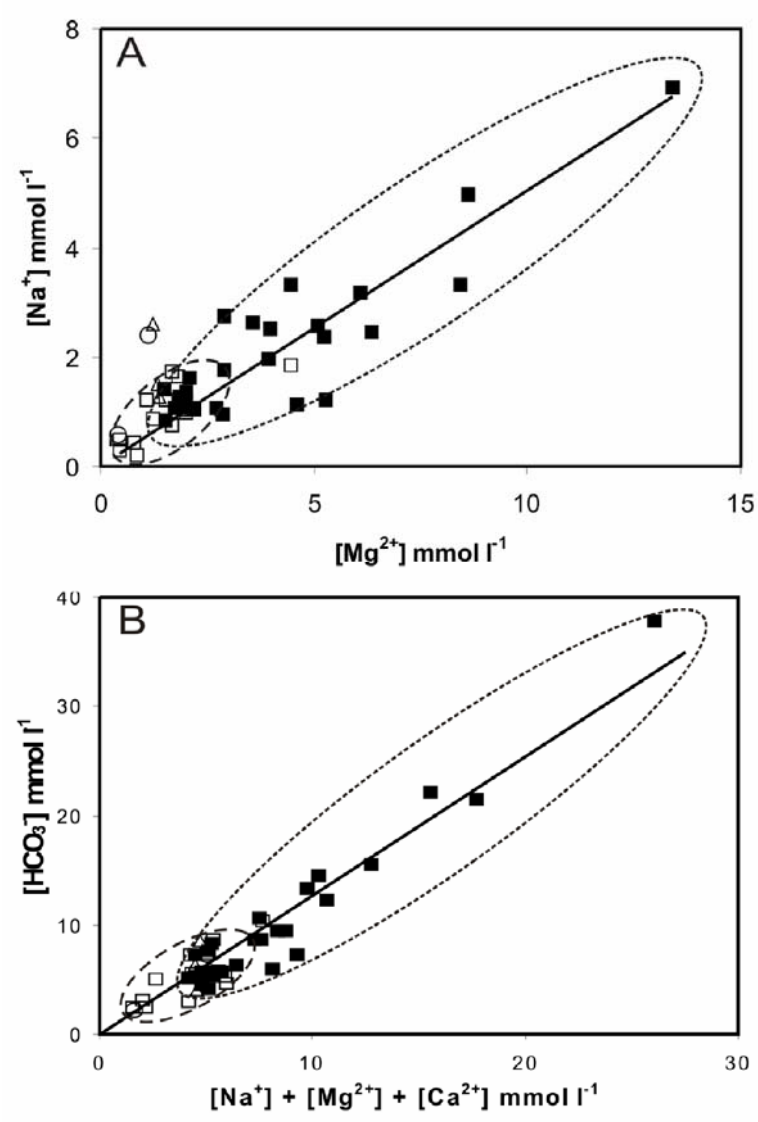

Fig. 11. Composition of water from deep wells (■) and shallow wells (□), spring water (Δ) and surface water (o) from the Axum area: (A) Sodium versus magnesium concentration; regression line: $[Na^+] = 0.505\ [Mg^{2+}]$ ($R^2 = 0.80$); (B) Sum of sodium, magnesium and calcium versus bicarbonate concentration; regression line: $[HCO_3^-] = 1.27\ ([Na^+] + [Mg^{2+}] + [Ca^{2+}])$ ($R^2 = 0.91$).

A similar equation can be obtained e.g., for augite dissolution liberating the cations Mg^{2+}, Ca^{2+}, and Fe^{2+} in the solution.

Weathering of the primary silicates release cations like Ca^{2+}, Mg^{2+}, and Na^{+} into the groundwater. Mg^{2+} and Na^{+} concentrations are linearly correlated with a slope close to 0.5 (Fig. 11A). One mole CO_2 is consumed by each equivalent of Ca^{2+} and Na^{+}. The scatter of Mg^{2+} and Na^{+} may be related to the heterogeneities of the aquifer and individual reaction paths. Groundwater from deep wells contains the highest Na^{+} and Mg^{2+} concentrations up to 6.9 and 13.4 mmol l^{-1}, respectively (see Appendix III), whereas significantly lower concentrations of Na^{+} and Mg^{2+} were measured in shallow groundwater and spring waters (see Fig. 11A). In contrast, liberation of K^{+} during silicate weathering is less important as $[Na^{+}]/[K^{+}]$ ratios of groundwaters lay between 6 and 200 with an average of ≈ 50 (see individual data in Appendix III).

The strong correlation of $[Na^{+}]+[Mg^{2+}]+[Ca^{2+}]$ versus $[HCO_3^{-}]$ verifies the above silicate dissolution (Fig. 11B), where the deep and shallow groundwater can be distinguished by high and low ion concentrations, respectively. The relationship between the concentration of HCO_3^{-} and dissolved cations according to the overall reactions (23) to (25) indicates that silicate weathering in the study area is controlled by the uptake of CO_2.

6.4. Dissolved Fe and Mn

Redox behaviour of groundwater can be monitored by analysing *Eh*, dissolved oxygen, iron species, sulfur species, and nitrogen species. Despite the lack of direct *Eh* measures, *Eh* of a solution is determined using dissolved O_2 content as an important parameter to understand the redox process (White et al., 1991). The dissolved oxygen concentration is related to *Eh* using equation 17 in section 2.4.

The dissolved oxygen concentration in Axum aquifers ranges from below 1 mg l^{-1} to 8 mg l^{-1}. The consumption of O_2 by oxidation of organic matter decreases the dissolved oxygen content in groundwater rapidly at greater depth. Thus, the oxidation of other reduced species and mineral phases in groundwater becomes significant. The presence of abundant Fe is addressed to the Fe(II)–Fe(III) redox behaviour. Accordingly, high amounts of dissolved iron are mostly accompanied with low concentrations of $O_{2(aq)}$ and vice versa (e.g. solutions AW7 and AW16 in Appendix III).

Iron concentrations above the WHO maximum level of 0.5 mg l^{-1} are observed in groundwaters (see Appendix III). The dissolved Fe concentrations in the aquifer ranged from below detection limit (0.001 ppm) to greater than 10 mg l^{-1} and manganese concentrations varied widely from below detection limit (0.001 ppm) to 0.48 mg l^{-1}. The high manganese concentrations are variable but follow roughly related trend to iron, reflecting their similar geochemical controls. The high Fe^{2+} concentration in groundwater is indicative of reducing conditions, since the original source for iron is the dissolution of Fe(II)–silicates (such as, pyroxene and olivine) or ferric oxyhydroxides (Appelo and Postma, 2005). Both Fe and Mn are soluble in water in their reduced form and are more mobile than the oxidized forms, which form insoluble oxy-hydroxides. The most common cause of reducing reactions is decay of organic matter. Iron is consumed as an electron acceptor during oxidation of organic matter. Therefore, if the local environment is in reduced condition, the water will have higher concentrations of iron.

The exposure of the solutions to the Earth's atmosphere allows absorption of gaseous oxygen from the atmosphere, which results in the oxidation of dissolved Fe(II) to Fe(III) and the precipitation of Fe(III)–O–OH-phases (e.g. Cornell and Schwertmann, 1996). A fast oxidation of Fe(II) to ferric oxides or hydroxides occur at near-neutral pH according to the reaction

$$Fe(II) + 2OH^- + 1/4O_2 + 1/2H_2O = Fe(OH)_{3(s)} \quad (26)$$

The relevant influence of pH and *Eh* on Fe species concentrations is shown by plotting the concentration on a predominance diagram, where the ranges of major of iron species are given (Fig.12).

The pattern of the groundwater fits fairly well with the presence of $Fe(OH)_3$ as the solid controlling dissolved iron concentration. Obviously, groundwater containing iron concentrations up to about 10 mg l^{-1} is falling in the stability field of the $Fe(OH)_3$. All the samples fall in the oxic condition is due to the fact that high Fe content is kinetically controlled and Fe-O-OH precipitation is an ongoing process. Small amount of dissolved oxygen in the samples invoke the plot automatically close to the upper stability field of *Eh-pH* diagram.

Fe^{2+} is oxidized to Fe^{3+} and precipitated as $Fe(OH)_3$ at the given *Eh-pH* conditions rather fast, while the Mn^{2+} ion can remains in solution for longer time periods (see also Mukherjee and Fryar, 2008).

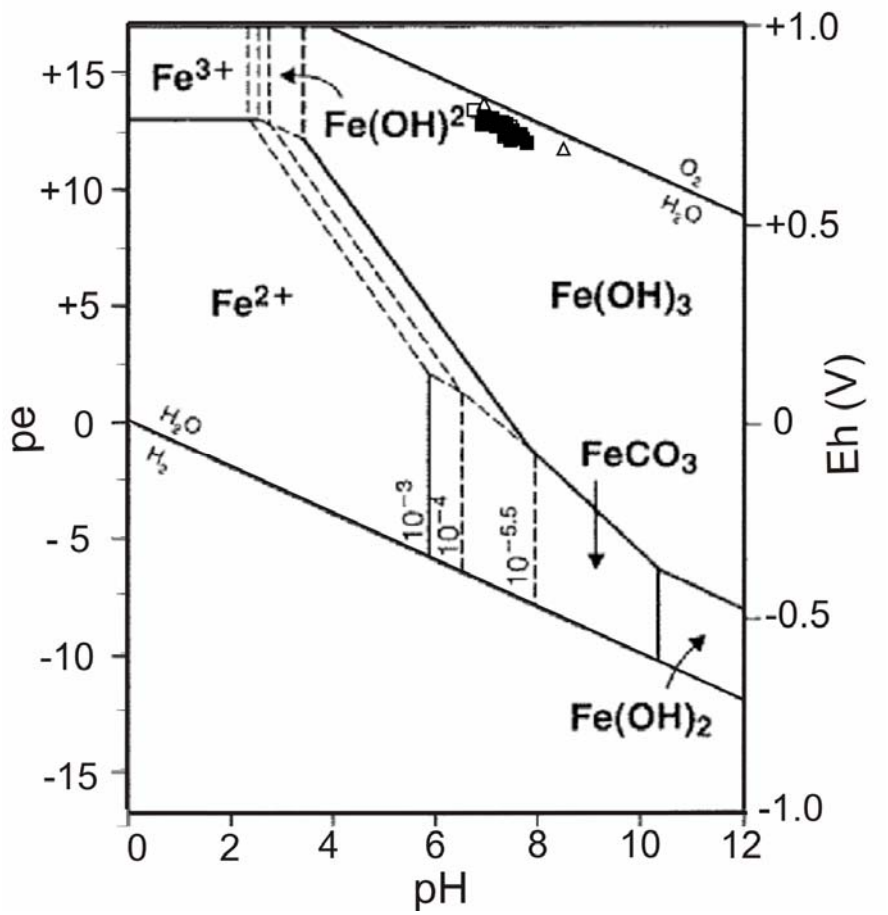

Fig. 12. Stability diagram for iron species and (hydro)oxides in the system Fe-H_2O-CO_2 at 25^0C, DIC =$10^{-2.5}$mol l^{-1}. Solid/solution boundaries are specified for different [Fe^{2+}]. Heavy lines indicate "realistic" boundaries (after Appelo and Postma, 2005). Deep wells (■) and shallow wells (□), spring water (Δ) and surface water (o) from the Axum area.

Locally, groundwater quality can be considered unsuitable for drinking or domestic use because of the presence of dissolved iron and manganese. However, elevated concentrations of these elements may not pose a direct health risk, but contribute to undesirable tastes, unacceptable appearance and unpleasant odour of the drinking water. The precipitation of excessive iron gives an objectionable reddish-brown colour to the water that readily stains both plumbing fixtures and laundry.

6.5. Trace elements

Analytical results of trace element in groundwaters are reported in Appendix IV. The concentration of Cd, Cs, Th and La were below detection limits in most of the samples. The mean content of Al (60 μg l^{-1}) and Zr (30 μg l^{-1}) in shallow wells are higher than those in deep wells. The concentration of Al depends on the extent of weathering of aluminosilicate and neoformation.

The concentration of trace metals is further illustrated in Fig. (13). Contrary to the major ions chemistry, the trace ion compositions of groundwater are much variable. The highest concentrations coincide with high mineralized solutions suggesting elevated leaching of the host rocks.

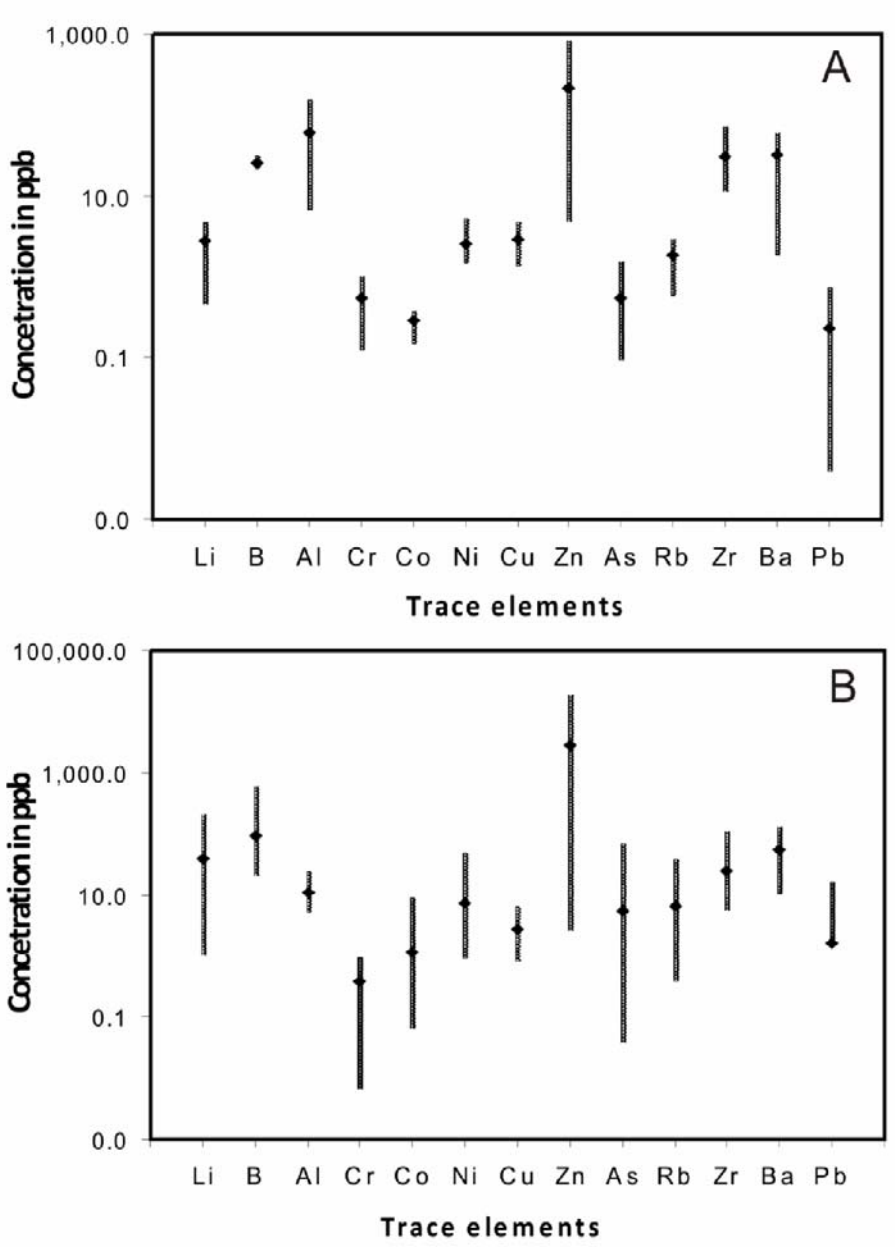

Fig. 13. Plots showing the distribution of trace elements in groundwater from (A) shallow and (B) deep wells. The line represents the range of minimum and maximum values with average values.

The trace elements loading of Axum groundwater are relatively low and lay with in the WHO guideline values except for Zn. It may be possible that the increase of Zn concentration could be

somewhat attributed to the corrosion of pump parts where it is used as an anticorrosion agent in coated iron pipelines to protect against corrosion.

6.6. Anthropogenic impact

The influence of human activities is evident in municipal as well as shallow wells as the average concentration of nitrate from shallow groundwater is 0.06 mmol l^{-1} NO_3^-. In several water points the nitrate concentration has exceeded WHO recommended value of 50 mg l^{-1} (0.8 mmol l^{-1}) for drinking water (WHO, 2004). For instance, wells AW14, AW15, AW20, AW22 and AW32 with elevated NO_3^- and Cl^- content are located close to or within Axum town indicating the vulnerability of the groundwaters to pollutants from different source. Common sources of nitrates in drinking water are from agricultural fertilizers, human and animal wastes, through poorly designed septic systems and untreated sewage discharges and leaky landfills. In principle, both NO_3^- and Cl^- are indicative of an anthropogenic impact. However, no significant correlation between NO_3^- and Cl^- concentration (Fig. 14) exists, which is probably related to due to the non-conservative behaviour of NO_3^- and as chloride in groundwater originates from sewage and industrial effluents as well as from natural sources.

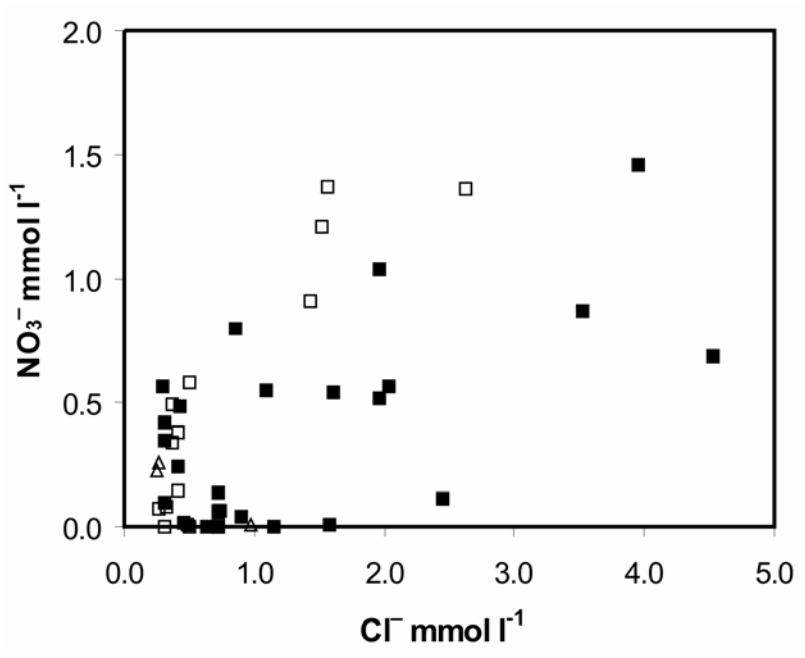

Fig. 14. Relationship of NO_3 versus Cl concentration for water from deep wells (■) and shallow wells (□), spring water (Δ) and surface water (o) from the Axum area.

Nitrate in groundwater is stable under the oxidizing condition and can be denitrified to N_2 or NH_4^+ in anoxic zones (Slomp and Cappellen, 2004). Nitrate contamination in groundwater of Axum is much more prevalent at shallow depths and generally decline as depth increases due to denitrification. Bacteria degrade organic carbon using oxygen as the terminal electron acceptor but if oxygen is not replenished quickly enough, the environment becomes anaerobic and then nitrates are used as electron acceptors leading to denitrification.

High concentrations of nitrate in the groundwaters is a common occurrence in unprotected shallow wells in many part of Ethiopia (e.g. Kebede et al., 2005; Demlie et al., 2008; Tilahun and Merkel, 2009), mostly as a result of leaking effluent from domestic waste. In urban areas, the high level of nitrate and accompanied high content of chloride are suspected to gain from human and animal waste effluent. Inadequate disposal of human and animal waste contributes to high nitrate concentration. Nitrate concentrations are likely to be worst in areas where traditionally hand-dugs have been used as drinking water supply. These drinking water sources are very close to the Earth's surface and human activities close to these waters can potentially pollute the drinking water. Human waste disposal and agriculture are the two major nitrate sources. Harm to human infant, by reducing the ability of blood to transport oxygen, has been cited as one of the health hazard associated with presence of high concentrations of nitrate in drinking water.

7. Isotope geochemistry

7.1. Introduction

A primary challenge for groundwater quality change is to understand the origin of groundwater and its chemical constituents in groundwater. In order to accomplish the task, the isotopic characteristics of the groundwater were used as tracer to efficiently assess the hydrologic and the hydrochemical variability (Alemayehu et al., 2011). Groundwater in its natural state contains environmental isotopes and their compositions and variations in the aquifer are important for assessing water resource quality problems unsolved by conventional methods.

In this section, the isotope data of groundwater interpreted with respect to geological and hydrogeological conditions of the study area are presented. The stable isotope of hydrogen ($^{2}H/^{1}H$) and oxygen ($^{18}O/^{16}O$) provides useful information about the interaction of the surface water versus groundwater and shallow versus deep well aquifers. The stable isotope ratios carbon ($^{13}C/^{12}C$) was used to trace the origin DIC. $^{87}Sr/^{86}Sr$ ratios are mainly used as tracers of water-rock interaction by providing information about the dominant geochemical reactions and mixing processes.

7.2. Stable isotopic composition of the water

The global meteoric water line (GMWL) and the local meteoric water line of the Addis Ababa area (LMWL) are plotted in Fig. 15. Because of the lack of isotope data from rainfall in the study area, it is assumed that the Addis Ababa meteoric water line generally applies for Ethiopia (Rozanski et al., 1996). The isotopic composition of rainwater for Addis Ababa station is given by equation of $\delta^{2}H = 7.5\ \delta^{18}O + 12.9$ ($r^{2}=0.95$) using data obtained from the IAEA-GNIP database (IAEA, 2008). In general, the impact of latitude and altitude on the isotopic composition of rainfall may be significant (Gat and Dansgaard, 1972), but appears to have little effect on the spatial variation of the isotopic composition of Ethiopian rainfall (Kebede et al., 2005). Thus, it is warranted to use the Addis Ababa meteoric line for Axum and the slope and intercept of the regression line drawn through Addis Ababa long-term $\delta^{2}H$ and $\delta^{18}O$ rainfall data differ only slightly from the GMWL (see Fig. 15).

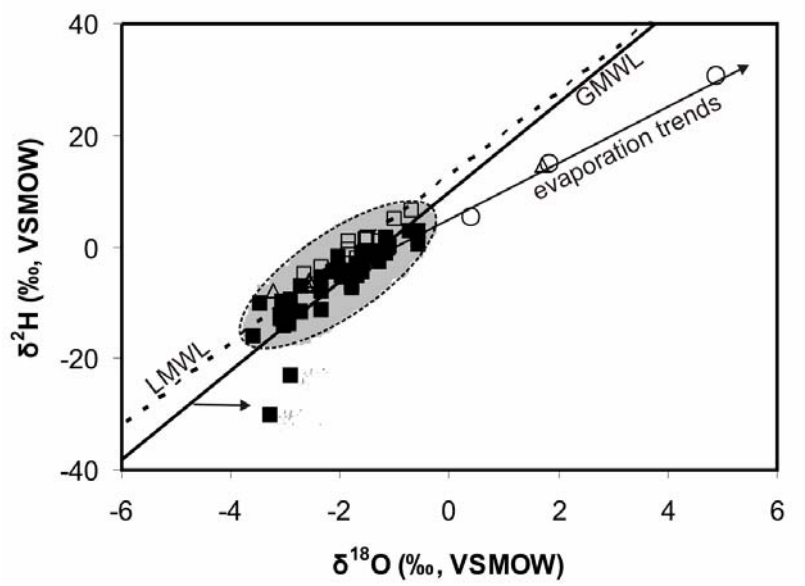

Fig. 15. Relationship between δ^2H and $\delta^{18}O$ values of water from deep wells (■) and shallow wells (□), spring water (Δ) and surface water (o) from the Axum area. LMWL (dashed line) denotes the linear regression for the local meteoric water line of Addis Ababa. GMWL (solid line) refers to the global meteoric water line of Craig (1961).

The δ^2H(VSMOW) and δ^{18}O(VSMOW)-values of groundwater and surface water range from about –30 to 30 ‰ and –5.1 to 4.8 ‰, respectively (Fig. 15). The isotope data clearly indicate that the groundwaters are of meteoric origin as δ^2H and δ^{18}O values of the sampled solutions plot along or close to the LMWL and GMWL. However, for two groundwaters (AW8 and AW16) a δ^{18}O shift to more positive values may be attributed to oxygen isotope exchange between the host rock and aqueous solution (e.g. Schofield and Jankowski, 2004). Strong interaction of basaltic rock with groundwater follows from the elevated solutes (Appendix V).

Although, the isotopic composition of all sampled solutions indicates the meteoric origin, their isotope signatures can be modified by evaporation of rain during infiltration as indicated by isotope values plotting below the meteoric water line (Clark and Fritz, 1997). The δ^2H and δ^{18}O values for the analysed surface waters and one spring water plot below the LMWL and GMWL (see evaporation line on Fig. 15). Evaporation results in discrimination of ^{18}O and ^{2}H versus ^{16}O and H, respectively, and heavier isotopes are accumulated in the remaining solution (e.g. Allison, 1982). The isotopic composition of shallow groundwater reflects the local precipitation values (Clark and Fritz, 1997) and there exist no clear evidence from isotopic composition to entail the effect of evaporation in shallow wells during recharge (Alemayehu et al., 2011). But, if rainwater is infiltrated slowly into the ground, significant evaporation may take place prior infiltration.

7.3. Stable carbon isotopes and source of CO_2

The chemical composition of the sampled groundwater from the Axum area clearly indicates weathering of local basalts by the uptake of gaseous CO_2 (Alemayehu et al., 2010). The stronger the weathering is, the higher the TDS and DIC content. These relationships can be followed by the overall increase of [DIC] at elevated internal partial pressures of CO_2, PCO_2, according to regression line in Fig. 16

$$\log(DIC) = 0.54\ PCO_2 + 1.84\ (R^2 = 0.51) \qquad (27)$$

Low PCO_2 refers to high pH, typical for shallow groundwater (e.g. solution 25 with pH 7.5), whereas high PCO_2 is related to low pH (e.g. solution AW16 with pH 6.9). Consequently, the chemical data display the uptake of CO_2 as crucial parameter for groundwater evolution in the study area. To decipher sources of CO_2 and conditions during groundwater evolution, the $^{13}C/^{12}C$ isotopic distribution of DIC has been successfully used as a groundwater tracer for possible carbon sources (e.g. Clark and Fritz 1997; Cartwright et al., 2002; Federico et al., 2002; Jin et al., 2009).

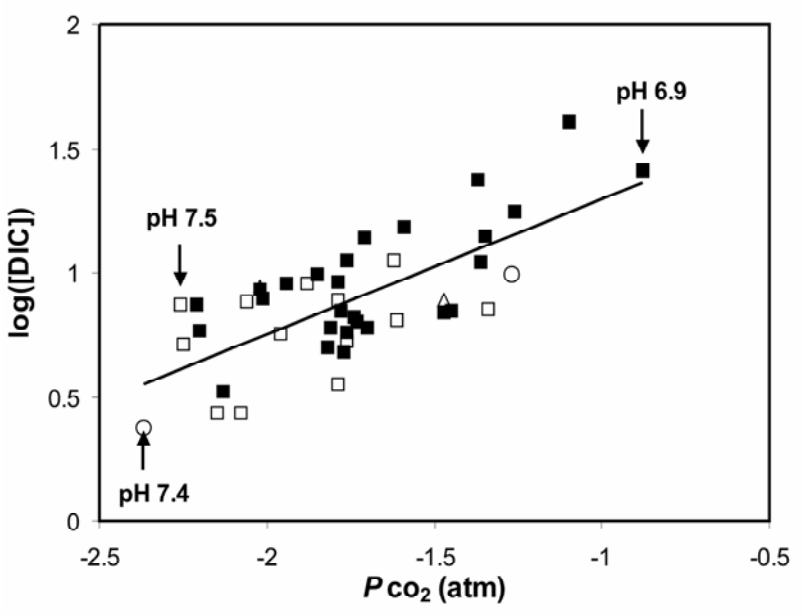

Fig. 16. Concentration of dissolved inorganic carbon, [DIC] in mmol l^{-1}, and the calculated internal partial pressure of CO_2 (PCO_2 in atm from equation (27)) of water from deep wells (■) and shallow wells (□), spring water (Δ) and surface water (o) from the Axum area.

The $\delta^{13}C_{DIC}$ values of the analysed groundwaters range from –12 to +1 ‰ (VPDB; Appendix V). Such a wide $\delta^{13}C_{DIC}$ range could reflect multiple carbon sources and variability in DIC evolution. Highest $\delta^{13}C_{DIC}$ values are measured for deep groundwater with elevated [DIC] (e.g. solution AW16 with $\delta^{13}C_{DIC}$ = +1.1 ‰; Fig. 17), whereas shallow wells display a lower $\delta^{13}C_{DIC}$ range from –12.0 to –7.3 ‰ with an average of –10 ±1.5 ‰.

As shown by the stable isotopes of H_2O, all groundwaters are of meteoric origin and thus acquire – beside negligible amounts of CO_2 from the Earth's atmosphere – biogenic CO_2 during infiltration through soils. As the mean $PCO_2 = 10^{-1.9}$ atm of shallow groundwater lays within the typical values for soil CO_2, the respective average $\delta^{13}C_{DIC}$ = –10 ‰ may be referred to CO_2 from soil horizons. Considering an open system with respect to soil CO_2 during evolution of shallow groundwater, the $\delta^{13}C_{CO2}$ = –17 ±2 ‰ is calculated for gaseous CO_2 based on the Eqs. 20 and 21.

$\delta^{13}C$ values of local soil CO_2 are not available, but Terwilliger et al. (2008) established the occurrence of C_3 and C_4 plants from soils along various elevations transects in Ethiopia. The stable carbon isotopic composition of CO_2 produced by respiration in a soil corresponds to $\delta^{13}C$ of the organic matter. Variation in isotopic compositions can be caused by local characteristics and essentially by the proportion of C_3 and C_4 plants. Average $\delta^{13}C_{CO2}$ values generated from C_3 and C_4 plants are about –23 and –9 ‰, respectively, if CO_2 diffusion effects in soils are considered (Vogel, 1993; Clark and Fritz, 1997). Assuming a C_3:C_4 ratio of 1:1 for soil CO_2 production in the study area yields $\delta^{13}C_{CO2} \approx$ –16 ‰, which is equivalent to the estimated soil CO_2 from the analysed $\delta^{13}C_{DIC}$ values considering isotopic equilibrium and high availability of CO_2. In semi-arid regions, where high evapotranspiration and extended warmer periods prevail, carbon isotopic equilibrium may be attained through long residence time of percolating water in the unsaturated zone (Jin et al., 2009). Moreover, the consumption of CO_2 by silicate weathering is slow compared to soil CO_2 production rates. Hence, in most cases the weathering of silicate in shallow aquifers may remain at quasi open system conditions with respect to soil CO_2.

For deep groundwater, $\delta^{13}C_{DIC}$ values up to about +1 ‰ are obtained at elevated PCO_2 of $10^{-0.9}$ atm (see solution AW16; Appendix V). Such ^{13}C enriched DIC indicates that beside soil CO_2, magmatic carbon may be reasonably assumed as additional CO_2 source. The typical $\delta^{13}C$ values of CO_2 from magmatic origin range from –8 to –5 ‰ (e.g. Hoefs, 1997). Sheppard (1986) postulated

that isotopic fractionation between CO_2 in magma and CO_2 gas can enrich gaseous CO_2 by about 2 ‰. For groundwater AW16 with the highest PCO_2 an open system with respect to magmatic CO_2 may be considered and fractionation between CO_2 gas and DIC is about –6 ‰ at the given pH of 6.9 (α_{DIC} = 1.006). Accordingly, a $\delta^{13}C_{CO2}$ value of about -5 ‰ is obtained for groundwater from the isotopic composition of the DIC, which is in general agreement with the isotopic composition of CO_2 from magmatic origin (Alemayehu et al., 2010).

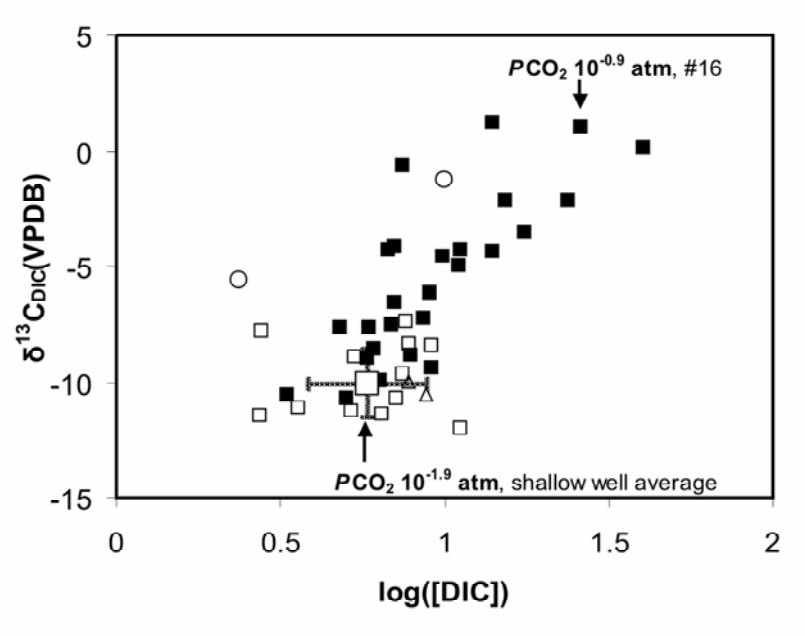

Fig. 17. $\delta^{13}C_{DIC}$ (VPDB) values in ‰ versus dissolved inorganic carbon concentration ([DIC] in mmol l^{-1}) of water from deep wells (■) and shallow wells (□), spring water (Δ) and surface water (o) from the Axum area. □: average values of groundwater from shallow wells. The $\delta^{13}C_{DIC}$ values indicate the presence of magmatic CO_2 (enriched in ^{13}C) and in the presence of soil gas (enriched in ^{12}C).

Thus, the analysed $\delta^{13}C_{DIC}$ range can be explained by the origin of CO_2 from two sources. The isotopically heavier deep groundwater indicates the presence of magmatic CO_2 at high PCO_2 causing strong silicate weathering. Low $\delta^{13}C_{DIC} \approx -10 \pm 1.5$ ‰ indicates soil CO_2 at lower PCO_2 and less silicate weathering. The intermediate carbon isotope signatures of DIC of the groundwaters in Fig. 17 are explicable as mixtures of the two end members: magmatic and soil CO_2. The isotopic composition of DIC may somewhat be influenced by dissolution of locally occurring calcite filling veins. But the calcite filling veins are mostly of magmatic origin (Gebresilassie, 2009) and their carbon isotope signature may overlap with that of magmatic CO_2.

The shift to more positive $\delta^{13}C_{DIC}$ values for the surface waters is attributed to enrichment of ^{13}C versus ^{12}C in DIC due to CO_2 outgassing (Appendix V; Doctor et al., 2008).

7.4. Strontium content and $^{87}Sr/^{86}Sr$ ratios

Strontium concentrations of water samples from the Axum aquifer range from 2 to 17 µmol l^{-1} (Appendix V). Fig. 18 illustrates the relationship between Sr^{2+} and Ca^{2+} content in deep and shallow groundwater. In general, elevated Sr^{2+} content is corresponding to high Ca^{2+} concentration in groundwater. The dominant source for both, Sr^{2+} and Ca^{2+} is the weathering of siliceous rocks and in particular plagioclase of the basalts within the aquifer. Variability of $[Ca^{2+}]$ and $[Sr^{2+}]$ may be due to carbonate formation and adsorption or ion exchange on clay minerals, zeolites etc. (Cartwright et al., 2007; Fridriksson et al., 2009). Thus, the $[Ca^{2+}]/[Sr^{2+}]$ ratio from about 0.2 to 0.6 in Fig. 19 is related to combined effects of weathering, adsorption and ion exchange phenomena, and discrimination of Sr^{2+} versus Ca^{2+} during calcite formation (e.g. Tang et al., 2008; Wiegand, 2009). Although, adsorption and ion exchange phenomena as well as calcite precipitation may modify the $[Ca^{2+}]/[Sr^{2+}]$ ratio in the groundwater, the Sr isotope composition of the solution remain unchanged (e.g. Shand et al., 2009; Wiegand, 2009)

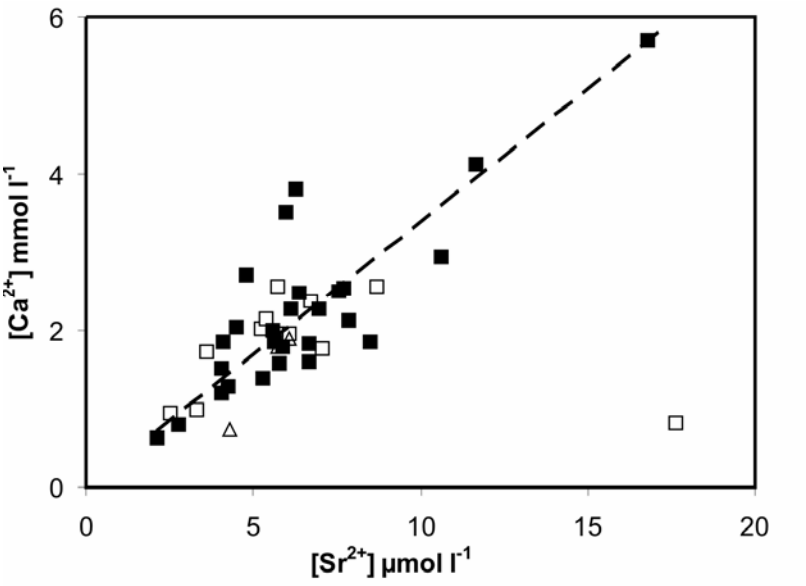

Fig. 18. Correlation between Ca^{2+} and Sr^{2+} concentration of water from deep wells (■) and shallow wells (□), spring water (Δ) and surface water (o) from the Axum area. Regression line: $[Ca^{2+}]$ (mmol l^{-1}) = 0.34 $[Sr^{2+}]$ (µmol l^{-1}) (R = 0.67).

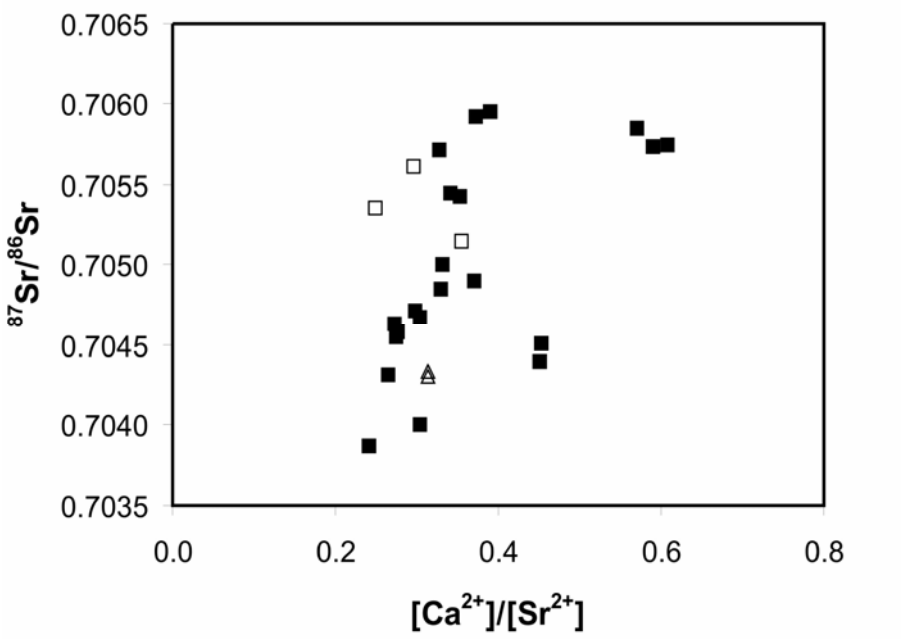

Fig. 19. $^{87}Sr/^{86}Sr$ ratios versus ($[Ca^{2+}]/[Sr^{2+}]$ ratios of water from deep wells (■) and shallow wells (□), spring water (Δ) and surface water (o) from the Axum area. $[Ca^{2+}]$ and $[Sr^{2+}]$ denote concentrations in mmol l^{-1}, mmol l^{-1} and µmol l^{-1}, respectively.

The analysed $^{87}Sr/^{86}Sr$ ratios of the groundwater samples from 18 sites vary between 0.70387 and 0.70595 (Appendix V). No significant relationship between Sr isotope distributions and $[Ca^{2+}]/[Sr^{2+}]$ ratios is displayed in Fig. 19 which may be caused by rather complex behaviour of Ca^{2+} and Sr^{2+} during above mentioned liberation and immobilization processes. However, the measured $^{87}Sr/^{86}Sr$ ratios are within the typical range for mantle derived mafic rocks from 0.703 and 0.706 (Faure and Mensing, 2005). The $^{87}Sr/^{86}Sr$ ratio of locally occurring LT and HT basalts ranges from 0.7030 to 0.7043, respectively (Pik et al., 1999) and the adjacent flood basalt provinces have $^{87}Sr/^{86}Sr$ ratios up to 0.706 (Yemen; Backer et al., 1996) and 0.707 (Djibouti; Vidal et. al., 1991). In principle, the release of $^{87}Sr/^{86}Sr$ due to weathering of silicate rocks depends on the individual weathering behaviour of solids with distinct Sr isotope ratios (e.g. Brantley et al., 1998; Bain and Bacon**,** 1994; Cartwright et al., 2007; Shand et al., 2009). For young basalt areas weathering of minerals produces insignificant differences in Sr isotope ratios in water-rock interactions (e.g. Chadwick et al., 2009; Raiber et al., 2009; Shand et al., 2009). This is because the radiogenic production of ^{87}Sr is limited due to very low Rb/Sr ratios and relatively short decay times of ^{87}Rb in the present basalt. The weathering rates of basalts are rapid and major minerals as well as glassy components contain rather homogeneous isotope distribution since the time scale of solidification was very short (e.g. Chadwick et al., 2009). Therefore, the

variations in $^{87}Sr/^{86}Sr$ isotope ratios of groundwaters caused by natural radioactive decay are negligible and the analysed $^{87}Sr/^{86}Sr$ range indicates clearly weathering of basaltic aquifer.

$^{87}Sr/^{86}Sr$ isotope ratios may also suggest a mixed input from underlying basement rocks. Miller et al. (2009) reported the $^{87}Sr/^{86}Sr$ ratios of metavolcanoes and metasediments from the basement between 0.7047 and 0.7063 and Tadesse et al. (2000) determined $^{87}Sr/^{86}Sr = 0.7057$ for a syn-tectonic granitoid. Thus the variations in aqueous $^{87}Sr/^{86}Sr$ can be related to differences in initial sources and mineralogical changes along flow paths as well as to respective reactivity and residence times of the groundwater concerning basalt rocks and the basement.

7.5. Stable isotopes distribution in dissolved sulfate

Sulfate ions in the groundwater could originate from various sources including dissolution of sulfate minerals, oxidation of sulfide minerals and anthropogenic source. Sulfate concentrations in the groundwater are low and vary widely from below 1 to 133 mg l^{-1} with a mean value of 32 mg l^{-1}. The highest SO_4^{2-} concentration is found in high mineralized groundwater with low oxygen content. The predominance of SO_4^{2-} concentration in the anaerobic part of the aquifer is associated with high concentrations of Fe. In order to gain further insight into the process, the stable sulphur isotopic composition of dissolved SO_4^{2-} were determined.

The $\delta^{34}S$ values of aqueous sulfate from the sampled wells exhibit a considerable variation (Fig. 20). Sulfate in the investigated groundwater samples is characterized by positive $\delta^{34}S$ values ranging between 6 and 19 ‰ VCDT. No SO_4^{2-} bearing evaporate has been reported from the area. However, the range of isotopic values can reflect a variety of mechanisms for sulfur isotope fractionation depending on environmental factors (Toran and Harris 1989).

The most likely source of sulfate in the groundwater is the oxidation of volcanic sulfur species (SO_2 and H_2S). Sulfides from igneous rocks typically have $\delta^{34}S$ values from –10 to 10‰ with an average of ~0‰ (Thode, 1991). The $\delta^{34}S$ of sulphate from the majority of groundwater samples lies between 6 and 13 ‰ which is roughly match up with the $\delta^{34}S$ values from 1.8 to 9 ‰ for volcanic rock samples of the area (Gebreslassie, 2009). Apparently, the slightly variation of $\delta^{34}S$ of the groundwater samples than volcanic rock samples suggests that the isotopic composition can be influenced by other processes. Bacterial sulfate reduction is a relevant factor for the

enrichment of $\delta^{34}S$ because bacteria consume $^{32}SO_4$ in preference to $^{34}SO_4$ during sulfate reduction leading to the gradually ascend of $\delta^{34}S$ values as reduction proceeds (Canfield 2001; Brunner and Bernasconi 2005). Thus, high $\delta^{34}S$ value of +19 ‰ could indicate sulfate reduction. The occurrence of bacterial sulfate reduction process locally and possible reoxidation of sulfide that return isotopically light sulfur to solution is essential process controlling the isotopic composition. Both oxidation and reduction of sulfur can take place along a flowpaths (Mukherjee and Fryar, 2008). Hence, the relationship between the SO_4^{2-} content and $\delta^{34}S$ value (Fig. 20) is not always explained by sulfate reduction alone.

Given the elevated contents of Fe and SO_4^{2-} in the anaerobic zone of the aquifer (see sample AW16), it is possible that the dissolved Fe(II) will react with reduced sulfur species present in the water to form Fe-sulfide minerals that latter oxidized (Appelo and Postma, 2005).

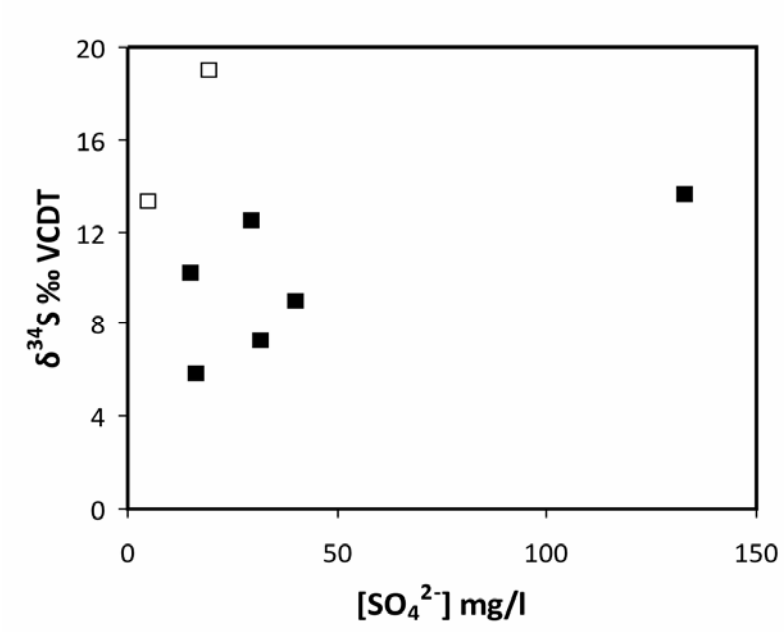

Fig. 20. $\delta^{34}S$ variation vs. SO_4^{2-} concentration for selected deep wells (■) and shallow wells (□).

8. Geochemical modelling and hydrogeochemical evolution

8.1. Mineral-solution equilibria

Speciation and saturation calculations were performed for the groundwater using *PHREEQC* geochemical model (Parkhurst & Appelo 1999) for minerals contributing to water chemistry according to Eq. (11). Mineral-solution equilibria calculations are useful in predicting the thermodynamic tendency of a mineral to be dissolved or precipitated in a groundwater system (Deutsch, 1997).

Most of the groundwaters are saturated or are very close to saturation with respect to carbonate minerals such as calcite, dolomite, and siderite. Speciation calculations conducted (see Section 2.3) suggests that calcite could be precipitating from groundwater due to ongoing CO_2 degassing. In addition, the progressively increasing in Ca^{2+} and HCO_3^- concentrations owing to increased water-rock interaction would ultimately result in saturation with respect to calcite. In contrast, the modelling also predicts that all sampled solutions are undersaturated with respect to sulfates such as gypsum and anhydrite related to the absence of sulfate bearing mineral in the aquifer (Fig. 21).

The thermodynamic saturation states and mineralogical evidences indicate that the elevated concentrations of cations and silica in the CO_2-rich (originated from volcanic source) are undoubtedly the result of enhanced dissolution of silicate minerals in basaltic aquifer. The chemical evolution is the result of weathering of primary aluminosilicate minerals leading to the formation and precipitation of carbonate and clay minerals..

Besides cations, silicic acid is transferred into the groundwater by silicate weathering. The current $Si(OH)_4$ concentration of a groundwater depends on mineral assemblages, solution chemistry, weathering rates and immobilization of $Si(OH)_4$ by formation of secondary silicate and adsorption phenomena (e.g. Appello and Postma, 2005). However, the analysed groundwaters in the Axum area display highest concentrations of silicic acid especially in deep groundwater with elevated DIC up to 40 mmol l^{-1} (e.g. 0.79 and 0.83 mmol l^{-1} of $Si(OH)_4$ in solutions AW7 and AW19, respectively; see Appendix III) versus shallow groundwater with [DIC] ≤ 11 mmol l^{-1} and a mean $[Si(OH)_4]$ = 0.38 ±0.12 mmol l^{-1}. All groundwaters, except the spring water AW1, are supersaturated with respect to quartz (solubility of 0.18 mmol l^{-1} $Si(OH)_4$ at 25°C; Rimstidt,

1997; see also $SI_{quartz} > 0$), but undersaturated with respect to amorphous silica (solubility of 1.9 mmol l^{-1} $Si(OH)_4$ at 25°C; Rimstidt and Barnes, 1980). Nevertheless, quartz has little control on silica concentration in solution. Highest [$Si(OH)_4$] values are reached in CO_2-rich deep groundwater, where silicic acid content suggests prolonged water-rock interaction, in spite of all uncertainties due to the secondary silica fixation e.g. by leached layer formation and neoformation of silicates.

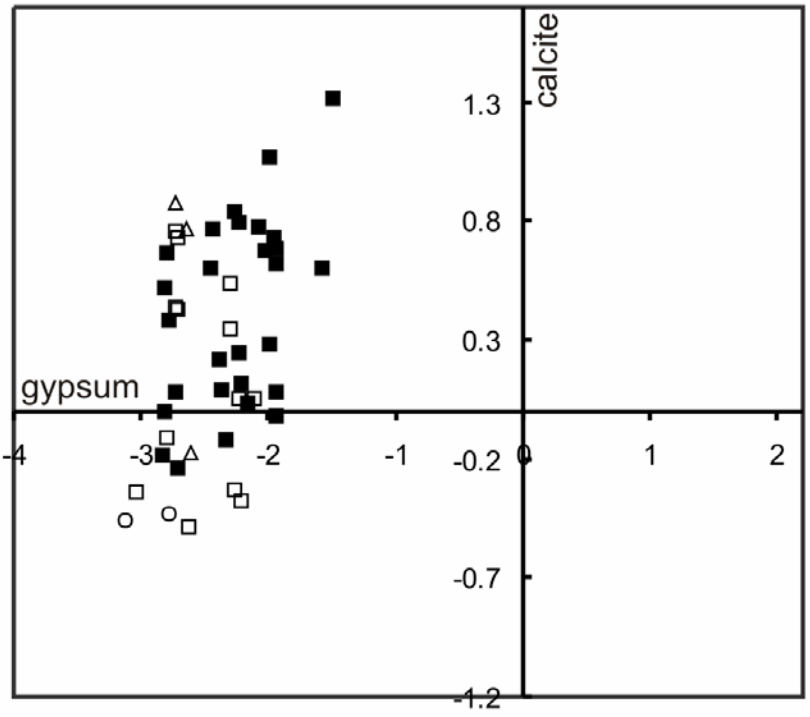

Fig. 21. Saturation indexes of calcite and gypsum from deep wells (■) and shallow wells (□), spring water (Δ) and surface water (o) of the Axum area.

The thermochemically stable minerals within an aqueous phase can be determined using mineral stability diagrams. Despite of the simplifications, the stability diagram are useful to decipher the chemical composition of the aqueous solution with that of the mineral phases in equilibrium. The stability diagrams assume equilibrium between the aqueous and mineral phases. In Figs. 22A and B the chemical composition of all sampled solutions are plotted within the predominant areas for relevant solids in the $CaO-Al_2O_3-SiO_2-H_2O$ and $Na_2O-Al_2O_3-SiO_2-H_2O$ system, respectively. For both systems the solution chemistry of the analysed groundwater plots in the field of kaolinite or close to the equilibrium line between kaolinite and montmorillonite suggesting they are the secondary minerals formed by the weathering of basaltic rocks. Thus, weathering of primary

silicates like plagioclase is an ongoing process to form secondary silicates like kaolinite and montmorillonite. Predominant areas of anorthite or albite can be reached by rise in pH and/or $[Ca^{2+}]$ or $[Na^{+}]$, respectively.

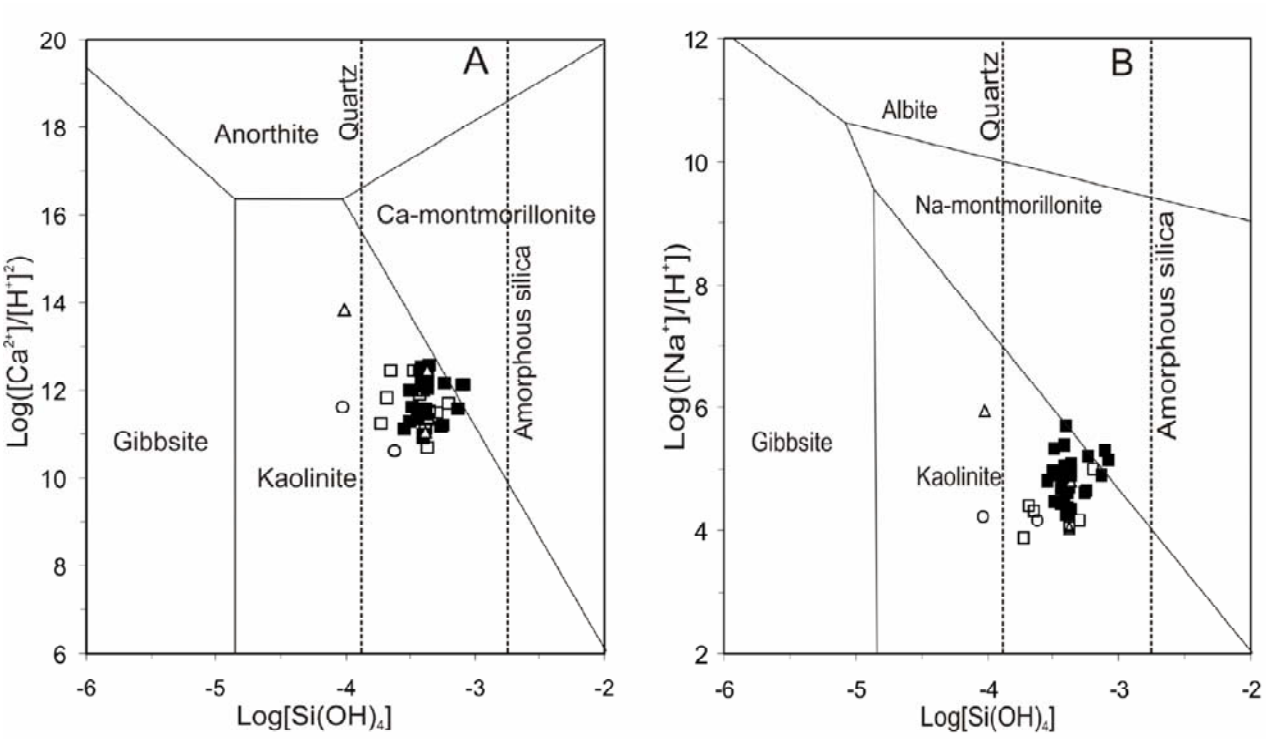

Fig. 22. Predominant phase diagram for Na_2O-Al_2O_3-SiO_2-H_2O (A) and CaO-Al_2O3-SiO_2-H_2O system (B), wherein the chemical compositions of the sampled solutions from the Axum area are plotted. Solubility constants from Tardy (1971) were used for construction (25°C and 1 atm). Symbols are given in Fig. 19.

The rocks in Axum have abundant plagioclase and clays and it seems reasonable to assume that slow weathering rates of silicate minerals may favour kaolinite rather than montmorillonite as the weathering product depends on hydrological conditions as well as weathering rate (Tardy 1971). In several deep groundwaters, kaolinite may be preferentially formed attributed to equilibrium between aluminosilicate minerals and kaolinite, as described by the reactions 23 and 24. But in response to further weathering, montmorillonite can be produced from kaolinite (Stumm and Morgan, 1996) by the following reactions

$$7Al_2Si_2O_5(OH)_4 + Ca^{2+} + 8H_4SiO_4 \rightarrow 6Ca_{0.16}Al_{2.33}Si_{3.67}O_{10}(OH)_2 + 2H^{+} + 23H_2O \qquad (28)$$

Similarly, albite weathering to smectite in the presence of, e.g. pyroxene is given in the Eq.

$$3NaAlSi_3O_8 + Mg^{2+} + 4H_2O \rightarrow 2Na_{0.5}Al_{1.5}Mg_{0.5}Si_4O_{10}(OH)_2 + 2Na^+ + Ha_4SiO_4 \quad (29)$$

The weathering of aluminosilicate to smectite consumes no protons (Appelo and Postma, 2005). However, it has to be pointed out that individual reaction between solids and aqueous solutions are complex, especially considering silicates like montmorillonite with highly variable chemistry and crystallinity as well as high adsorption and cation exchange capacities. Reactions involving dissolution-precipitation of basaltic rocks as well as adsorption and ion exchange related to clay minerals significantly influence the change in major ion composition of the groundwater. The secondary minerals (smectite clays, zeolites and calcite) precipitations also result in removal of calcium, iron and silica from the groundwaters.

8.2. Conceptual hydrogeochemical model

Developing a conceptual model is the first step to understand the reactions deriving the groundwater evolution. The work described here invokes the use of modelling for better understanding of hydrogeochemical processes. Schematic illustration depicts the different groundwater types and the interaction processes between groundwater and hosting rocks. The chemical characteristics of these groundwaters are the result of a chemical processes driven by the input of CO_2. The biogenic CO_2 input (derived from decay of organic matter) and inorganic volcanic CO_2 drives the weathering of silicates that controls the groundwater chemistry of the study area (Alemayehu et al., 2011).

The hydrochemical characteristics of shallow wells are mainly determined by weathering reactions of mostly soil-induced dissolution. Meteoric water infiltrates in groundwater at recharge zones of shallow aquifer with bicarbonate type water. A deep more saline groundwater is formed in the crystalline bedrock by water-rock interactions. The composition of groundwaters is interpreted in the light of the role of CO_2 flux from deep-seated source and its influence on the groundwater chemistry. The spatial distribution of major ions in Axum groundwater reveals a marked heterogeneity, which is likely to reflect uptake of CO_2 and extent of water-rock interaction. It is proposed that the processes giving rise to the chemistry of Axum groundwaters occur within the volcanic sequence is CO_2-induce weathering of silicates (Fig. 23). The geological and structural conditions of the study area could promote the release of CO_2 into the

groundwater. The occurrence and role of externally controlled PCO_2 in the groundwater can be verified using the analytical model.

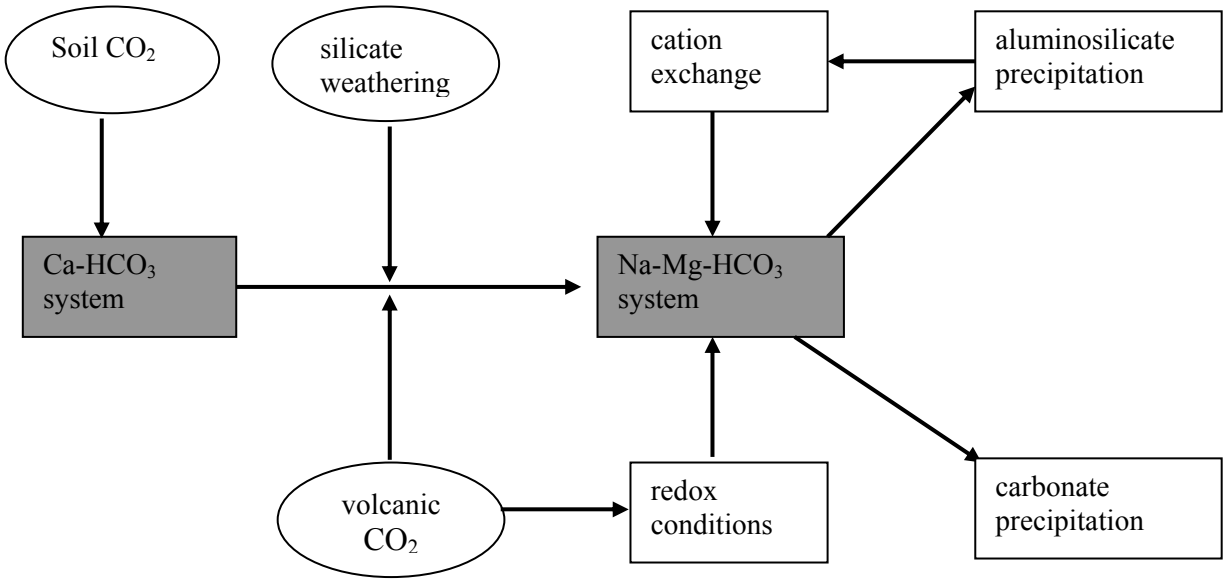

Fig. 23. Hydrogeochemical processes controlling the chemical characteristics of groundwater from Axum aquifer.

8.3. Inverse geochemical modelling

Inverse geochemical modelling was used to generate the evolution of the chemical composition of groundwater using chemical, mineralogical and gas data (Parkhurst, 1997; Hidalgo and Cruz-Sanjulian, 2001; Sharif et al., 2008). The mass-balance calculations were performed assuming open-system conditions with respect to CO_2. The precipitation/dissolution of potential phase was determined from general trends of chemical data and accounts for the changes in major-ion water chemistry between the initial and final waters along a virtual flowpath (Hidalgo and Cruz-Sanjulian, 2001; Sharif et al., 2008). The mass transfer along flow direction for two consequentive water points was considered. The shallow groundwater (well AW23) was assumed to represent a recharged solution, whereas groundwater from well AW16 denotes the final groundwater chemical composition (see Appendix VI). The two water points are chosen because of their defined hydraulic head difference with distance of 200 meters apart.

In the inverse geochemical modelling primary mineral phases constraint includes plagioclase, pyroxene, olivine, and k-feldspar. The uptake of carbon dioxide (gas) and hydrogen sulfide (gas)

are considered. Uptake of CO_2 from soil and volcanic origin was verified by isotopic data. The presence of H_2S gas was also noticed by the odour during sampling and its oxidation is assumed to account for sulfate concentration in the groundwater. Precipitation of calcite, kaolinite, Ca-montmorillonite, siderite and $Fe(OH)_3$, was considered once the solution reached respective supersaturation. The exchange reactions involving Na^+, Ca^{2+}, and Mg^{2+} on exchange sites were included in the model as a source for excess of Na^+ in the groundwater.

The results of mass transfer from solid phase into the solutions are shown in Table 1, where positive values indicate dissolution and negative values precipitation. Moreover, for Mg-Na and Ca-Na exchange, negative values indicate that Ca^{2+} and Mg^{2+} are absorbed by aquifer media and positive indicate that Na^+ enters groundwater where X is the exchanger. The reaction paths model indicates plausible pathways for the chemical evolution. These flowpaths were shown to have valid geochemical models for different scenarios (see Table M1, M2 and M3).

Table 1. The mole transfer of geochemical modelling for proposed reaction paths calculated using PHREEQC. The thermodynamic data of solid phases are taken from PHREEQC database (Parkhurst and Appelo, 1999). The amount of dissolved and precipitated minerals is expressed as mmol/kg water and individual chemical reactions assumed in the inverse modeling are given in Appendix VI.

Mineral phases	Reaction paths		
	M1	M2	M3
CO_2(g)	25.8	26.3	23.1
H_2S (g)	0.82	0.82	0.82
plagioclase An70	2.8	11.9	7.5
diopside	–	1.7	–
olivine	6.5	0.2	1.9
$Fe(OH)_3$(a)	-2.2	–	–
calcite	–	-5.1	-0.2
kaolinite	-2.7	–	–
montmorillonite	–	-8.9	-5.7
siderite	-4.1	–	-1.7
CaX2	–	-1.5	-1.5
NaX	5.7	2.9	4.3
MgX2	-2.8		

In the reaction path, e.g. M2, the mole transfer between the two water points are 11.9 mmol/kg H_2O, 1.7 mmol/kg H_2O and 0.2 mmol/kg H_2O for plagioclase, pyroxene and olivine, respectively. Significant amount of CO_2 uptake gas (+26.3 mmol/kg H_2O) leads to considerably increases in HCO^-_3 and at the same time calcite precipitates (−5.1 mmol/kg H_2O). Elevated Na^+ concentration in deep groundwaters is likely related to the ion exchange (Ca^{2+} and Mg^{2+} replacing Na^+ in smectite clays). The CaX_2 (–1.5 mmol/kg H_2O), i.e. Ca^{2+} is absorbed by exchanger site, and 2.9 mmol/kg H_2O of Na^+ enters into the solution. Thus the sharp increase of Na^+ concentration is also accounted for cation exchange reactions.

9. Conclusions

The present study has demonstrated that the application of hydrochemical characteristics together with multi-isotopic techniques enabled to constrain the groundwater chemical evolution in the volcanic dominated aquifers of the Axum area. It examined the dominant geochemical processes that control groundwater chemistry and distinguish the baseline major ion concentrations in contrast to anthropogenic impact.

The apparent incongruent weathering of basalts through hydrolysis of silicates and formation of secondary minerals, plus associated ion exchange reactions derives variation in groundwater chemistry. The major Axum aquifers consist of primarily plagioclase, clinopyroxene, olivine with minor amounts secondary minerals. Clay minerals (kaolinite and smectite clays, zeolites and calcite) influence the mobility of the elements through cation adsorption and ion-exchange reactions which further modify the water by enriching of Na^+.

Isotope data support the hypothesis that the dominant dissolved solids input is contributed from deep groundwater inflow. Stable isotopic composition of the water indicates that the groundwater of the Axum area is essentially of meteoric origin as they plot close to the local meteoric water line. However a slightly positive $\delta^{18}O$ shift refers to groundwater with highest PCO_2 $10^{-0.9}$ atm content documenting strong water-rock interaction that tend to increase the major ion concentrations. The geochemical trends can be established by $\delta^{13}C_{DIC}$ values which indicate flow paths of CO_2. In recharge areas where a significant soil zone is present, CO_2 can be generated by microbial oxidation of soil organic matter. Uptake of additional CO_2 derived from an inorganic deep supply of volcanic origin is evident from isotopically heavy value of $\delta^{13}C_{DIC}$ (+1 to -5‰). Given the high CO_2 content of deep groundwater from volcanic aquifer, it is suggested that pockets of CO_2 may occur within volcanic rocks and structural discontinuities promotes the migration of deep gases/fluids into the groundwater system.

The $^{87}Sr/^{86}Sr$ ratios of groundwater from 0.7038 to 0.7059 documented the weathering of basaltic rocks with possible mixing from basement. Beside the lengthy interaction of groundwater with basalts, the weathering rate controls the Sr concentration and $^{87}Sr/^{86}Sr$ ratios. The consumption of CO_2 was facilitated by the weathering of basaltic rocks leading to elevated cation concentrations

and progressively buffering the solutions. Inverse geochemical modelling validated silicate reactions at high CO_2 accompanied by precipitation secondary minerals and ion exchange results in change in groundwater chemistry.

Although most of the trace element concentrations are within the desirable of WHO (2004) limits, the major and minor ions composition in certain groundwater indicates that they are not suitable for drinking purpose. The presence of high concentration of NO_3^-, exceeding the permissible value of WHO, mostly at shallow depths pose a serious threat to the quality of the groundwater resources, and consequently to the public health. Reducing conditions prevail in the deep aquifers enhance the mobilization Fe^{2+} and Mn^{2+} in the groundwater. Nevertheless, the redox conditions alone cannot account for elevated elemental concentrations as they can be mobilized by CO_2-rich water due to increase mineral solubility. The sulfate concentration of the groundwater is general low except in CO_2-rich water sample suggesting a link with the upward leakage of volcanic origin mineralized waters along fracture zones.

10. Suggestions for further research

The following recommendations provide scientific contexts to future groundwater assessment plan by defining key research targets.

- The management approach for better groundwater quality supply is essentially based on monitoring, regulation and community awareness. The most appropriate means for controlling, for e.g. elevated nitrate content is to prevent the pollutant from source. Potential contaminant point sources such as livestock facilities or sewage disposal areas should be placed away from the wells to avoid groundwater contamination from surface. Follow up testing and monitoring of domestic wells should be carried out for potential changes in groundwater quality to ensure that the groundwater does not become degraded by land use changes, over-extraction and contamination.
- One of the major challenges in the study area is the occurrence of iron contents exceeding the desirable limit of WHO (2004). There are various existing methods to remove both soluble ferrous and insoluble ferric iron from the water. However, in-situ iron removal through injection of oxygenated water has proven to be a viable technique for removing the iron in groundwater (Appelo et al., 1999). Practically, dissolved iron can be removed from a solution by precipitating ferric hydroxide ($Fe(OH)_3$) or keeping the dissolved Fe in dissolved state by adding sequestering agent. Precipitation is usually done by oxidising it to the ferric form by making a contact with oxygen while keeping pH above 6. Another technique is to sequestered iron by adding sequestering agent to the water supply while the iron is in the ferrous state (dissolved form) to keep the iron in the clear water state. However; successful reduction of iron requires proper identification of iron, exchange and sorption of Fe^{2+} contact time, total hardness, pH, kinetics of oxidation, and iron bacteria. The processes can be model for in-situ removal of iron in groundwater. So further work should look at the operational flow of the above factors that make sure in-situ removal of Fe from groundwater more effective.
- The thesis has dealt with the groundwater chemical evolution of Axum. The groundwater dynamics and the potential productivity of the aquifer need to be studied for further groundwater development and management strategies of the region. The groundwater

potentiality of the area has to be assessed through integration of the models and making quantitative estimate of the groundwater resources through water balance. Developing geological or hydrogeological models that signify three-dimensional groundwater system is required in order to better represent the complexity of the groundwater systems. Therefore, further research should focus on improve understanding hydrogeology system and groundwater potential analysis to generate of potential groundwater zone to meet the population demand.

- The variation in the chemical of groundwater of Axum reflects the deep-sited source of carbon and sulfur contribution to the groundwater system. Geological structures play important role in the occurrence and movement of groundwater. So understanding and conceptualisation of groundwater dynamics through interconnected openings by transverse faults would greatly help to determine the connectivity of the aquifers to mantle release/ the Rift Valley that would supply volcanic origin gases. Further research need to be done to constraints depths of groundwater circulation, inter-basin relationship, groundwater flow dynamics and continuity faults and tectonic structures responsible for facilitating groundwater movement along transects.
- Future work should involve determination of the residence time of the groundwater using tritium content or ^{14}C. It would be important tool in understanding groundwater dynamics and age in similar geological settings.

References

Abay Engineering, 2006. The hydrogeological study of Axum Town Water Supply Project 107 pp.

Aiken, G.R., Kaplan, L.A., Weishaar, J., 2002. Assessment of relative accuracy in the determination of organic matter concentrations in aquatic systems. Journal of Environmental Monitoring 4, 70-74.

Alemayehu, T., Dietzel, M., Leis, A., 2010. Evolution of groundwater in volcanic aquifer of Axum, Ethiopia: Isotopic and hydrochemical evidence. In: Birkle, P., Torres-Alvarado I.S. (Eds), Water-Rock Interaction XIII. Proceedings of the 13th International Conference on Water-Rock Interaction (WRI-13), Guanajuato, Mexico, 16–20 August 2010.– 47–50, London (CRC Press, Taylor & Francis Group).

Alemayehu, T., Leis, A., Eisenhauer, A., Dietzel, M., 2011. Multi-proxy approach ($^{2}H/H$, $^{18}O/^{16}O$, $^{13}C/^{12}C$ and $^{87}Sr/^{86}Sr$) for the evolution of carbonate-rich groundwater in basalt dominated aquifer of Axum area, Northern Ethiopia- Chemie Erde-Geochemistry- in press

Allison, G.B., 1982. The relationship between ^{18}O and deuterium in water in sand columns undergoing evaporation. Journal Hydrology 55, 163–169.

Amiotte-Suchet P., Aubert, D., Probst, J. L., Gauthier-Lafaye, F., Probst, A., Andreux, F., and Viville D., 1999. $\delta^{13}C$ pattern of dissolved inorganic carbon in a small granitic catchment: the Strengbach case study (Vosges mountains, France). Chemical Geology 159, 129–145.

Appelo, C.A.J., Postma, D., 2005. Geochemistry, groundwater and pollution, 2nd edition, A.A. Balkema publishers, Rotterdam.

Appelo, C.A. J., Drijver, B., Hekkenberg, R., de Jonge, M.**,** 1999. Modeling in situ iron removal from groundwater. Groundwater 37, 811–817.

Asrat, A., 2002.The rock-hewn churches of Tigrai, Northern Ethiopia: A geological perspective. Geoarchaeology 17, 649–663.

Ayenew, T., Kebede, S., Alemyahu, T., 2007. Environmental isotopes and hydrochemical study as applied to surface water and groundwater interaction in the Awash River basin. Hydrological Processes 8**,** 1548–1563.

Ayenew, T., Molla, D., Wohnlich, S., 2008. Hydrogeological framework and occurrence of groundwater in the Ethiopian aquifers. Journal of African Earth Sciences 52, 97–113.

Atekwana, E.A., Krishnamurthy, R.V., 1998. Seasonal variations of dissolved inorganic carbon and ^{13}C of surface waters: application of a modified gas evolution technique. Journal of Hydrology 205, 265–278.

Avigad, D., Stern, R.J., Beythc, M., Miller, M., McWilliams, O., 2007. Detrital zircon U–Pb geochronology of Cryogen N.ian diamictites and Lower Paleozoic sandstone in Ethiopia (Tigrai): Age constraints on Neoproterozoic glaciation and crustal evolution of the southern Arabian–Nubian Shield. Precambrian Research 154, 88–106.

Bain, D.C., Bacon, J.R., 1994. Strontium isotopes as indicators of mineral weathering in catchments. Catena 22, 201–214.

Barnes, C. J., Allison, G. B., 1988. Tracing of water movement in the unsaturated zone using stable isotopes of Hydrogeology and oxygen. Journal of Hydrology 100, 143–176.

Baker, J., Thirlwall, M., Menzies, M.A., 1996. Sr–Nd–Pb isotopic and trace element evidence for crustal contamination of plume-derived flood basalts: Oligocene flood volcanism in western Yemen. Geochim. Cosmochim. Acta 60, 2559–2581.

Beccaluva, L., Bianchini, G., Natali, C., Siena, F., 2009. Continental flood basalts and mantle plumes: a case study of the Northern Ethiopian Plateau. Journal of Petrology 50, 1377–1403.

Bertrand, G., Celle-Jeanton, H., Huneau, F., Loock, S., Renac, C., 2010. Identification of different groundwater flowpaths within volcanic aquifers using natural tracers for the evaluation of the influence of lava flows morphology (Argnat basin, Chaîne des Puys, France). Journal of Hydrology 391, 223–234.

Bowser, C.J. Jones, B.F., 1990. Geochemical constraints on groundwaters dominated by silicate hydrolysis: An interactive spreadsheet, Mass Balance Approach; Chem. Geol., 84, 33–35.

Böttcher, M.E., Schnetger, B., 2004. Direct measurement of the content and isotopic composition of sulfur in black shales by means of combustion-isotope-ratio-monitoring mass spectrometry (C-irmMS). In: de Groot, P. (Ed.), Handbook of Stable Isotope Analytical Techniques: Amsterdam (Elsevier), 597–603.

Brantley, S.L., Chesley, J.T., Stillings**,** L.L., 1998. Isotopic ratios and release rates of strontium measured from weathering feldspars. Geochim. Cosmochim. Acta 62, 1493**–**1500.

Brunner, B., Bernasconi, S.M., 2005. A revised isotope fractionation model for dissimilatory sulfate reduction in sulfate reducing bacteria. Geochim. Cosmochim. Acta 69, 4759–4771.

Canfield, D.E., 2001. Isotope fractionation by natural populations of sulfate-reducing bacteria. Geochim. Cosmochim. Acta 65, 1117–1124.

Cartwright, I., Weaver, T., Tweed, S., Ahearne, D., Cooper, M., Czapnik, K., Tranter, J., 2002. Stable isotope geochemistry of cold CO_2-bearing mineral spring waters, Daylesford, Victoria, Australia: sources of gas and water and links with waning volcanism. Chem. Geol. 185, 71–91.

Cartwright, I., Weaver, T., Petrides, B., 2007. Controls on $^{87}Sr/^{86}Sr$ ratios of groundwater in silicate-dominated aquifers: SE Murray Basin, Australia. Chemical Geology 246, 107–123.

Chadwick, O.A., Derry, L.A., Bern, C.R., Vitousek, P.M., 2009. Changing sources of strontium to soils and ecosystems across the Hawaiian Islands. Chemical Geology 267, 64**–**76.

Christidis, G. E., 1998. Comparative study of the mobility of major and trace elements during alteration of an andesite and a rhyolite to bentonite, in the islands of Milos and Kimolos, Aegean, Greece. Clays and Clay Minerals 46, 379**–**399**.**

Clark, I.D., Fritz, P., 1997. Environmental isotopes in hydrogeology. Lewis Publisher, New York.

Cornell, R.M., Schwertmann, U., 1996. The iron oxides: Structure, reactions, occurrences and use. VCH, New York.

Craig, H., 1961. Isotopic variations in meteoric waters. Science 133, 1702–1703.

Dafny, E., Burg, A., Gvirtzman, H., 2006. Deduction of groundwater flow regime in a basaltic aquifer using geochemical and isotopic data: The Golan Heights, Israel case study. Journal of Hydrology 330, 506–524.

D'Andrea, A. C., Manzo, A., Harrower, M. J., Hawkins, A L., 2008. The Pre-Aksumite and Aksumite settlement of NE Tigrai, Ethiopia. Journal of Field Archaeology 33, 151–176.

Demlie, M., Wohnlich S., Ayenew, T., 2008. Major ion hydrochemistry and environmental isotope signatures as a tool in assessing groundwater occurrence and its dynamics in a fractured volcanic aquifer system located within a heavily urbanized catchment, central Ethiopia. Journal of Hydrology 353, 175–188.

Deutsch, W.J., 1997. Groundwater Geochemistry: Fundamentals and application to contamination. Lewis publishers, New York.

Devecon Engineers and Architects, 1995. Water supply and sanitation study of Axum, Ministry of Water Resources, unpublished report.

Dietzel M., Kirchhoff, T., 2002. Stable isotope ratios and the evolution of acidulous groundwater. Aquatic Geochemistry 8, 229–254.

Doctor, D.H., Kendall, C., Sebestyen, S.D., Shanley, J.B., Ohte, N., Boyer, E.W., 2008. Carbon isotope fractionation of dissolved inorganic carbon (DIC) due to outgassing of carbon dioxide from ahead water stream. Hydrological Processes 22, 2410–2423.

Edmunds, W. M., Carrillo-Rivera, J. J., Cardona, A., 2002. Geochemical evolution of groundwater beneath, Mexico City. Journal of Hydrology 254, 1–24.

Eggleton, R. A., Foudoulis C., Varkevisser, D., 1987. Weathering of Basalt: Change in rock chemistry and mineralogy. Clays and Clay Minerals 35, 161–169.

Elango, L., Kannan, R., 2007. Rock-water interaction and its control on chemical composition of groundwater, In: Sarkar, D., Datta, R., Hannigan, R., (Eds.), Concepts and applications in environmental geochemistry, Elsevier Science, pp. 229–246.

Epstein, S., Mayeda, T., 1953. Variation of O^{18} content of waters from natural sources. Geochim. Cosmochim. Acta 4, 213–224.

Ethiopian Health and Nutrition research Institute and Drug Administration and Control Authority (EHNRI/DACA), 2006. Laboratory and epidemiological investigation into the cause of unspecified liver disease in Tseda Amba Village, Tahtay Keraro Woreda, Tigray.

EWE, (German Water Engineering GmbH) 1973. Eight towns water supply project. Engineering report of Axum. Ministry of Interior Municipalities Department, Addis Ababa, Ethiopia

Faure, G., Mensing, T.M., 2005. Isotopes: Principles and Applications. 3rd Edition. John Wiley and Sons, New York.

Federico, C., Aiuppa, A., Allard, P., Bellomo, S., Jean-Baptiste, P., Parello, F., Valenza, M., 2002. Magma-derived gas influx and water-rock interactions in the volcanic aquifer of Mt. Vesuvius, Italy. Geochim. Cosmochim. Acta 66, 963–981.

Fietzke, J., Eisenhauer, A.,2006. Determination of temperature-dependent stable strontium isotopes ($^{88}Sr/^{86}Sr$) fractionation via bracketing standard MC-ICP-MS, Geochemistry Geophysics Geosystems **7**.

Flaathen, T.K., Gislason, S.R., Oelkers, E.H., Sveinbjörnsdóttir, Á.E., 2009. Chemical evolution of the Mt. Hekla, Iceland, groundwaters: A natural analogue for CO_2 sequestration in basaltic rocks. Applied Geochemistry 24, 463–474.

Frape, S.K., Fritz, P., McNutt, R.H., 1984. Water-rock interaction and chemistry of groundwaters from the Canadian Shield. Geochim. Cosmochim. Acta 48, 1617–1627.

Fridriksson, T., Arnórsson, S., Bird, D.K., 2009. Processes controlling Sr in surface and ground waters of Tertiary tholeiitic flood basalts in Northern Iceland. Geochim. Cosmochim. Acta 73, 6727–6746.

Gat, J.R., Dansgaard, W., 1972. Stable isotope survey of the freshwater occurrences in Israel and the Jordan rift Valley. Journal of Hydrology 16**,** 177–211.

Gebresilassie, S., 2009. Nature and characteristics of metasedimentary rock hosted gold and base metal mineralization in the Workamba area, central Tigray, Northern Ethiopia, PhD thesis Ludwig-Maximilians University, Munich.

Getaneh, W., 2002. Geochemistry provenance and depositional tectonic setting of the Adigrat Sandstone northern Ethiopia. Journal of African Earth Sciences 35, 185–198.

Gislason, S.R., Wolff-Boenisch, D., Stefansson, A., Oelkers, E.H., Gunnlaugsson, E., Sigurdardottir, H., Sigfusson, B., Broecker, W.S., Matter, J.M., Stute, M., Axelsson, G., Fridriksson, T., 2010. Mineral sequestration of carbon dioxide in basalt: A pre-injection overview of the CarbFix project, International Journal of Greenhouse Gas Control 4, 537–545.

Godderis, Y., Roelandt, C., Schott, J., Pierret, M.C., Francois, L.M., 2009. Towards an integrated model of weathering, climate, and biospheric processes, In: Oelkers, E. H. Schott, J., (Eds.), Thermodynamics and Kinetics of Water-Rock Interaction, Mineralogical Soc Amer. 70, 411–434.

Hidalgo, M.C.-L., Cruz-Sanjulian, J., 2001. Groundwater composition, hydrochemical evolution and mass transfer in a regional detrital aquifer Baza basin, southern Spain. Appl. Geochem. 16, 745–758.

Hagos, M., Koeberl, C., Kabeto, K., Koller, F., 2010. Geochemical characteristics of the alkaline basalts and the phonolite-trachyte plugs of the Axum area, northern Ethiopian. Austrian Journal of Earth Sciences 103, 153-170

Hoefs, J., 1997. Stable isotope geochemistry. Springer-Verlag, Berlin.

Hofmann, C., Courtillot, V., Feraud, G., Rochette, P., Yirgu, G., Ketefo, E. and Pik, R. (1997). Timing of the Ethiopian flood basalt event and implications for plume birth and global change. Nature 389, 338-341.

Horita, J., Ueda, A., Mizukami, K., Takatori, I., 1989. Automatic δD and $\delta^{18}O$ analyses of multi-water samples using H_2- and CO_2-water equilibration methods with a common equilibration set-up. Applied Radiation and Isotopes 40, 801–805.

IAEA, 2008. Isotope Hydrology Information System, the ISOHIS Database. International Atomic Energy Agency, (available at: http://isohis.iaea.org).

Jin, L., Ogrinc, N., Hamilton, S.K., Szramek, K., Kanduc, T., Walter, L.M., 2009. Inorganic carbon isotope systematics in soil profiles undergoing silicate and carbonate weathering (Southern Michigan, USA). Chemical Geology 264, 139–153.

Kebede, S., Travi, Y., Alemayehu, T., Ayenew, T., 2005. Groundwater recharge, circulation and geochemical evolution in the source region of the Blue Nile River, Ethiopia. Applied Geochemistry 20, 1658–1676.

Kebede, S., Travi, Y., Asrat, A., Alemayehu, T., Ayenew, T., Tessema, Z., 2007. Groundwater origin and flow along selected transects in Ethiopian rift volcanic aquifers. Hydrogeology Journal 16**,** 55–73.

Kebede S., Travi Y., S. Stadler, 2010. Groundwaters of the Central Ethiopian Rift: diagnostic trends in trace elements, $\delta^{18}O$ and major elements. Environmental Earth Sciences 61, 1641–1655.

Kieffer, B. Arndt, N., Lapierre, H., Bastien, F., Bosch, D., Pecher, A., Yirgu, G., Ayalew, D., Weis, D., Jerram, D.A., Keller, F., Meugniot, C., (2004). The transition from Plateau to Shield volcanism in Ethiopia: a petrological and geochemical study of the Simien, Choke and Guguftu volcanoes and underlying flood basalts. Journal of Petrology, 45, 793-834.

Kim K 2002 Plagioclase weathering in a groundwater system of sandy, silicate aquifer. Hydrological Processes*,* 16, 1793–806.

Kumpulainen, R.A., Uchman, A., Woldehaimanot, B, Kreuser, T., Ghirmay, S., 2006. Trace fossil evidence from the Adigrat Sandstone for an Ordovician glaciation in Eritrea, NE Africa. Journal of African Earth Sciences 45, 408–420.

La Tour, T. E., 1989. Analysis of Rocks Using X-ray Fluorescence Spectrometry. The Rigaku Journal Vol. 6/ No. 1

Le Bas, M.L., Le Maitre, R.W., Streckeisen, A., Zanettin, B., 1986. A chemical classification of volcanic rocks based on the total alkali – silica diagram. Journal of Petrology 27, 745–750.

Massmann G. Tichomirowa M., Merz C. and Pekdeger A., 2003. Sulfide oxidation and sulfate reduction in a shallow groundwater system (Oderbruch Aquifer, Germany). Journal of Hydrology 278, 231-243

Miller, N., Stern, R.J., Avigad, D., Beyth M., Schilman, B., 2009. Cryogenian carbonate-slate sequences of the Tambien Group, N. Ethiopia: pre-"Sturtian" chemostratigraphy and regional correlations. Precambrian Research 170, 129–156.

Mook, W.G., Bommerson, J.C., Stavermann, W.H., 1974. Carbon isotope fractionation between dissolved bicarbonate and gaseous carbon dioxide. Earth Planet. Sci. Lett. 22, 169–176.

Morrison, J., Brockwell, T., Merren, T., Fourel, F., Philips, A.M., 2001. On-line high-precision stable hydrogen isotopic analyses on nanoliter water samples. Anal. Chem. 73, 3570–3575.

Mukherjee, A., Fryar, A. E., 2008. Deeper groundwater chemistry and geochemical modeling of the arsenic affected western Bengal basin, West Bengal, India. Applied Geochemistry 23, 863-894.

Nakayama, K., Kakamura, T, 2005. X-ray Fluorescence Analysis of Rare Earth Elements in Rocks Using Low Dilution Glass Beads.

Nesbitt, H. W., Young, G. M. 1984. Prediction of some weathering trends of plutonic and volcanic rocks based on thermodynamic and kinetic considerations. Geochim. Cosmochim. Acta 48, 1523–1534.

Parkhurst, D.L., 1997. Geochemical mole-balance modeling with uncertain data. Water Resources Research 33, 1957–1970.

Parkhurst, D.L., Appelo, C.A.J., 1999. User's guide to PHREEQC (version 2) –A computer program for speciation, batch-reaction, one-dimensional transport and inverse geochemical calculations. U. S. Geological Survey, Water-Resources Investigations Report 99–4259.

Peiffer, S., Klemm, O., Pecher, K., Hollerung, R., 1992. Redox measurements in aqueous solutions- A theoretical approach to data interpretation, based on electrode kinetics. Journal of Contaminant Hydrology 10, 1–18.

Pik, R., Deniel, C., Coulon, C., Yirgu, G., Hoffmann, C., Ayalew, D., 1998. The northwestern Ethiopian Plateau flood basalts: classification and spatial distribution of magma types. Journal of Volcanol. Geothem. Res. 81, 91–111.

Pik, R.E., Daniel, C., Coulon, C., Yirgu, G., Marty, B., 1999. Isotopic and trace element signatures of Ethiopian flood basalts: Evidence for plume–lithosphere interactions. Geochim. Cosmochim. Acta 63, 2263–2279.

Raiber, M., Webb, J.A., Bennetts, D.A., 2009. Strontium isotopes as tracers to delineate aquifer interactions and the influence of rainfall in the basalt plains of southeastern Australia. Journal of Hydrology 367, 188–199.

Rimstidt, J.D., 1997. Quartz solubility at low temperatures. Geochim. Cosmochim. Acta 61, 2553–2558.

Rimstidt, J.D., Barnes, H.L., 1980. The kinetics of silica-water reactions. Geochim. Cosmochim. Acta 44, 1683–1699.

Rozanski, K., Araguas-Araguas, L., Gonfiantini, R., 1996. Isotope patterns of precipitation in the East African region. In: Johnson, TC., Odada, E., (Eds.), The liminology, Climatology, and Paleoclimatology of the east African lakes. Gordon and Breach, Toronto, 79–93.

Rueedi J., Cronin A. A, Taylor R. G. and Morris B. L., 2007. Tracing sources of carbon in urban groundwater using $\delta^{13}C_{TDIC}$ ratios. Environmetal Geology 52, 541–557.

Schmid, T., Koch, M., DiBlasi, M.C., Hagos, M., 2008. Spatial and spectral analysis of soil surface properties for an archaeological area in Aksum, Ethiopia, applying high and medium resolution data. Catena 75, 93–101.

Schofield, S., Jankowski, J., 2004. Hydrochemistry and isotopic composition of Na–HCO_3 rich groundwaters from the Ballimore region, central New South Wales, Australia. Chemical Geology 211, 111–134.

Shand, P., Darbyshire, D.P.F., Love, A.J., Edmunds, W.M., 2009. Sr isotope in natural waters: Applications to source characterization and water-rock interaction in contrasting landscapes. Applied Geochemistry 24, 574–586.

Sharif, M.U., Davis, R.K., Steele, K.F., Kim, B., Kresse, T.M., Fazio, J.A., 2008a. Inverse geochemical modeling of groundwater evolution with emphasis on arsenic in the Mississippi River Valley alluvial aquifer, Arkansas, USA. J. Hydrol. 350, 41-55.

Singhal, B. B. S. and Gupta, R. P., 1999. Applied Hydrogeology of Fractured Rocks, Kluwer Academic Publishers, Dordrecht.

Slomp, C. P., Cappellen, P. V., 2004. Nutrient inputs to the coastal ocean through submarine groundwater discharge: controls and potential impact. Journal of Hydrology 295, 64-86

Srinivasamoorthy, K., Chidambaram, S., Prasanna, M. V., Vasanthavihar, M., Peter, J. Anandhan, P., 2008. Identification of major sources controlling groundwater chemistry from a hard rock terrain – A case study from Mettur taluk, Salem district, Tamil Nadu, India. Journal of Earth System Science. 117: 49–58.

Sheppard, S.M.F., 1986. Characterization of isotopic variations in natural waters. In: Valley, J.W., Taylor, H.P., O'Neil, J.R., (Eds.), Stable Isotopes in High-Temperature Geological Processes, Reviews in Mineralogy 16, Mineralogical Society of America, 165–184.

Spötl, C., 2005. A robust and fast method of sampling and analysis of $\delta^{13}C$ of dissolved inorganic carbon in ground waters. Isotopes in Environmental and Health Studies 41, 217–221.

Stetzenbach, K. J., Hodge, V. F., Guo, C., Farnham, I. M., Johannesson, K. H., 2001. Geochemical and statistical evidence of deep carbonate groundwater within overlying volcanic rock aquifers/aquitards of southern Nevada, USA. Journal of Hydrology 243, 254–271.

Stumm, W., Morgan, J.J., 1996. Aquatic Chemistry - Chemical Equilibria and Rates in Natural Waters. John Wiley and Sons, New York.

Tadesse-Alemu, A., 1998. Geochemistry of Neoproterozoic granitoids from the Axum area, northern Ethiopia. Journal of African Earth Sciences 27, 437–460.

Tadesse, T., Hoshino, M., Sawada, Y., 1999. Geochemistry of low-grade metavolcanic rocks from the Pan-African of the Axum Area, northern Ethiopia. Precambrian Research 99, 101–124.

Tadesse, T., Hoshino, M., Suzukp, K., Zumi, S., 2000. Sm-Nd, Rb-Sr and Th-U-Pb zircon ages of syn- and post-tectonic granitoids from the Axum area of northern Ethiopia. Journal of African Earth Sciences 30, 313–327.

Tang, J., Köhler, S.J., Dietzel, M., 2008. Sr^{2+}/Ca^{2+} and $^{44}Ca/^{40}Ca$ fractionation during inorganic calcite formation: I. Sr incorporation. Geochim. Cosmochim. Acta 72, 3718–3732.

Tardy, Y., 1971. Characterization of the principal weathering types by the geochemistry of waters from European and African crystalline massifs. Chemical Geology 7, 253–271.

Terwilliger, V.J., Eshetu, Z., Colman, A., Bekele, T., Gezahgne, A., Fogel, M.L., 2008. Reconstructing palaeoenvironment from $\delta^{13}C$ and $\delta^{15}N$ values of soil organic matter: a calibration from arid and wetter elevation transects in Ethiopia. Geoderma 147, 197–210.

Thode, H. G., 1991. Sulfur isotopes in nature and the environment: an overview. In: Krouse, H. R., Grinenko, V. A., (Eds), Stable Isotopes, Natural and Anthropogenic Sulfur in the Environment. 1–21, John Wiles & Sons.

Thode, H.G., Shima, M., Rees, C.E., Krishnamurty, K.V., 1965. Carbon-13 isotope effects in systems containing carbon dioxide, bicarbonate, carbonate and metal ions. Canadian Journal of Chemistry 43, 582–595.

Tilahun, K., Merkel, B. J., 2009. Assessment of groundwater vulnerability to pollution in Dire Dawa, Ethiopia using DRASTIC Environmental Earth Sciences 59, 1485–1496.

Toran, L. Harris, R. F., 1989. Interpretation of sulfur and oxygen isotopes in biological and abiological sulfide oxidation. Geochim. Cosmochim. Acta 53, 2341–2348.

Vidal, P., Deniel, C., Vellutini, P.J., Piguet, P., Coulon, C., Vincent, J., Audin, J., 1991. Changes of mantle source in the course of a rift evolution. Geophysical Research Letters 18, 1913–1916.

Vogel, J.C., 1993. Variability of carbon isotope fractionation during photosynthesis. In: Ehleringer, J.R., Hall, A.E., Farquhar, G.D., (Eds.), Stable Isotopes and Plant Carbon-Water Relations 29–46. Academic Press, San Diego.

Vogel, J.C., Grootes, P.M., Mook, W.G., 1970. Isotopic fractionation between gaseous and dissolved carbon dioxide. Z. Phys. 230, 225–238.

WHO, 2004. Guidelines for Drinking-Water Quality. Third Edition: Vol I – Recommendations. World Health Organization, Geneva.

Wiegand, B.A., 2009. Tracing effects of decalcification on solute sources in a shallow groundwater aquifer, NW Germany. Journal of Hydrology 378, 62–71.

White, A.F., Peterson, M.L., Solbau, R.D., 1991. Measurement and interpretation of low levels of dissolved oxygen *i*n ground water. Ground Water 28,584–590

Yidana, S.M., Ophori, D., Banoeng-Yakubo, B., 2007. Hydrogeological and hydrochemical characterization of the Voltaian Basin: the Afram Plains area, Ghana. Environmental Geology 53, 1213–1223.

Yoshimura, K., Nakao, S., Noto, M., Inokura, Y., Urata, K, Chen, M., Lin, P. W., 2001. Geochemical and stable isotope studies on natural water in the Taroko Gorge karst area, Taiwan–chemical weathering of carbonate rocks by deep source CO_2 and sulfuric acid. Chemical Geology 177, 415–430.

Zanettin, B., Bellieni, G., Visentin, E.J., 2006. Stratigraphy and evolution of the trachy-rhyolitic volcanism of the Senafe area (Eastern Eritrean Plateau). Journal of African Earth Sciences 45, 478–488.

Appendices

Appendix I. Whole-rock geochemical analysis

Appendix II. Mineralogical analysis

Appendix III. Hydrochemical analysis

Appendix IV. Trace elements analysis of water

Appendix V. Isotope geochemistry analysis

Appendix VI. Phreeqc input file

Appendix I

Whole-rock geochemical analysis-X-ray fluorescence

X-ray fluorescene (XRF) analysis provides the chemical composition of the bulk solids. The solid samples were initially grounded and dried at 110 °C for overnight to remove remaining moisture. Samples are usually prepared as glass discs for major element analyses and pressed powder pellets for trace-element analyses using a Philips MAGIX PRO spectrometer at the laboratory of Institute of Applied Geosciences, Graz University of Technology.

The rock samples were crushed using a jaw crusher with a stainless steel jaw crusher and then pulverized into powder by an agate mortar to produce fine particle size of no larger than 100 microns. This aliquot powder was weighed accurately and thoroughly mixed with lithium tetraborate flux ($Li_2B_40_7$) for the determination of major components (SiO_2, Al_2O_3, Fe_2O_3, TiO_2, CaO, MgO, K_2O, Na_2O and P_2O_5). Fused glass disks were created in such a way that constituent powder of 1g was mixed homogeneously with 6g diLithumbetraborat. This mixture was melted at 1030°C for 12 minutes and the molten sample poured into Pt-Au crucible and allows to quench for few minutes. The fused glass technique effectively homogenises the samples to get the representative analysis of the bulk samples. The method minimizes the mineralogical effects of the samples and produce a more accurate and precise analysis.

Trace-elements were determined using pressed powder pellets for higher resolution. The pellets were made by mixing of rock powder of 12g with pulviser wax of 3g and pressing the mixture at 20 tons pressure for 20 seconds. The finished pellet is uniform in composition, density, and mass per unit area, and has a smooth finish.

Major and trace element analyses for rocks from the Axum area.

Rock type	phonolite	phonolite	phonolite	phonolite	trachyte	trachyte	trachyte	basalt	basalt	basalt	basalt	siltstone	siltstone	siltstone
sample	**AR1**	**AR2**	**AR3**	**AR4**	**AR5**	**AR6**	**AR7**	**AR8**	**AR9**	**A10**	**A11**	**A12**	**A13**	**A14**
SiO_2	56.45	56.99	62.63	60.33	66.50	66.63	62.43	49.51	48.06	52.05	47.88	74.93	83.29	79.22
TiO_2	bdl	bdl	bdl	0.08	bdl	0.19	0.13	1.71	1.75	2.7	3.27	0.48	0.49	0.59
Al_2O_3	18.05	17.64	15.97	16.65	16.10	16.49	18.23	13.54	13.47	14.92	14.24	14.27	9.56	10.79
Fe_2O_3	6.53	6.76	5.81	6.09	3.66	2.95	5.15	11.3	10.84	13.64	15.07	3.51	2.25	4.18
MnO	0.34	0.39	0.53	0.37	0.28	bdl	0.32	0.12	0.30	0.15	0.32	bdl	bdl	bdl
MgO	0.20	0.17	0.12	bdl	bdl	bdl	bdl	5.57	5.86	1.08	3.64	bdl	bdl	bdl
CaO	1.55	1.14	0.57	1.43	0.36	0.46	bdl	10.01	12.74	4.49	7.82	0.09	bdl	bdl
Na_2O	8.34	9.37	7.74	8.35	5.71	6.68	7.55	2.36	2.33	3.89	3.27	0.08	0.06	0.06
K_2O	4.86	5.01	5.11	5.02	5.38	5.33	4.45	0.69	0.27	3.59	1.70	0.16	0.08	0.12
P_2O5	0.05	bdl	0.02	0.03	bdl	0.02	0.03	bdl	0.18	0.83	0.85	0.03	0.03	0.02
LOI	3.67	2.61	1.62	1.72	1.86	1.23	1.80	5.22	4.20	3.18	2.00	6.39	4.20	4.80
Sum	**100.0**	**100.1**	**100.1**	**100.1**	**99.9**	**100.0**	**100.1**	**100.0**	**100.0**	**100.0**	**100.1**	**99.9**	**100.0**	**99.8**
						Trace element (ppm)								
Sc	2.1	2.2	3.4	4.5	2.4	0.7	1.2	30.0	30.4	18.1	24.9	9.0	9.3	5.7
V	0.9	5.5	1.7	0.8	3.3	trace	2.3	249.7	237.8	161.2	235.1	67.7	27.1	57.1
Cr	97.9	211.4	17.1	120.4	5.4	17.0	0.9	175.0	200.5	28.6	152.2	50.2	29.2	176.8
Co	trace	3.1	trace	1.5	trace	trace	2.6	45.2	39.0	11.3	38.5	1.8	2.0	5.7
Ni	33.9	67.2	9.2	41.3	5.4	8.4	11.4	75.2	84.7	20.5	60.1	14.2	9.8	39.1
Cu	11.3	14.1	8.7	12.6	14.6	7.2	13.4	63.3	93.1	30.0	36.2	40.2	12.8	10.4
Zn	271.8	259.3	251.4	168.2	116.7	91.6	217.1	78.5	80.0	117.3	126.0	9.8	10.3	5.3
Ga	48.4	49.5	45.6	37.0	27.7	38.5	32.4	18.1	17.5	21.2	20.5	12.9	8.1	10.4
Ge	1.7	1.9	1.7	1.4	0.9	1.5	1.4	0.2	0.1	0.6	bdl	0.4	0.3	0.5
As	29.5	29.5	25.7	27.4	24.4	22.5	22.4	24.7	26.7	29.2	31.4	18.1	15.6	16.4
Se	4.5	4.2	4.0	3.4	3.3	3.4	3.2	4.0	3.5	4.4	4.6	2.0	1.9	2.7
Br	6.8	10.1	4.5	5.5	4.1	3.7	4.0	5.0	5.5	6.9	6.6	3.1	3.5	3.7

Rb	268.5	279.8	396.1	215.5	208.7	233.6	129.2	12.6	7.1	54.5	35.1	3.9	2.0	3.4
Sr	236.6	55.6	15.8	45.8	30.5	10.8	14.1	351.2	342.0	526.9	707.5	92.6	64.8	79.1
Y	154.6	122.4	94.2	80.6	42.3	73.1	55.8	24.0	25.0	44.5	44.5	4.1	4.6	3.5
Zr	1342.2	1360.8	2006.6	1041.2	503.5	488.6	1522.4	126.3	126.4	518.6	338.2	137.7	155.8	210.1
Nb	246.2	256.2	331.8	182.6	144.4	197.0	188.0	7.0	7.2	21.6	19.6	4.5	3.7	6.0
Mo	18.7	16.4	1.0	6.6	3.2	3.0	5.1	1.0	2.5	1.9	4.8	0.8	0.1	2.9
Ag	9.6	7.7	7.4	6.6	4.5	8.2	9.0	12.0	11.3	9.3	12.6	5.0	7.2	4.5
Cd	9.1	9.0	6.4	5.4	5.3	8.0	5.9	6.8	7.5	6.0	7.8	5.8	6.1	4.9
Sn	8.8	8.8	13.8	7.6	8.2	8.0	7.6	1.4	bdl	2.3	0.9	1.5	3.9	2.3
Ba	296.6	122.4	bdl	bdl	201.8	0.3	180.5	96.7	392.8	1005.1	776.1	31.5	bdl	424.9
La	332.6	263.4	275.1	133.6	92.7	180.5	108.5	22.4	17.9	64.6	62.2	13.1	21.8	12.9
Ce	376.7	432.3	406.0	262.1	153.2	240.0	208.4	27.4	27.9	102.3	101.8	11.9	36.7	16.4
Nd	212.1	182.3	146.2	92.6	52.8	115.2	62.7	16.8	12.6	68.0	57.1	7.8	5.3	2.2
Sm	29.9	26.7	30.5	22.2	10.0	21.0	6.5	bdl	12.2	12.8	0.2	4.7	bdl	bdl
Yb	7.1	5.9	9.8	3.1	1.0	7.0	2.2	bdl	bdl	bdl	bdl	bdl	bdl	bdl
Hf	27.5	26.3	37.4	16.7	14.3	13.4	24.4	1.2	3.4	11.6	8.1	3.7	3.2	3.9
Ta	15.0	17.9	24.2	8.5	10.8	12.3	8.0	bdl	bdl	bdl	0.0	bdl	bdl	bdl
W	9.4	10.1	7.5	6.5	7.2	6.9	7.8	1.8	0.8	1.1	0.0	bdl	bdl	bdl
Ti	11.6	11.1	9.7	11.4	9.2	9.6	9.5	12.8	13.7	14.5	16.8	7.7	7.6	7.8
Pb	22.5	22.0	30.9	14.2	21.4	17.2	5.6	bdl	1.1	8.0	4.5	5.4	3.8	9.0
Bi	5.5	5.3	4.6	4.5	4.0	3.8	4.1	5.6	4.6	6.4	7.1	2.8	2.1	2.7
Th	32.7	30.8	50.6	24.0	20.5	26.5	20.1	3.5	3.2	4.5	4.3	4.6	3.6	2.8

bdl: below detection limit

Appendix II

Mineralogical analysis by X-ray diffraction

The mineralogical analysis was carried out by XRD PANalytical X'Pert Pro series diffractometer equipped with a cobalt-target tube anticathode. XRD pattern provides mineral identification, particularly for fine grained minerals that can not be easily studied by optical microscope. Mineral phases were identified by comparing diffraction patterns with standards. Therefore, the computer program X'pert Highscore Plus with database ICDD (International Center for diffraction Data) was used.

Sample preparation

The rock samples were crushed using a jaw crusher with a stainless steel jaw crusher and then pulverized into powder by an agate mortar to produce fine particle size of no larger than 100 microns. The pulverized samples were pressed at a pressure of 7 tons weight of load to make a compact sample with correct height and smooth surface.

Mineralogical composition of the rocks from Axum

	Basalt	Phonolite-trachyte	Quaternary sediment*	Sandstone/siltstone
Major minerals	plagioclase, clinopyroxene olivine K-feldspar	plagioclase K-feldspar quartz nepheline	quartz, Na-rich plagioclase K- feldspar	quartz K-feldspar
Minor minerals	kaolinite smectite chlorite	analcim phillipsite nosean chlorite	smectite kaolinite illite, chlorite calcite and dolomite	kaolinite Fe-Mn-oxide

* Schmid, et al. (2008)

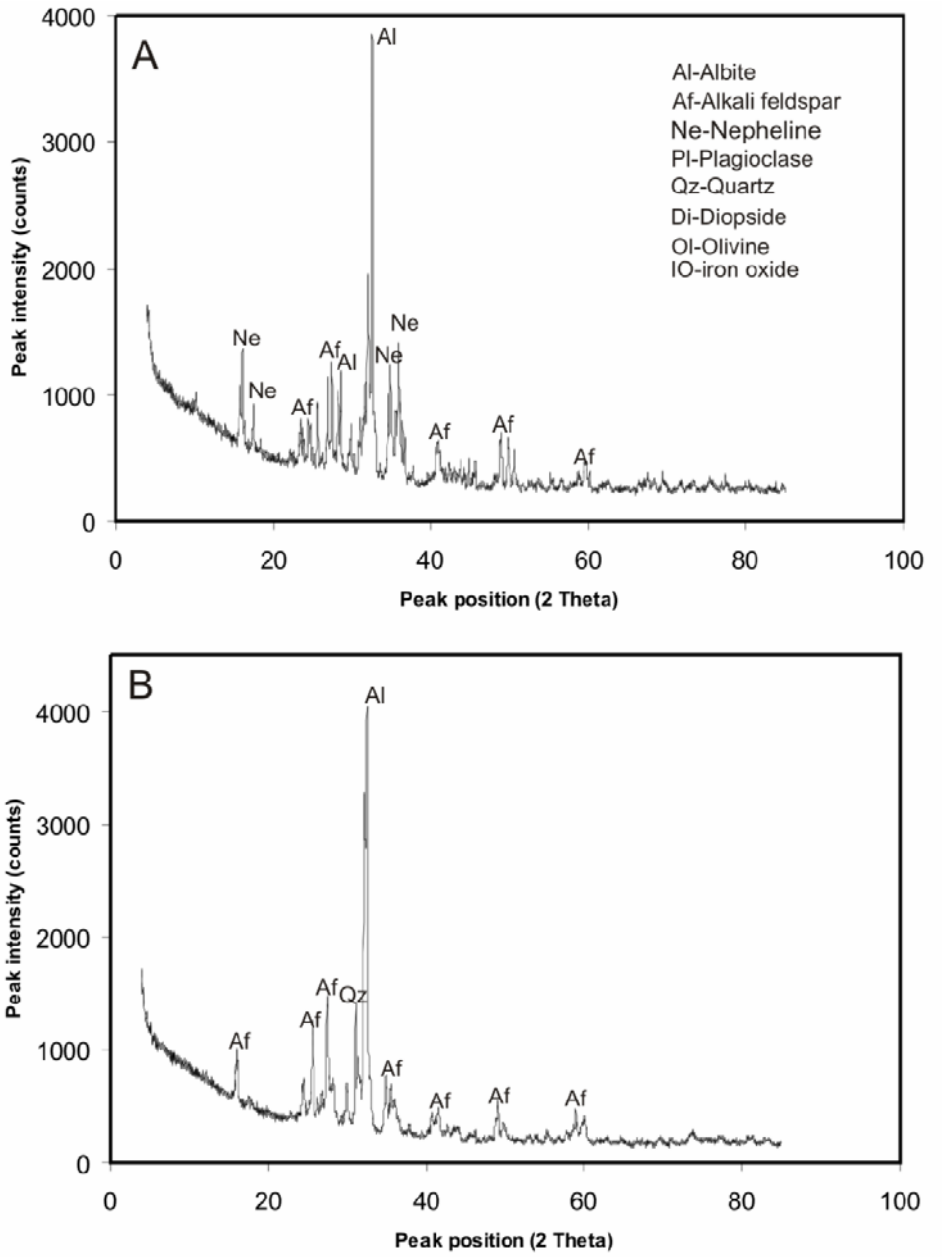

Appendix 2a.Characteristic XRD pattern of rocks from the study area (A) Phonolite (B) Trachyte

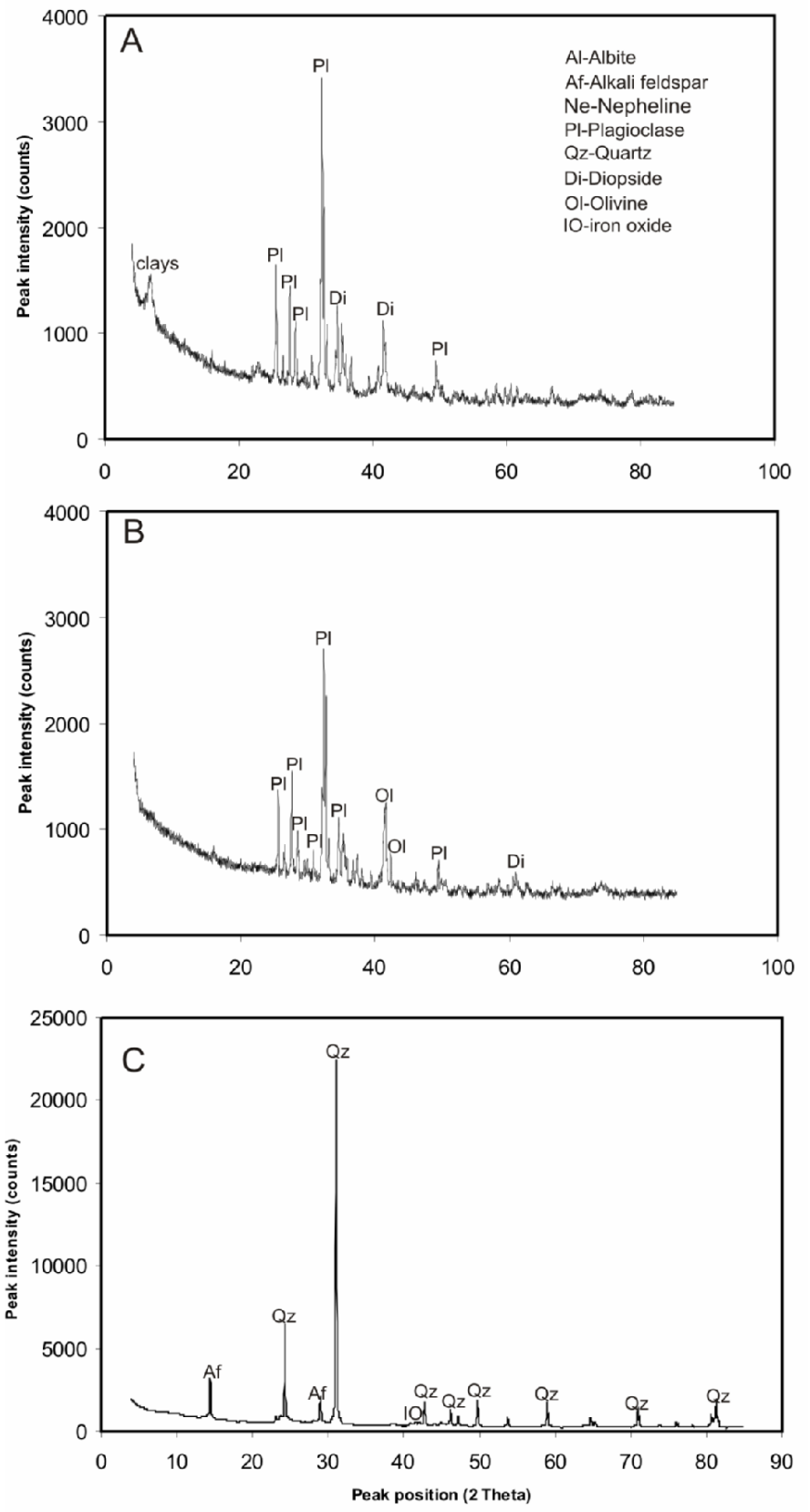

Appendix 2b. XRD scan of Aquifer rocks from Axum, (A) and (B) Basalt and (C) sandstone/siltstone

Appendix III

Physicochemical data of deep and shallow groundwater as well as spring and surface water from the Axum area (see sampling sites in Fig.1). $O_{2(aq)}$ and (TDS) total dissolved solids content is given in mg l^{-1}. Concentrations of dissolved compounds are in mmol l^{-1} except for ∑Fe and Sr^{2+} in µmol l^{-1}.

No	Site/Well name	Sampling date	pH	$O_{2(aq)}$ mg/L	Temp °C	TDS mg/L	Ca^{2+}	Mg^{2+}	Na^{+}	K^{+}	$Si(OH)_4$	∑Fe	Sr^{2+}	HCO_3^-	Cl^-	NO_3^-	SO_4^{2-}
Springs																	
AW1	Mayberki	19/12/08	8.57	10	21.7	440	0.74	1.23	2.61	0.05	0.10	0.5	4.28	3.95	0.97	0.01	0.18
AW2	St.Yared	21/12/08	6.99	6.5	17.1	504	1.80	1.39	1.28	0.13	0.42	2.1	5.73	6.29	0.26	0.26	0.11
		10/10/09	7.70	4.5	24.5	536	1.90	1.35	1.49	0.11	0.43	bdl	6.05	8.50	0.25	0.23	0.11
Surface water																	
AW3	AdiTsehafti	21/12/08	6.82	9.7	12.0	504	1.51	1.12	2.4	0.11	0.24	1.7	4.88	7.20	0.51	0.03	0.08
AW4	MayNigus	20/12/08	7.47	9.0	19.6	176	0.65	0.39	0.59	0.07	0.09	bdl	2.13	2.19	0.21	0.00	0.06
Deep wells																	
AW5	AdiBandras	19/12/08	7.24	3.0	24.0	680	2.27	1.26	1.86	0.07	0.32	bdl	6.94	5.69	2.45	0.11	0.16
		09/10/09	7.74	3.0	25.0	464	1.57	1.41	1.50	0.06	0.38	bdl	5.79	7.20	0.42	0.24	0.08
AW6	MayHaret	20/12/08	7.18	6.8	23.9	592	2.13	1.22	1.99	0.01	0.36	2.1	7.83	5.29	0.86	0.80	0.17
AW7	APW2	20/12/08	7.17	bdl	21.2	1386	3.52	3.18	6.09	0.33	0.74	42.6	5.96	15.48	0.73	0.00	0.42
		09/10/09	7.44	0.5	23.5	1264	3.82	3.31	8.44	0.33	0.79	53.6	6.29	22.20	0.72	0.00	0.39
AW8	W1	20/12/08	7.07	3.5	22.4	848	1.86	2.52	3.96	0.18	0.55	0.6	4.12	9.39	0.74	0.06	0.33
		09/10/09	7.57	6.8	24.1	840	2.04	2.58	5.09	0.17	0.58	bdl	4.50	13.30	0.72	0.06	0.32
AW9	W5	20/12/08	7.17	4.0	23.1	576	2.28	1.08	1.75	0.05	0.42	0.8	6.11	4.19	2.03	0.56	0.44
		09/10/09	7.70	2.6	23.4	624	2.49	1.08	2.13	0.05	0.44	bdl	6.39	5.70	1.95	0.51	0.42
AW10	W4	20/12/08	7.34	7.5	22.2	536	0.64	1.13	4.61	0.07	0.31	0.0	2.10	6.39	0.31	0.10	0.17
		10/10/09	7.65	6.0	25.8	552	0.81	1.20	5.27	0.04	0.32	bdl	2.74	8.70	0.48	0.01	0.16
AW11	W6	20/12/08	7.31	2.8	22.0	480	1.21	1.06	2.7	0.04	0.36	0.3	4.05	5.49	0.3	0.35	0.09
		10/10/09	7.65	6.2	25.0	472	1.29	0.95	2.85	0.02	0.39	bdl	4.25	7.60	0.31	0.41	0.09
AW12	May Hinto	20/12/08	7.24	3.0	22.8	440	1.78	0.84	1.54	0.12	0.41	0.3	5.87	5.19	0.29	0.56	0.08
AW13	APW5	21/10/08	7.24	2.8	24.3	536	1.83	1.14	1.85	0.02	0.38	0.7	6.65	4.49	1.09	0.55	0.31
		10/10/09	7.50	3.8	28.9	776	2.94	1.75	2.88	0.02	0.43	bdl	10.61	8.70	1.96	1.04	0.31
AW14	A-7	21/12/08	7.21	bdl	16.6	968	2.50	2.74	2.90	0.16	0.41	1.1	7.54	5.89	3.94	1.46	0.48
		10/10/09	7.82	4.2	26.5	952	1.51	3.33	4.44	0.21	0.38	bdl	4.07	7.30	4.54	0.69	0.72

AW15	A-4	21/12/08	6.98	5.8	24.7	648	1.85	1.61	2.08	0.09	0.40	0.0	5.62	5.80	1.61	0.54	0.22
		10/10/09	7.56	4.3	24.1	936	2.54	2.64	3.58	0.13	0.41	bdl	7.72	9.40	3.52	0.87	0.50
AW16	Arequiti-2	21/12/08	6.94	bdl	25.9	1768	4.12	4.97	8.62	0.59	0.28	191	11.64	21.48	1.15	0.00	1.10
		09/10/09	7.38	bdl	25.4	2168	5.71	6.94	13.4	0.90	0.39	31.7	16.78	37.79	1.57	0.01	1.39
AW17	Arequiti-1	21/12/08	6.94	6.5	23.2	512	1.40	1.35	2.02	0.06	0.39	0.3	5.30	5.70	0.43	0.48	0.11
		10/10/09	7.54	5.7	24.9	672	1.60	1.96	3.95	0.12	0.43	bdl	6.64	10.60	0.46	0.01	0.21
AW18	APW3	10/10/09	7.48	0.5	23.0	904	2.72	2.37	5.22	0.24	0.82	81.2	4.77	14.50	0.64	0.00	0.22
AW19	Mayshum	10/10/09	7.69	6.0	24.6	544	2.01	1.03	2.18	0.05	0.42	bdl	5.59	8.30	0.73	0.14	0.16
Shallow wells																	
AW20	HamedGebz	19/12/08	7.17	2.5	21.2	848	2.57	1.72	1.68	0.06	0.44	bdl	8.67	4.69	2.63	1.36	0.22
AW21	St. Gebriel	19/12/08	7.43	5.5	22.5	704	2.38	1.64	1.82	0.05	0.4	bdl	6.70	5.29	1.52	1.21	0.20
AW22	Ezana Park	19/12/08	7.03	3.0	23.3	520	1.77	0.75	1.68	0.10	0.42	1.3	7.08	3.00	1.57	1.37	0.26
AW23	May Siye	21/12/08	7.12	5.4	24.4	512	2.03	1.22	1.08	0.02	0.42	1.3	5.25	5.59	0.41	0.38	0.32
AW24	Zorat_2	19/12/08	7.32	4.0	23.0	256	0.99	0.43	0.77	0.05	0.51	0.8	3.33	2.50	0.32	0.08	0.05
AW25	Zorat_1	09/10/09	7.51	4.2	21.5	224	0.94	0.21	0.85	0.10	0.21	bdl	2.53	3.10	0.41	0.14	0.10
AW26	Adiberekti	09/10/09	7.71	nm	23.5	328	1.73	0.48	0.43	0.07	0.22	bdl	3.61	5.00	0.27	0.08	0.20
AW27	Mayhakay	09/10/09	7.24	nm	24.0	680	0.83	0.29	0.46	0.01	0.19	163	17.63	2.50	0.31	0.00	0.15
AW28	Adikelkel	10/10/09	7.39	4.2	22.5	472	2.15	0.86	1.24	0.02	0.38	bdl	5.38	7.20	0.37	0.34	0.07
AW29	GolgolAwle	10/10/09	7.57	5.2	24.0	576	2.57	1.22	1.54	0.02	0.42	bdl	5.74	8.70	0.37	0.49	0.07
AW30	Mayguala	10/10/09	7.69	3.6	26.3	528	1.95	1.03	2.01	0.02	0.34	bdl	6.06	7.40	0.50	0.58	0.08
AW31	Shhtanbo	10/10/09	7.41	2.0	27.7	648	1.33	1.86	4.44	0.13	0.63	bdl	bdl	10.40	0.50	0.00	0.13
AW32	Africa hotel	11/10/09	6.81	3.8	21.7	496	1.96	0.97	2.01	0.01	0.42	bdl	5.69	5.40	1.43	0.91	0.23

bdl: below detection limit

nm: not measured

Appendix IV

Trace element analysis results, concentration is given in ppb

No	Site/Well name	Li	B	Al	Cr	Co	Ni	Cu	Zn	As	Se	Rb	Zr	Ba	Pb	U
AW1	Mayberki	1.2	54.6	21.9	0.3	0.7	3.4	2.4	4.5	0.5	1.7	1.0	13.6	72.1	0.1	1.7
AW2	St.Yared	22.6	47.5	32.7	0.1	1.1	2.4	1.0	1.4	1.3	0.9	3.5	37.5	127.6	0.0	2.1
		4.1	16.1	bdl	bdl	0.5	15.0	1.7	1.0	0.0	1.1	6.2	0.2	15.3	bdl	1.7
AW3	AdiTsehafti	22.6	47.5	32.7	0.1	1.1	2.4	1.0	1.4	1.3	0.9	3.5	37.5	127.6	0.0	2.1
AW4	MayNigus	bdl	18.1	41.7	0.1	0.2	1.1	1.3	1.3	0.4	0.5	1.4	20.5	59.6	0.1	0.4
AW5	AdiBandras	2.0	33.3	7.4	0.9	0.8	8.8	2.4	17560.0	0.3	2.2	1.9	19.6	43.7	15.5	0.4
		3.4	32.7	bdl	bdl	0.3	1.6	4.6	161.0	bdl	1.2	2.7	0.3	17.5	3.8	0.6
AW6	MayHaret	4.8	41.7	5.9	0.3	0.6	1.7	6.0	11.2	4.2	3.6	0.4	14.2	24.5	0.5	0.4
AW7	APW2	160.5	156.8	15.8	0.4	3.0	7.6	5.6	39.5	0.5	0.8	18.0	36.4	98.9	0.0	0.5
		64.8	130.1	bdl	bdl	2.8	9.2	5.6	46.5	bdl	0.6	19.1	0.4	114.2	3.9	0.4
AW8	W1	21.4	94.8	6.7	0.2	0.4	1.7	3.0	18.1	0.4	2.5	6.1	14.2	125.0	1.3	0.4
		9.6	75.5	bdl	bdl	0.3	2.0	8.8	15.5	bdl	0.8	5.8	bdl	102.9	5.8	0.4
AW9	W5	2.3	30.4	6.6	0.7	0.2	4.2	3.4	41.2	0.1	3.4	3.1	9.4	20.1	0.2	2.2
		3.7	20.0	bdl	bdl	bdl	9.5	1.3	2.9	bdl	2.8	2.6	bdl	11.5	3.5	2.2
AW10	W4	23.1	105.8	9.3	0.1	0.1	1.1	2.3	18.7	0.1	0.6	2.2	12.0	10.7	1.4	0.4
		9.8	87.1	bdl	bdl	0.7	1.3	4.3	26.4	0.4	0.4	2.5	0.5	12.0	bdl	0.3
AW11	W6	9.6	44.6	5.6	0.1	0.1	0.9	2.3	61.8	0.1	0.8	1.2	5.7	40.8	1.6	0.2
		5.1	41.3	bdl	bdl	0.6	121.4	10.9	20.7	0.1	0.8	1.5	0.3	11.8	bdl	0.1
AW12	May Hinto	1.1	22.3	9.0	0.2	0.1	4.0	3.2	2.7	0.0	4.3	2.9	6.1	39.5	0.2	0.9
AW13	APW5	1.5	24.2	17.8	0.3	0.3	3.9	1.2	14.3	0.3	0.6	0.5	20.8	64.2	0.1	0.3
		5.3	81.7	bdl	11.7	4.1	70.5	6.1	14.7	2.9	1.4	3.8	2.4	6.3	bdl	0.7
AW14	A-7	54.1	41.7	12.1	0.9	0.4	6.5	0.9	111.7	0.6	1.6	4.8	19.0	23.4	0.0	1.8
		31.0	44.0	n.n.	1.6	0.5	6.2	8.8	132.2	0.4	1.6	7.3	0.2	18.6	bdl	0.7
AW15	A-4	27.7	40.5	22.5	0.4	0.3	3.1	1.9	4.9	0.4	1.1	3.4	24.8	47.8	0.1	1.0
		25.0	38.9	n.n.	1.3	0.7	8.1	0.9	66.3	bdl	1.3	5.1	0.3	32.5	bdl	2.3
AW16	Arequiti-2	199.7	549.4	14.6	0.0	8.8	46.7	1.9	17350.0	64.6	1.5	35.9	106.2	111.8	0.0	2.1
		111.3	612.7	bdl	bdl	4.1	20.8	2.9	83.7	7.8	1.0	48.4	1.8	86.7	7.7	2.5
AW17	Arequiti-1	10.7	40.6	6.7	bdl	0.2	5.1	1.1	30.3	0.4	1.2	2.5	24.6	44.8	0.0	0.3

		11.8	63.7	bdl	bdl	0.7	2.0	1.7	104.9	bdl	0.9	5.7	bdl	97.7	3.7	0.6
AW18	APW3	58.8	81.2	bdl	bdl	3.3	8.2	4.1	83.9	bdl	1.1	15.2	bdl	134.6	3.8	0.1
AW19	Mayshum	8.7	59.1	bdl	bdl	0.5	2.1	2.2	42.4	0.1	1.4	7.4	0.3	2.2	bdl	6.4
AW20	HamedGebz	4.6	27.2	9.2	0.7	0.4	2.1	1.4	19.1	1.4	2.5	2.2	15.5	56.1	0.0	1.4
AW21	St. Gebriel	3.4	30.3	20.8	1.0	0.3	2.2	1.9	244.4	0.6	1.4	2.5	15.7	1.9	0.3	1.4
AW22	Ezana Park	3.1	22.1	146.5	0.7	0.3	1.6	2.1	5.0	0.4	1.1	1.3	69.4	15.0	0.1	0.3
AW23	May Siye	0.5	22.7	113.8	0.3	0.3	1.7	4.4	10.6	0.2	1.7	0.6	43.5	31.0	0.0	0.4
AW24	Zorat_2	2.5	24.7	7.0	0.1	0.1	5.1	4.6	797.3	0.1	0.6	2.8	11.6	58.5	0.7	0.1
AW25	Zorat_1	4.6	27.1	bdl	bdl	0.4	1.0	20.5	461.1	0.3	1.2	3.3	0.5	67.4	2.8	0.2
AW26	Adiberekti	2.2	29.1	bdl	bdl	0.5	1.8	2.9	206.2	0.1	0.8	3.4	0.2	95.6	2.6	0.4
AW27	Mayhakay	2.6	29.0	bdl	bdl	48.1	26.5	7.2	93.9	0.7	0.6	0.9	0.1	179.2	2.9	0.1
AW28	Adikelkel	1.2	24.5	bdl	bdl	bdl	1.9	4.5	834.6	bdl	1.2	1.6	bdl	427.4	5.4	0.5
AW29	GolgolAwle	1.0	25.7	bdl	bdl	0.0	3.4	2.9	27.1	bdl	1.3	1.8	bdl	365.2	1.6	0.5
AW30	Mayguala	1.2	28.7	bdl	bdl	bdl	1.6	3.6	4425.5	bdl	2.0	0.5	bdl	169.4	2.7	0.4
AW31	Shhtanbo	3.0	44.9	bdl	bdl	bdl	1.2	1.5	64.9	bdl	0.6	3.3	bdl	115.2	1.8	0.8
AW32	Africa hotel	2.0	21.9	bdl	bdl	0.4	3.9	0.5	14.8	bdl	1.1	1.3	0.1	44.2	bdl	2.6

bdl: below detection limit

Appendix V

Isotope signatures (δ^2H, $\delta^{18}O$, $\delta^{13}C$ in ‰ and $^{87}Sr/^{86}Sr$), DIC (mmol l^{-1}) and PCO_2 (atm).

No.	Coordinate		δ^2H	$\delta^{18}O$	$\delta^{13}C$	$^{87}Sr/^{86}Sr$	DIC	Log
	X	Y	‰	‰	‰			PCO_2
AW1	474582	1560677	14.8	1.7			3.95	-3.24
AW2	469766	1564473	-6.1	-2.6	-9.9	0.70433	7.73	-1.47
	469766	1564473	-7.9	-3.3	-10.6		8.76	-2.02
*			-6.9	-2.6		0.70431		
AW3	468633	1565545	5.3	0.4	-1.2		9.89	-1.27
AW4	463509	1560632	15.0	1.8	-5.5		2.36	-2.37
*			30.7	4.9				
AW5	476941	1558543	0.1	-1.1	-9.9	0.70571	6.33	-1.73
	476941	1558543	1.6	-1.2	-10.5		3.30	-2.13
*			-1.4	-1.6				
AW6	462256	1557914	-1.6	-1.5	-10.1	0.70463	5.98	-1.70
AW7	463266	1559530	-5.5	-1.9	-3.5	0.70574	17.5	-1.26
	463266	1559530	-5.1	-2.0	-2.1		23. 6	-1.37
*			-7.3	-1.8		0.70575		
AW8	466030	1559858	-14.2	-3.1	-4.9	0.70440	10.9	-1.36
	466030	1559858	-12.8	-3.1	-4.3		13.9	-1.71
*			-22.9	-2.9		0.70451		
AW9	466142	1560033	2.9	-0.6	-7.6	0.70592	4.79	-1.77
	466142	1560033	2.8	-0.7	-7.6		5.87	-2.20
*			0.4	-0.6		0.70596		
AW10	467291	1559514	-4.8	-1.8	-6.5	0.70401	6.99	-1.78
	467291	1559514	-4.6	-2.1	-6.1		9.03	-1.94
*			-6.6	-1.8				
AW11	466996	1559504	-4.6	-1.6	-8.5	0.70471	6.04	-1.81
	466996	1559504	-1.7	-2.1	-8.8		7.89	-2.01
*			-5.2	-1.7		0.70467		
AW12	466341	1559695	-0.9	-1.3	-8.9		5.80	-1.76
*			-2.7	-1.3				
AW13	467842	1559661	-1.2	-1.2	-10.7	0.70455	5.00	-1.82
	467842	1559661	-2.8	-1.6	-9.3		9.13	-1.79
*			1.4	-1.2		0.70458		
AW14	470699	1560989	-6.8	-2.7	-4.3	0.70501	6.67	-1.74
	470699	1560989	-9.5	-2.9	-0.6		7.41	-2.21
*			-11.5	-2.7		0.70491		
AW15	471628	1560884	-4.1	-1.9	-4.1	0.70485	6.98	-1.45
	471628	1560884	-9.8	-3.1	-4.5		9.83	-1.85
*			-11.6	-2.8		0.70485		
AW16	470358	1556962	-13.6	-2.9	1.1	0.70543	25.8	-0.88
	470358	1556962	-15.9	-3.6	0.1		40.3	-1.10

*			-30.0	-3.3		0.70545		
AW17	470031	1558054	-0.1	-1.2	-7.5	0.70432	6.88	-1.47
	470031	1558054	-7.9	-2.4	-4.2		11.1	-1.76
*			-11.2	-2.4		0.70387		
AW18	462895	1559472	-5.3	-2.4	-2.1		15.3	-1.59
*			-2.8	-1.7		0.70585		
AW19	469975	1562729	-10.1	-3.5	-7.2		8.56	-2.02
*			-11.1	-3.1				
AW20	471600	1560490	-0.9	-1.5	-8.9	0.70561	5.32	-1.76
AW21	472131	1561576	-1.9	-1.7	-9.9	0.70515	5.66	-1.96
AW22	470284	1561471	-6.5	-2.5	-11.0	0.70535	3.56	-1.79
AW23	470176	1557251	1.0	-1.3	-11.4		6.43	-1.61
AW24	474342	1562731	-4.1	-2.1	-7.7		2.74	-2.15
AW25	474361	1562533	-0.4	-1.9	-9.6		7.39	-2.26
AW26	475443	1553432	1.1	-1.9	-11.2		5.16	-2.25
AW27	475481	1553277	1.6	-1.5	-11.4		2.73	-2.08
AW28	469617	1553735	6.5	-0.7	-8.3		7.77	-1.79
AW29	469167	1553838	5.1	-1.0	-8.4		9.10	-1.88
AW30	462006	1557104	1.3	-1.5	-7.3		7.63	-2.06
AW31	462571	1553681	-3.7	-2.4	-12.0		11.1	-1.62
AW32	471178	1561610	-4.7	-2.7	-10.7		7.12	-1.34

*****additional sampling campaign in summer 2009 for $\delta^{2}H$, $\delta^{18}O$ and $^{87}Sr/^{86}Sr$ analysis.

Appendix VI

Phreeqc input file

```
SELECTED_OUTPUT
        file       L:\Project\Study area\phreeqc_aqua\in5_3.xls #_llnl.xls
        -solution          true
        -charge_balance true
        -reaction          false
        -temperature     true
        -alkalinity        true
        -ionic_strength true
        -water  true
        -percent_error  true
SOLUTION 1 #AW23
        units     mg/l
        pH         7.12
        pe         4
        temp      24.4
       redox     pe
        K          .86
        Na         24.8
        Ca         81.34
        Mg        29.8
        Cl         14.43
        Fe         .07
        N(+5)    23.65
        S(+6)    30.4
        Si         25.5      as SiO2
        O(0)   5.4 O2(g)  -0.88
        Alkalinity          321.7119  as HCO3

SOLUTION 2  #AW16
        units     mg/l
        pH         6.94
        pe         4
        temp      25.9
        redox     pe
        K          23.68
        Na         198.56
        Ca         165.8
        Mg        120.98
        Cl         41.02
        Fe         10.64
        N(+5)    .14
        Mn        .41
        S(+6)    105.89
        Si         16.9      as SiO2
        O(0)   1   O2(g) -1.60
        Alkalinity          1411.93  as HCO3
INVERSE_MODELING 1
```

```
   -solutions      1 2
          -uncertainty    0.025  0.025
          -phases
                    Kaolinite  pre # only precipitate
                    Ca-Montmorillonite pre # precipitate
                    CO2(g) diss
                    H2S(g)
                    N2(g)  pre # denitrification
                    Pyrolusite # maganese in subsurface
                    Fe(OH)3(a)
                    Plagioclase diss #only dissolves
                    Diopside diss
                    Olivine diss
                    SiO2(a)
                    Calcite pre
                    Siderite    pre
                    K-feldspar diss
                    Halite diss   # only dissolve
                    CH2O diss
                    CaX2
                    MgX2
                    NaX
          -balances
                    ph 0.1
                    Cl
                    S(6)
                    Mn
                    N(+5)
          -mineral_water false

PHASES
Plagioclase      #An70
Na0.3Ca0.7Al1.7Si2.3O8 + 6.3H2O + 1.7H+ = 0.3Na+ + 0.7Ca+2 +1.7Al(OH)3 + 2.3H4SiO4
           log_k = 0
CH2O
          CH2O+ H2O = CO2 + 4H+ + 4e-
                              log_k = 0.0
Olivine
          MgFeSiO4  + 4H2O + 4CO2  = Mg+2 + Fe+2 + H4SiO4 + 4HCO3-
          log_k = 0.0

Diopside    # clinopyroxine
          CaMgSi2O6 + 4CO2 + 6H2O = Ca+2 + Mg+2 + 4HCO3- + 2H4SiO4
          log_k = 0.0
EXCHANGE_SPECIES
X- = X-; log_k 0
X- + Na+ = NaX; log_k 0.0 # define the half-reactions of ion exchange
2X- + Ca+2 = CaX2; log_k 0.8

End
```